Production of Cascade Hyperons in Hadron- and Photon-induced Reactions

by

Benjamin C. Jackson

(Under the Direction of Professor Kanzo Nakayama)

Abstract

Towards a better understanding of multi-strangeness physics, various aspects of Ξ hyperon production are investigated in the reactions $\bar{K} + N \to K + \Xi$ and $\gamma + N \to K + K + \Xi$. First $\bar{K} + N \to K + \Xi(\Xi^*)$ is treated in a model-independent manner and a minimum set of spin observables is established that will determine the spin-parity of the produced $\Xi(\Xi^*)$, two of the basic quantum numbers that specify a baryon. In addition, a calculation for all observables is done within a simple effective lagrangian model in an effort to learn about the reaction dynamics. Here $S = -1$ hyperon resonances contributions are reported which are important production mechanisms for Ξ baryons. The $\gamma + N \to K + K + \Xi$ reaction has a more complicated spin structure and we derive the most general spin structures consistent with basic symmetry principles. The effect of parity conservation on spin observables is investigated. A gauge-invariant model is described which is consistent with the calculation for the $\bar{K} + N \to K + \Xi$ reaction.

Index words: Baryon spectroscopy, $S = -2$ baryons, $\bar{K}$-induced reactions, Cascade photoproduction

Production of Cascade Hyperons in Hadron- and Photon-induced Reactions

by

Benjamin C. Jackson

B.S., Physics, Georgia Institute of Technology, 2004

A Dissertation Submitted to the Graduate Faculty
of The University of Georgia in Partial Fulfillment
of the
Requirements for the Degree

Doctor of Philosophy

Athens, Georgia

2015

Production of Cascade Hyperons in Hadron- and Photon-induced Reactions

by

Benjamin C. Jackson

Approved:

Major Professor:	Kanzo Nakayama
Committee:	Michael Bachmann
	Michael Geller

Electronic Version Approved:

Julie Coffield
Interim Dean of the Graduate School
The University of Georgia
May 2015

Production of Cascade Hyperons in Hadron- and Photon-induced Reactions

Benjamin C. Jackson

April 21, 2015

Acknowledgments

Firstly, I would like to thank my PhD. advisor, Professor Kanzo Nakayama. His instruction and guidance is why my research is possible. His passion for research and high standards are traits that I hope to exemplify during my career. I would like to thank Professors Helmut Haberzettl and Yongseok Oh, who have taught me much about physics, writing, presenting and professionalism. I would like to thank my committee members, Professors Michael Geller and Michael Bachmann who both took the time to be a part of this work.

I would like to thank all of my fellow students, both past and present, who have helped foster a positive and enjoyable environment in our department. I would like to thank all of my friends who have been supportive and encouraging over the many years of my studies. A special acknowledgment must be made for Jennifer Kvapil, whose selfless help over the final year of my graduate studies was much needed and always given with eagerness.

Finally, I would like to dedicate the entirety of my time at UGA to my family. My father and mother, Charlie and Debra Jackson, and my sister, Caroline Jackson, have waited a long time for the completion of this work. I do this for them as much as for myself. I hope I have made them proud.

Contents

List of Figures

List of Tables

Chapter 1

Introduction and Motivation

1.1 Standard Model of Particle Physics

The Standard Model of Particle Physics is founded on the belief that all fundamental interactions are mitigated via an exchange of *gauge bosons*. The four fundamental forces are the strong nuclear force, weak nuclear force, electromagnetic force and gravity. It is common to separate gravity from the discussion of the other forces for at least three reasons: gravity is nearly 40 orders of magnitude weaker than the electromagnetic force, and thus has a very small effect at the level of particle interactions, the gauge boson associated with gravity, the graviton, has not been observed and a testable quantum theory of gravity that agrees with the theory of General Relativity has not yet been formally developed. String theory may be a possible candidate theory which unifies the four fundamental interactions. The three remaining forces each have gauge bosons which result in demanding the quantum field theory describing the free fermions be invariant under *local* $U(1)_Y \times SU(2)$ and $SU(3)_c$. This $U(1)_Y \times SU(2)$ symmetry unifies the electromagnetic and the weak interaction into the electroweak interaction and the formal theory was developed by Glashow, Weinberg, and Salam for which they were awarded the Nobel Prize in 1979. The $U(1)_Y \times SU(2)$ invariance reduces to $U(1)_{em}$ symmetry after spontaneous symmetry breaking caused by the Higgs mechanism. This $U(1)_{em}$ symmetry of fermions with electromagnetic charge results in the photon. The remaining gauge particles after the symmetry breaking are the three gauge bosons, Z^0, W^+

and W^-. The photon is massless while the other three have masses over 80 GeV. The $SU(3)_c$ is the color charge symmetry of the quarks. The formal theory of quarks and the color-charge carrying gluons is Quantum Chromodynamics (QCD) is generally believed to be the correct theory explaining the strong interaction. The $SU(3)_c$ symmetry results in eight massless gluons which interact with the quarks as well as each other. This self interaction is a feature of any *non-Abelian* gauge theory and is also seen in the weak sector of the electro-weak interaction. This self interaction is an important reason why fundamental calculations of processes involving the strong interaction are very difficult.

The other difficulty is due to the growing coupling of the interaction as distance becomes larger. This means that the strong interaction is inherently non-perturbative in the low-energy regime. Add this to the self-interacting aspect of QCD and you have a very difficult problem to solve. One place to study this non-perturbative regime of QCD is hadronic systems: color neutral systems of quarks. The statement of color neutrality is a statement of *confinement*. Confinement is seen experimentally as the lack of isolated quarks, i.e., a single quark which is not part of a hadronic system has never been observed. Confinement is seen theoretically as the requirement that closed systems of quarks *must* form color neutral objects or, put another way, they must be invariant under $SU(3)_c$ transformations, i.e., color singlets. These statements actually extend to any state made of particles with color charge. This means that physical states of single gluons have not been observed either and predicted states of multiple gluons, or glueballs, must be color singlets as well.

This concept of color charge has been introduced in [1], and is a vital addition to the quantum description of baryons because it allows $\{qqq\}$ states to exist when all three quarks are identical and occupy the ground state. Without color charge, three identical spin-1/2 fermions would not be allowed in the same state due to the Pauli Exlusion Principle. The discoveries of the Δ^{++} $\{uuu\}$, Δ^- $\{ddd\}$, and Ω^- $\{sss\}$ confirm the existence of these states and demand that quarks must carry an additional quantum number (color). The possible color-neutral states are usually grouped in 2 or 3 categories. Systems containing a quark $\{q\}$ carrying color charge and and anti-quark $\{\bar{q}\}$ carrying anti-color charge can form a color singlet state and are called mesons $\{q\bar{q}\}$. Systems containing three quarks can be created so that they are color singlets and are called baryons $\{qqq\}$. Quark

configurations not included in these two possibilities fall into an exotic category which contains states such as the tetraquark $\{qq\bar{q}\bar{q}\}$, pentaquark $\{qqqq\bar{q}\}$, and states made from coupled hadronic states into hadronic 'molecules', amongst others. A non-trivial quark state, say $\{qq\bar{q}\bar{q}\}$, may have the same quark content as a hadronic molecule, $\{q\bar{q}+q\bar{q}\}$. The distinction between a non-trivial quark state and a hadronic molecule is not clear but it has been confirmed that these exotic quark states exist. Recently, two new four-quark states were discovered, $Z_b(10610)$ and $Z_b(10650)$ [2–4]. One of the purposes of hadron physics is to investigate the quark structure of hadrons. A review of heavy quarkonia can be found in Ref. [5]

Quarks come in 6 varieties. The up (u), down (d) and strange (s) quarks have relatively low mass, approximately 2.3, 4.8 and 95 MeV respectively [6]. The charm (c) quark, bottom (b) quark and top (t) quark are all much more massive. Their masses are listed as approximately 1.3, 4.2, and 173 GeV respectively [6]. The three lightest quarks have a mass which is comparable to zero on the hadronic scale of ~ 1 GeV. This mass structure leads to two near symmetries, chiral symmetry and iso-spin symmetry. If the masses of the quarks are zero, the lagrangian for the quarks can be separated into left and right handed spinor fields.

$$\mathcal{L}_0 = \sum_{a=\mathrm{u,d,s,c,t,b}} \bar{\Psi}_a i\not{D}\Psi_a = \sum_a \left(\bar{\Psi}_{L,a} i\not{D}\Psi_{L,a} + \bar{\Psi}_{R,a} i\not{D}\Psi_{R,a}\right) \tag{1.1}$$

$$\Psi_{R,L} = \frac{1 \pm \gamma_5}{2}\Psi \tag{1.2}$$

The lagrangian now has $SU(6)_L \times SU(6)_R$ symmetry because the L and R portions of the fields are decoupled. This chiral symmetry can be written as a vector, $V = L+R$, and axial-vector, $V = L-R$, symmetry. While the ground state, vacuum, does have the vector symmetry, it does not share the axial-vector symmetry and thus spontaneously breaks the chiral symmetry. There should appear massless Nambu-Goldstone bosons (NGBs) as a result of this spontaneous symmetry breaking and they should have $J^P = 0^-$ due to the ground state breaking the axial symmetry. Though a set of very low mass 0^- mesons do exist and are considered to be the Nambu-Goldstone bosons predicted, they have non-zero mass and do not have an $SU(6)$ symmetry. The non-zero mass is a result of the mass terms in the original lagrangian. While the mass of the quarks explicitly breaks chiral

symmetry, the three least massive quarks, {u,d,s}, are light enough that the chiral symmetry is nearly realized and therefore the NGBs are seen with a *near* $SU(3)$ structure.

As just mentioned, the other near symmetry that is seen is $SU(3)$ iso-spin symmetry. This symmetry can be seen from the free lagrangian of the {u,d,s} quarks

$$\mathcal{L}_0 = \sum_{a=\text{u,d,s}} \bar{\Psi}_a i \not{D} \Psi_a - m_a \bar{\Psi}_a \Psi_a \,. \tag{1.3}$$

The mass terms are included here and the lagrangian has $SU(3)$ symmetry *when* the masses of {u,d,s} are all equal. The masses of u and d are *nearly* equal and this leads to a very good $SU(2)$ symmetry which is expressed in the meson sector as the quark structures $\{u\bar{u}, d\bar{d}, u\bar{d}, d\bar{u}\}$ splitting into iso-spin singlet and iso-spin triplet states. The $SU(2)$ 0^- singlet is the η_8 state and the triplet is $\{\pi^+, \pi^0, \pi^-\}$ with all four having equal masses. The mass difference, $\Delta m = m_s - m_u \approx m_s - m_d \neq 0$, does explicitly break the $SU(3)$ symmetry but because it is still small compared to the hadronic scale, the symmetry is nearly conserved. The full, nearly realized, $SU(3)$ symmetry results in eight states with similar masses. The 0^- octet contains $\{\eta_8, \pi^+, \pi^0, \pi^-, K^+, K^0, \bar{K}_0, K^-\}$. The states containing s quarks are more massive than states composed of only u and d, and the quite good $SU(2)$ symmetry is contained within this $SU(3)$ octet, i.e., $u\bar{s}$ states and $d\bar{s}$ states have nearly equal mass. The observed $SU(3)$ 0^- states number nine due to the $SU(3)$ singlet state, η_0, and are $\{\eta, \pi^+, \pi^0, \pi^-, K^+, K^0, \bar{K}_0, K^-, \eta'\}$. The physical η and η' states are mixtures of the octet, η_8, and singlet, η_0, states. Here we note that the peculiarly high mass of the physical η' ($\sim$ 958 MeV) is a consequence of QCD $U(1)_A$ axial vector anomaly [7–10, 12–14]. This 8-fold(+1) grouping of the low-mass mesons is often referred to as the '8-fold way' [15]. This $SU(3)$ iso-spin symmetry is seen in the baryonic sector as well, where states organize themselves into octets and decuplets. Fig. 1.1 is a visualization of this $SU(3)$ organization scheme.

1.2 Motivation for Studying Hadronic Systems

The $SU(3)$ organization scheme described above has been very successful in predicting and classifying the light hadrons. Unfortunately, it is incapable of explaining the mass discrepancy between

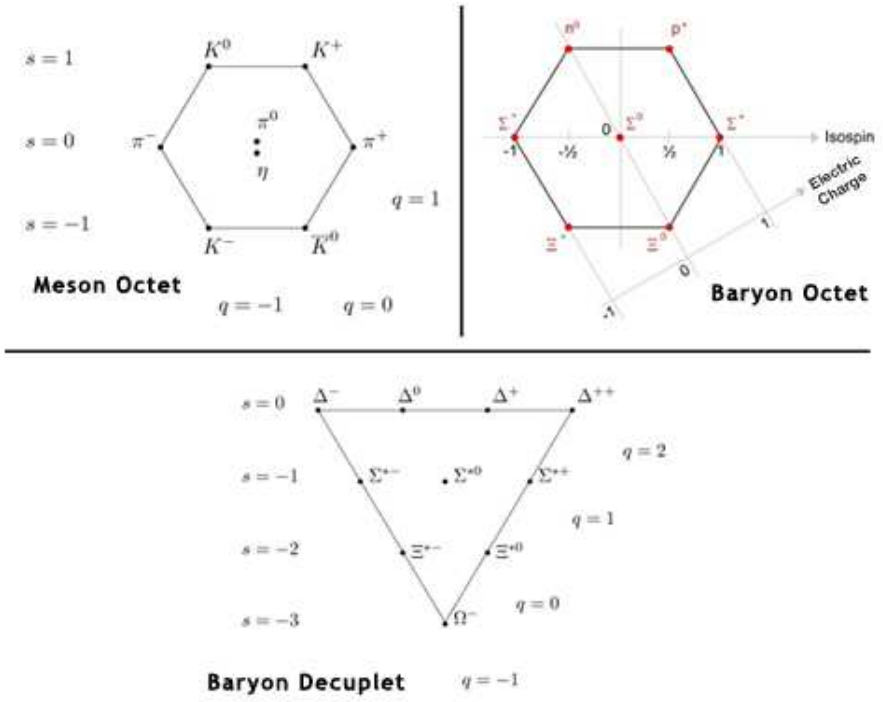

Figure 1.1: Meson 0^- octet, $\frac{1}{2}^+$ baryon octet and $\frac{3}{2}^+$ baryon decuplet. Image from [16]

the current quarks of the QCD lagrangian and the mass of the observed hadrons. The lightest baryons, the nucleons, have a mass of over 900 MeV while the up and down quark masses composing the nucleon are $\sim$ 15 MeV. Even the lightest NGB, the pion, has a mass of $\sim$ 14 times the mass of its quarks. Clearly most of the energy of the hadrons is not contained in the valence quark's mass but in the quark-gluon 'soup' inside the hadron. If one wishes to study this mixture or the valence quarks, a high energy scattering experiment must be conducted to probe this internal structure. But, as the energy is increased, the strong interaction becomes weaker and can be described perturbatively. This effect is referred to as *asymptotic freedom* and means that quarks are only free at very high energies, or very small separations. Fig. 1.2 shows this feature by α_S approaching zero as momentum transfer, Q, becomes larger than 100 GeV. Therefore, to examine the nonperturbative nature of the strong interaction, one must study systems where the quarks have low energies, i.e., low-energy hadrons. Fig. 1.2 again shows the strong coupling content, α_S,

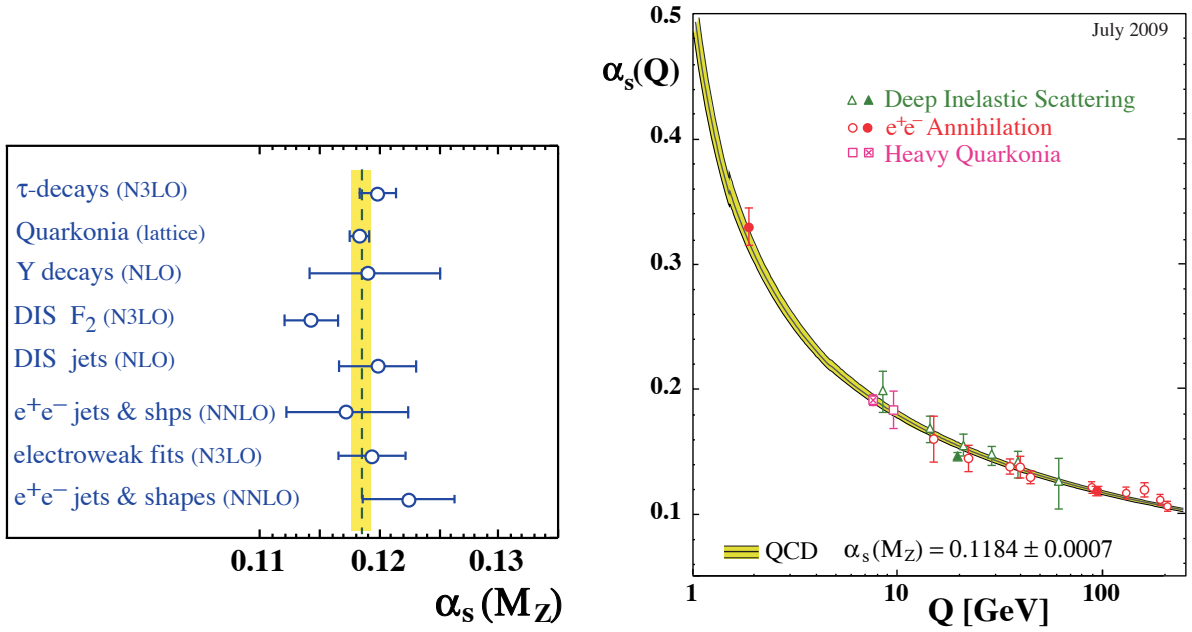

Figure 1.2: The figure on the left are values for the strong coupling constant, α_s at an energy scale of $Q = M_Z$ found using different channels. The figure on the right is a graph of α_s as a function of energy scale Q. Image from Ref. [17]

growing quickly as energy or momentum transfer drop below $\sim$ 10 GeV. For a sense of scale, the process $\bar{K} + N \to K + \Xi$ lives in the $Q < 10$ GeV region for the energies considered in this work.

In particular, hadron spectroscopy is an essential part of the investigation to understand the non-perturbative regime of QCD. The non-perturbative nature of QCD allows for poles in scattering amplitudes, i.e., resonances. In principle, an ab-initio approach to hadron resonance physics can be provided by lattice QCD (LQCD) simulation. Instead of a continuum gauge theory, a discrete statistical mechanical system is applied on a four-dimensional Euclidean lattice while exact gauge invariance is preserved [18]. The spectra of excited baryons observed in the recent lattice simulations [19,20] hold the promise of explaining the rich dynamics in the resonance energy region in the near future. Once quark masses drop towards the physical limit and finite volume effects are fully under control, a close comparison to experimental data will be possible [21–29]. Constituent quark models [30,31] have been developed to describe the resonance structure of hadrons. Some of these models organize hadrons in terms of $SU(6) \times O(3)$ supermultiplets [32] and some attempts

are made at adding relativistic effects [33]. Other relativistic and non-relativistic quark models calculate resonance features. Other approaches such as the dynamical Dyson-Schwinger [34] and the Skyrme model [35] also generate resonance spectra. Unitarized Chiral Perturbation Theory also provides a complementary picture of some of the low-lying resonances [36, 37]. Some of these attempts have been directed at the Ξ spectra and are discussed below.

These theoretical results must be compared with resonance parameters extracted from experimental data. This is no easy task and a quick glance at a list of nucleon resonances shows why. There are 11 N^* states below 2 GeV with a 3- or 4-star status and several more have been seen with less confidence [6]. Although resonances can be seen as peaks in cross section data, they are often much more difficult to discern. Because such resonances are so close in energy and many have large widths, extracting them from scattering data almost always requires a robust reaction theory. Such reaction theories, based on a coupled-channel approach, have been developed to various degree of sophistication and are being improved. So far, most of the experimentally extracted baryon resonances come from the pion-induced reaction experiments, especially the πN scattering, and about 16 nucleon resonances and 11 Δ resonances have been identified [6]. A number of Λ and Σ baryons, which are particles with strangeness quantum number $S = -1$, have been also discovered [6]. A review on the status of baryon spectroscopy is given, e.g., in Ref. [38, 39].

Effective field theories (EFTs) are a powerful tool to describe the strong interaction in the non-perturbative regime of QCD. EFTs are based on the assumption that the low-energy behavior of a theory should not strongly depend on the high energy dynamics. These omitted dynamics of the high-energy portion of the full theory are absorbed into the EFT's parameters, known as the low energy constants. The goal then is to find the most general lagrangian, involving only the low-energy degrees of freedom, that retains all of the symmetries of the full theory [40]. Below 1 GeV, the only degrees of freedom for a QCD EFT are the 0^- mesons and the nucleons. Chiral Perturbation Theory (χPT) is this QCD effective theory with pions and nucleons and is an expansion in terms of m_π/Λ_{QCD} or m_π/m_N. These expansions are not unitary. Unitarity is satisfied by solving the Bethe-Salpeter equation. Such an approach is known as Unitarized Chiral Perturbation Theory (UχPT). This approach generates resonances dynamically, i.e., resonances are generated through

the Bethe-Salpeter equation. Currently, both χPT and UχPT are only able to describe resonances for s- partial waves thus limiting their applicability [41], though there are efforts to include the p-wave [42, 43].

There are many different reaction theories which are applied in the extraction of resonances from scattering data. In K-matrix appraoches, the Bethe-Salpeter equation is solved but the real portion of the 2-body propagator is neglected. Though unitarity is preserved, the omission of the real dispersive parts of the two-body intermediate states leads to a violation of analyticity. The K-matrix approach is unable to dynamically generate resonances and the lack of analyticity renders pole extraction impossible in the complex plane. The usefulness of this approach comes from its ability to incorporate large amounts of data across many channels in the resonance analysis. The most promising reaction theories may be dynamical coupled-channel (DCC) approaches. The difficulties of overlapping resonances and broad widths described above is best solved with a DCC formalism. These models use effective lagrangians, which reflect the symmetries of QCD at tree level, and explicit resonances are contained in the models as s-channel diagrams while the background can be explicitly calculated with t- and u-channel diagrams. In this approach, unitarity is preserved via the Beth-Salpeter equation and thus resonances can be generated dynamically. This is extremely important if one wishes to discern the nature of these resonances. DCC approaches are also well suited for answering the 'missing resonance' problem. This is because resonances may couple to different channels and a DCC approach treats these simultaneously.

1.3 Multi-strangeness Baryon Systems

Although the multi-strangeness baryons ($S < -1$) have played an important role in the development of our understanding of strong interactions, and thus, should be an integral part of any baryon spectroscopy program, the current knowledge of these baryons is still extremely limited. For example, the prediction and discovery of the Ω baryon [44], with strangeness $S = -3$, has been a spectacular confirmation of how well the SU(3) flavor symmetry works in strong interactions. Nevertheless, more than a half century passed before the spin of $\Omega^-(1672)$ was recently confirmed [45,46]. Further gaps in our knowledge is shown by undiscovered Ξ resonances. The SU(3) flavor symmetry allows

as many $S = -2$ baryon resonances, Ξ, as there are N and Δ resonances combined (~ 27); however, until now, only eleven Ξ baryons have been discovered [6]. Among them, only three [ground state $\Xi(1318)1/2^+$, $\Xi(1538)3/2^+$, and $\Xi(1820)3/2^-$] have their quantum numbers assigned.[1] This situation is mainly due to the fact that multi-strangeness particle productions have relatively low yields. For example, if there are no strange particles in the initial state, Ξ is produced only indirectly and the yield is only of the order of nb in the photoproduction reaction [47], whereas the yield is of the order of μb [55] in the hadronic, $\bar{K}$-induced reaction, where the Ξ is produced directly because of the presence of an $S = -1$ $\bar{K}$ meson in the initial state. The production rates for Ω baryons with $S = -3$ are even lower [49].

The study of multi-strangeness baryons has started to attract a renewed interest recently. Indeed, the CLAS Collaboration at Thomas Jefferson National Accelerator Facility (JLab) plans to initiate a Ξ spectroscopy program using the upgraded 12-GeV machine, and measure the exclusive Ω photoproduction for the first time [52]. Some data for the production of the Ξ ground state, obtained from the 6-GeV machine, are already available [47]. They were analyzed in Ref. [53, 54]. J-PARC is going to study the Ξ baryons via the $\bar{K}N \to K\Xi$ process (which is the reaction of choice for producing Ξ) in connection to its program proposal for obtaining information on Ξ hypernuclei spectroscopy. It also plans to study the $\pi N \to KK\Xi$ reaction as well as Ω production [56, 57]. At the FAIR facility of GSI, the reaction $\bar{p}p \to \bar{\Xi}\Xi$ will be studied by the PANDA Collaboration [58].

While many upcoming experiments will be providing plenty of new results, theoretical studies of the Ξ baryons are hampered mainly by the scarcity of currently available experimental data. The existing theoretical models cannot be well constrained and, as a consequence, there is strong model-dependence in predictions of the Ξ spectrum. In particular, one of the current open issues in the Ξ spectrum concerns the low mass of the $\Xi(1690)$ and $\Xi(1620)$, i.e., the nature of the third lowest Ξ state [35]. Here, different approaches, such as the non-relativistic and relativistic quark models [33, 59, 60], one-boson-exchange model [61], large N_c model [62–66], QCD sum rules [67, 68], and Skyrme model [35], yield contradictory predictions for the nature of these resonances. The planned new experimental studies as mentioned above are expected to play a key role in addressing

[1] The parity of the ground state Ξ has not been measured explicitly yet, but its assignment is based on quark models and SU(3) flavor symmetry.

such open problems. Quite recently, lattice QCD calculations of the baryon spectra, including those of Ξ and Ω baryons, have been reported [19, 20].

Like the other research mentioned, this work is part of the global effort to ultimately understand confinement. Our part of this effort is trying to find evidence of resonances in scattering data, determine these resonances' properties such as mass, decay width, and various decay modes, and determine their quantum numbers, J^P. This work takes on these tasks on two fronts. First, we investigate the model-independent aspects of the Ξ baryon resonance production reactions, $\bar{K} + N \to K + \Xi(\Xi^*)$ and $\gamma + N \to K + K + \Xi(\Xi^*)$. The second is to investigate the dynamics of these reactions in a consistent model-dependent analysis. We investigate the available data for the $\bar{K} + N \to K + \Xi$ reaction and extract $S = -1$ resonance contributions. We also give predictions for yet-to-be-measured spin observables to assist in future experiment design. Chapter 2 is dedicated to these tasks for the $\bar{K}$ reaction, while Chapter 3 focuses on Ξ photoproduction. The $\gamma + N \to K + K + \Xi$ reaction is a much more complicated situation due to the 3-body final state, the added spin complexity of the photon, and the important basic requirement of gauge symmetry known as gauge invariance.

Chapter 2

$\bar{K} + N \to K + \Xi$

The reaction of choice for studying Ξ and Ξ^* hyperons is $\bar{K} + N \to K + \Xi(\Xi^*)$. It is the simplest reaction with open strangeness in the initial state. Reactions with S=-1 hyperon targets such as Λ or Σ have never been performed and are experimentally impractical. The $N + \bar{N} \to \Xi + \bar{\Xi}$ reaction is also an interesting reaction to study. This reaction should be studied in parallel with $\bar{K} + N \to K + \Xi$ as they both are expected to be dominated by the same reaction mechanism, Y^* production. There is already available cross section and recoil polarization data for the $\bar{K}$-induced reaction though it is very old and suffers from large uncertainties [69–82]. Luckily, new experiments at J-PARC are planned and will include Ξ production using pion and anti-kaon beams [56,57]. Data for the $N\bar{N}$ reaction is virtually nonexistent with less than 10 $\Xi\bar{\Xi}$ events recorded. Again, new experiments are planned using the PANDA detector at HESR at FAIR [58]. The expected cross sections are of the order of μb which is an order of magnitude higher than the $\gamma + N \to K + K + \Xi$ reaction. This chapter will focus on $\bar{K} + N \to K + \Xi$.

The purpose of theoretical and phenomenological calculations for these reactions is to identify and extract information on baryon resonances from experimental data which allow for a comparison with fundamental QCD calculations based on first principles, i.e., lattice QCD and/or QCD-based models. Note that a direct comparison of the QCD calculations with experimental data is not feasible at present. In this chapter, the task of resonance extraction is taken on in two ways. In Section 2.1, a model-independent calculation is performed. This calculation decomposes the

Ξ, or Ξ^* of $J \leq 3/2$, production amplitude into its most general form consistent with the most basic of symmetries, rotational invariance and parity conservation. Once these symmetries are taken into account, the reaction amplitude's spin structures are reduced by half, from $2 * (2J + 1)$ to $2J + 1$. From these spin-amplitudes, all observables can be calculated. Measurement of all possible observables is a huge and unneeded task, so a smaller set of observables is listed which can unambiguously determine these spin amplitudes. Further, these spin observables hold the key to determining the spin and parity of the produced Ξ or Ξ^*, fundamentally important information for comparing QCD computation results, and a set of measurements is listed which will determine these quantum numbers.

In Section 2.2, a model-based analysis of existing data is performed. These model calculations are important when trying to understand the production mechanisms. Due to the lack of exotic, S=-2, meson exchange, our model only includes $S = -1$ hyperon contributions as well as a four-point contact amplitude. Because this reaction is expected to be dominated by these hyperon exchanges, it provides a useful place to study their resonance spectra. Our goal is to determine if any Y^* resonances are indicated by the data and extract their masses, widths, and quantum numbers.

2.1 Model-Independent Analysis

In this section, we derive the most general structure of the amplitude for the reaction of

$$\bar{K}(q) + N(p) \to K(q') + \Xi(p') \ , \tag{2.1}$$

following the method used in Ref. [83]. In the present work, we consider the production of Ξ of spin-1/2 and -3/2 with both positive and negative parities. The method is quite general and, in principle, can be applied to extract the spin structure of any reaction amplitude. In the above

equation, the arguments denote the four-momenta of the respective particles.

The reaction in Eq. (2.1) is described in its center-of-momentum (CM) frame, where $\boldsymbol{q} = -\boldsymbol{p}$ and $\boldsymbol{q}' = -\boldsymbol{p}'$. For further convenience, we define the three mutually orthogonal unit vectors $\hat{\boldsymbol{n}}_i$ $(i = 1, 2, 3)$ in terms of the independent momenta available in the reaction, i.e.,

$$\hat{\boldsymbol{n}}_1 \equiv \frac{(\boldsymbol{p} \times \boldsymbol{p}') \times \boldsymbol{p}}{|(\boldsymbol{p} \times \boldsymbol{p}') \times \boldsymbol{p}|} \ , \tag{2.2a}$$

$$\hat{\boldsymbol{n}}_2 \equiv \frac{\boldsymbol{p} \times \boldsymbol{p}'}{|\boldsymbol{p} \times \boldsymbol{p}'|} \ , \tag{2.2b}$$

$$\hat{\boldsymbol{n}}_3 \equiv \frac{\boldsymbol{p}}{|\boldsymbol{p}|} \ , \tag{2.2c}$$

where $\boldsymbol{p}$ and $\boldsymbol{p}'$ denote the three-momenta of the nucleon and Ξ, respectively. Note that $\boldsymbol{p}$ and $\boldsymbol{p}'$ define the reaction plane, such that $\hat{\boldsymbol{n}}_2$ is perpendicular to the reaction plane. The coordinate-system setup is shown in Fig. 2.1. Throughout this work, the hat notation for vectors is used to indicate unit vectors, i.e., $\hat{\boldsymbol{a}} \equiv \boldsymbol{a}/|\boldsymbol{a}|$ for an arbitrary vector $\boldsymbol{a}$. The quantization axis is chosen to be along $\hat{\boldsymbol{n}}_3$. We also use the alternative Cartesian notation $i = x, y, z$ for the indices of the unit vectors $\hat{\boldsymbol{n}}_i$.

2.1.1 Production of Ξ with $J^P = \frac{1}{2}^{\pm}$

First, we consider spin-parity $J^P = \frac{1}{2}^{\pm}$ for the Ξ produced in reaction (2.1). Following the method of Ref. [83], the most general spin structure of the reaction amplitude, consistent with basic symmetries, is

$$\hat{M} = M_0' + M_2' \, \boldsymbol{\sigma} \cdot (\hat{\boldsymbol{p}} \times \hat{\boldsymbol{p}}') \ , \qquad \text{for } J^P = \tfrac{1}{2}^+ \ , \tag{2.3a}$$

$$\hat{M} = M_1' \, \boldsymbol{\sigma} \cdot \hat{\boldsymbol{p}}' + M_3' \, \boldsymbol{\sigma} \cdot \hat{\boldsymbol{p}} \ , \qquad \text{for } J^P = \tfrac{1}{2}^- \ , \tag{2.3b}$$

where $\boldsymbol{\sigma} = (\sigma_1, \sigma_2, \sigma_3)$ stands for the vector built up of usual Pauli spin operators.[1] Equations (2.3a) and (2.3b) are direct consequences of the amplitude's reflection symmetry about the reaction plane [84, 85], which is further exploited in our analysis presented below. Note that the coeffi-

[1] Note that the spin structure for the positive-parity Ξ in Eq. (2.3a) is identical to the familiar structure of the πN elastic scattering amplitude. However, obviously, the isospin structure is different.

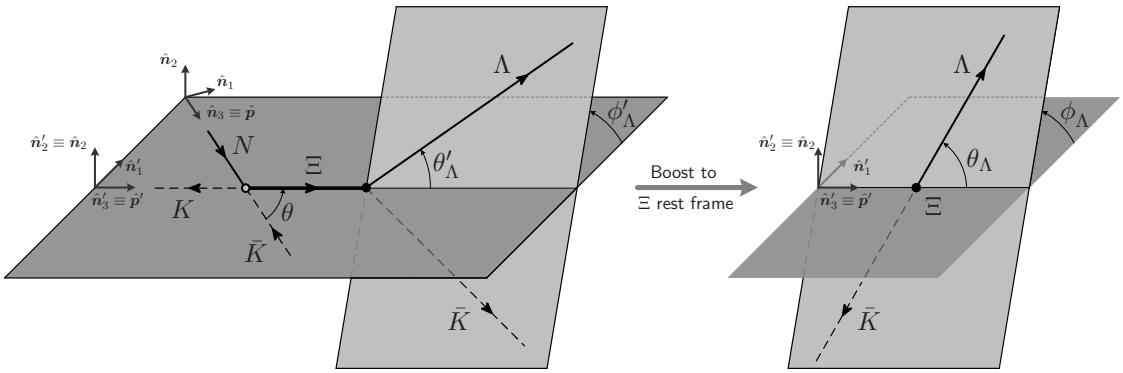

Figure 2.1: Coordinate systems used in describing the Ξ production reaction and its subsequent decay process. On the left, the production reaction $\bar{K}N \to K\Xi$ is shown in its center-of-momentum (CM) frame. The corresponding reaction plane (indicated in dark gray) contains the nucleon and Ξ momenta $\boldsymbol{p}$ and $\boldsymbol{p}'$, respectively. The basis vectors $\{\hat{\boldsymbol{n}}_1, \hat{\boldsymbol{n}}_2, \hat{\boldsymbol{n}}_3\}$ are defined in Eq. (2.2), with $\hat{\boldsymbol{n}}_3$ aligned with the nucleon momentum $\boldsymbol{p}$ and $\hat{\boldsymbol{n}}_2$ perpendicular to the reaction plane; θ indicates the Ξ emission angle. The (primed) frame $\{\hat{\boldsymbol{n}}'_1, \hat{\boldsymbol{n}}'_2, \hat{\boldsymbol{n}}'_3\}$ is obtained from $\{\hat{\boldsymbol{n}}_1, \hat{\boldsymbol{n}}_2, \hat{\boldsymbol{n}}_3\}$ by rotating the latter about the $\hat{\boldsymbol{n}}_2$ axis by θ, which aligns $\hat{\boldsymbol{n}}'_3$ with $\boldsymbol{p}'$ and leaves $\hat{\boldsymbol{n}}'_2 \equiv \hat{\boldsymbol{n}}_2$. The (light gray) plane tilted by the angle ϕ'_Λ about the $\hat{\boldsymbol{n}}'_3 \equiv \hat{\boldsymbol{p}}'$ axis is spanned by the momenta of the decay products Λ and $\bar{K}$. The polar and azimuthal angles of the decay product Λ in the rotated (primed) CM frame are indicated by θ'_Λ and ϕ'_Λ, respectively. In the boosted frame on the right, the decay process of the produced Ξ at rest is described in the $\{\hat{\boldsymbol{n}}'_1, \hat{\boldsymbol{n}}'_2, \hat{\boldsymbol{n}}'_3\}$ coordinate system. The polar and azimuthal angles of the decay product Λ are indicated here by θ_Λ and ϕ_Λ, respectively. For the latter angle, one has $\phi_\Lambda \equiv \phi'_\Lambda$ since the boost happens along the corresponding tilt axis.

cients M'_1 and M'_2 do not contain S-wave in the final state.

For further convenience, we rewrite Eq. (2.3) as

$$\hat{M} = M_0 + M_2\, \boldsymbol{\sigma} \cdot \hat{\boldsymbol{n}}_2 \ , \qquad \text{for } J^P = \tfrac{1}{2}^+ \ , \tag{2.4a}$$

$$\hat{M} = M_1\, \boldsymbol{\sigma} \cdot \hat{\boldsymbol{n}}_1 + M_3\, \boldsymbol{\sigma} \cdot \hat{\boldsymbol{n}}_3 \ , \qquad \text{for } J^P = \tfrac{1}{2}^- \ , \tag{2.4b}$$

using $\hat{\boldsymbol{p}}' = \cos\theta\, \hat{\boldsymbol{n}}_3 + \sin\theta\, \hat{\boldsymbol{n}}_1$ and $\hat{\boldsymbol{n}}_3 = \hat{\boldsymbol{p}}$. The respective coefficients in Eqs. (2.3) and (2.4) are related by

$$M'_0 = M_0 \ , \qquad M'_2 = \frac{1}{\sin\theta}\, M_2 \ , \tag{2.5a}$$

$$M'_1 = \frac{1}{\sin\theta}\, M_1 \ , \qquad M'_3 = M_3 - \frac{\cos\theta}{\sin\theta}\, M_1 \ . \tag{2.5b}$$

Following Ref. [83], one may also express these coefficients in terms of partial-wave matrix elements. The corresponding results are given in Appendix 2.4.1, which show, in particular, that the coefficients M_1 and M_2 vanish identically for Ξ scattering angles $\theta = 0$ and π, as can be seen in Eq. (3.34). The partial-wave expansions will become particularly relevant once sufficient experimental data become available to permit their full-fledged partial-wave analysis. The isospin structure of the amplitudes in Eq. (2.4) [or in Eq. (2.3)] is contained in the coefficients M_i as given explicitly by Eq. (3.34) in Appendix 2.4.1.

Once the spin structure of the reaction amplitude is determined, all the observables can be readily expressed in terms of the amplitudes M_i multiplying each spin structure. For the reaction under consideration, apart from the cross section ($d\sigma/d\Omega$), a complete set of observables includes the target asymmetry (T), recoil Ξ polarization (P), and the spin-transfer coefficient (K). For arbitrary spin orientations along directions $\hat{\boldsymbol{a}}$ and $\hat{\boldsymbol{b}}$, their coordinate-independent expressions are

$$\frac{d\sigma}{d\Omega} \equiv \frac{1}{2}\,\mathrm{Tr}[\hat{M}\hat{M}^\dagger]\ , \tag{2.6a}$$

$$\frac{d\sigma}{d\Omega}T_a \equiv \frac{1}{2}\,\mathrm{Tr}[\hat{M}\,\boldsymbol{\sigma}\cdot\hat{\boldsymbol{a}}\,\hat{M}^\dagger]\ , \tag{2.6b}$$

$$\frac{d\sigma}{d\Omega}P_a \equiv \frac{1}{2}\,\mathrm{Tr}[\hat{M}\hat{M}^\dagger\,\boldsymbol{\sigma}\cdot\hat{\boldsymbol{a}}]\ , \tag{2.6c}$$

$$\frac{d\sigma}{d\Omega}K_{ba} \equiv \frac{1}{2}\,\mathrm{Tr}[\hat{M}\,\boldsymbol{\sigma}\cdot\hat{\boldsymbol{b}}\,\hat{M}^\dagger\,\boldsymbol{\sigma}\cdot\hat{\boldsymbol{a}}]\ . \tag{2.6d}$$

For Cartesian directions $\hat{\boldsymbol{n}}_i$ enumerated by $i = 1, 2, 3$ $(= x, y, z)$, in particular, one obtains

$$\frac{d\sigma}{d\Omega}T_i = \frac{1}{2}\,\mathrm{Tr}[\hat{M}\sigma_i\hat{M}^\dagger]\ , \tag{2.7a}$$

$$\frac{d\sigma}{d\Omega}P_i = \frac{1}{2}\,\mathrm{Tr}[\hat{M}\hat{M}^\dagger\sigma_i]\ , \tag{2.7b}$$

$$\frac{d\sigma}{d\Omega}K_{ij} = \frac{1}{2}\,\mathrm{Tr}[\hat{M}\sigma_i\hat{M}^\dagger\sigma_j]\ . \tag{2.7c}$$

Of course, the T, P, and K observables for arbitrary directions in Eq. (2.6) can be expressed as linear combinations of the specific Cartesian expressions given in Eq. (2.7).

Due to symmetries of the reaction, eight observables vanish identically, i.e., $T_i = P_i = K_{iy} = K_{yi} = 0$ for $i = x, z$, and of the remaining eight, only four are independent for a given parity, which

completely determine the amplitudes M_i in Eq. (2.4). Indeed, for a positive-parity Ξ, we have

$$\frac{d\sigma}{d\Omega} = \frac{d\sigma}{d\Omega} K_{yy} = |M_0|^2 + |M_2|^2 \ , \tag{2.8a}$$

$$\frac{d\sigma}{d\Omega} K_{xx} = \frac{d\sigma}{d\Omega} K_{zz} = |M_0|^2 - |M_2|^2 \ , \tag{2.8b}$$

$$\frac{d\sigma}{d\Omega} T_y = \frac{d\sigma}{d\Omega} P_y = 2\,\mathrm{Re}\left[M_2 M_0^*\right] \ , \tag{2.8c}$$

$$\frac{d\sigma}{d\Omega} K_{xz} = -\frac{d\sigma}{d\Omega} K_{zx} = 2\,\mathrm{Im}\left[M_2 M_0^*\right] \ , \tag{2.8d}$$

and for a negative-parity Ξ, we obtain

$$\frac{d\sigma}{d\Omega} = -\frac{d\sigma}{d\Omega} K_{yy} = |M_1|^2 + |M_3|^2 \ , \tag{2.9a}$$

$$\frac{d\sigma}{d\Omega} K_{xx} = -\frac{d\sigma}{d\Omega} K_{zz} = |M_1|^2 - |M_3|^2 \ , \tag{2.9b}$$

$$\frac{d\sigma}{d\Omega} T_y = -\frac{d\sigma}{d\Omega} P_y = 2\,\mathrm{Im}\left[M_3 M_1^*\right] \ , \tag{2.9c}$$

$$\frac{d\sigma}{d\Omega} K_{xz} = \frac{d\sigma}{d\Omega} K_{zx} = 2\,\mathrm{Re}\left[M_3 M_1^*\right] \ . \tag{2.9d}$$

The respective first two relations in the two equation sets determine the magnitudes of the amplitudes M_0, M_2 and M_1, M_3, respectively, whereas the respective last two relations determine their phase differences. Therefore, apart from an irrelevant overall phase, the observables in Eqs. (2.8) and (2.9) determine the amplitudes M_i, $i = 0, \ldots, 3$, unambiguously. These results reveal that it is experimentally demanding to determine the reaction amplitude completely, for it requires measuring both the single- and double-polarization observables.

Comparing Eqs. (2.8a) and (2.9a), one obtains

$$K_{yy} = \pi_\Xi \ , \tag{2.10}$$

where π_Ξ stands for the parity of the produced Ξ. This result is actually a direct consequence of reflection symmetry, as exploited in Bohr's theorem [85, 86] and applied in Ref. [87]. It, therefore, provides a model-independent way of determining the parity of the Ξ resonance. Alternative

expressions extracted from Eqs. (2.8) and (2.9) are [87]

$$T_y = \pi_\Xi \, P_y \ , \tag{2.11}$$

which involves only single polarization observables and

$$K_{xx} = \pi_\Xi \, K_{zz} \quad \text{and} \quad K_{xz} = -\pi_\Xi \, K_{zx} \ . \tag{2.12}$$

These results are all consequences of the reflection symmetry about the reaction plane.

In Sec. 2.1.3, we will perform the analysis in terms of the spin-density matrix (SDM) elements, which are equivalent to the observables discussed here. The SDM elements are convenient quantities when dealing with spin observables, especially when higher-spin particles are produced in the reaction. They can be extracted from the information on the subsequent decay processes of the produced particles, in conjunction with the self-analyzing property of the decaying particles via a weak decay, without the explicit measurement of the spin polarizations of these produced particles.

2.1.2 Production of Ξ with $J^P = \frac{3}{2}^\pm$

We now turn to the spin-parity $J^P = \frac{3}{2}^\pm$. Again, following Ref. [83], the most general spin structure of the reaction amplitude is given by

$$\hat{M} = F_1' \, \boldsymbol{T}^\dagger \cdot (\hat{\boldsymbol{p}} \times \hat{\boldsymbol{p}}') + F_2' \, \boldsymbol{T}^\dagger \cdot \hat{\boldsymbol{p}}' \, \boldsymbol{\sigma} \cdot \hat{\boldsymbol{p}}' + F_3' \left[\boldsymbol{T}^\dagger \cdot \hat{\boldsymbol{p}} \, \boldsymbol{\sigma} \cdot \hat{\boldsymbol{p}}' + \boldsymbol{T}^\dagger \cdot \hat{\boldsymbol{p}}' \, \boldsymbol{\sigma} \cdot \hat{\boldsymbol{p}} \right] + F_4' \, \boldsymbol{T}^\dagger \cdot \hat{\boldsymbol{p}} \, \boldsymbol{\sigma} \cdot \hat{\boldsymbol{p}} \tag{2.13a}$$

for $J^P = \frac{3}{2}^+$ and

$$\begin{aligned} \hat{M} = G_1' \left[\boldsymbol{T}^\dagger \cdot \hat{\boldsymbol{p}} \, \boldsymbol{\sigma} \cdot (\hat{\boldsymbol{p}} \times \hat{\boldsymbol{p}}') + \boldsymbol{T}^\dagger \cdot (\hat{\boldsymbol{p}} \times \hat{\boldsymbol{p}}') \, \boldsymbol{\sigma} \cdot \hat{\boldsymbol{p}} \right] + G_2' \left[\boldsymbol{T}^\dagger \cdot \hat{\boldsymbol{p}}' \, \boldsymbol{\sigma} \cdot (\hat{\boldsymbol{p}} \times \hat{\boldsymbol{p}}') + \boldsymbol{T}^\dagger \cdot (\hat{\boldsymbol{p}} \times \hat{\boldsymbol{p}}') \, \boldsymbol{\sigma} \cdot \hat{\boldsymbol{p}}' \right] \\ + G_3' \, \boldsymbol{T}^\dagger \cdot \hat{\boldsymbol{p}}' + G_4' \, \boldsymbol{T}^\dagger \cdot \hat{\boldsymbol{p}} \end{aligned} \tag{2.13b}$$

for $J^P = \frac{3}{2}^-$. Here, $\boldsymbol{T}^\dagger$ stands for the (spin-1/2 $\to$ spin-3/2) transition operator. Its explicit representation may be found in Appendix 2.4.1. In contrast to the spin-1/2 case, each parity of

the spin-3/2 case has four independent amplitudes, F_i' and G_i' $(i = 1, \ldots, 4)$, respectively, and one needs at least eight independent observables to determine them completely apart from an irrelevant overall phase. From the above equations, it is obvious that only F_4' and G_4' contain an S-wave in the final state. Also, F_2' and G_2' contain only D- and higher-waves in the final state.

The amplitudes in Eq. (2.13) can be also rewritten as

$$\hat{M} = F_1\, \boldsymbol{T}^\dagger \cdot \hat{\boldsymbol{n}}_2 + F_2\, \boldsymbol{T}^\dagger \cdot \hat{\boldsymbol{n}}_1\, \boldsymbol{\sigma} \cdot \hat{\boldsymbol{n}}_1 + F_3 \left[\boldsymbol{T}^\dagger \cdot \hat{\boldsymbol{n}}_3\, \boldsymbol{\sigma} \cdot \hat{\boldsymbol{n}}_1 + \boldsymbol{T}^\dagger \cdot \hat{\boldsymbol{n}}_1\, \boldsymbol{\sigma} \cdot \hat{\boldsymbol{n}}_3\right] + F_4\, \boldsymbol{T}^\dagger \cdot \hat{\boldsymbol{n}}_3\, \boldsymbol{\sigma} \cdot \hat{\boldsymbol{n}}_3 \tag{2.14a}$$

for $J^P = \frac{3}{2}^+$ and

$$\begin{aligned}\hat{M} = G_1 \left[\boldsymbol{T}^\dagger \cdot \hat{\boldsymbol{n}}_3\, \boldsymbol{\sigma} \cdot \hat{\boldsymbol{n}}_2 + \boldsymbol{T}^\dagger \cdot \hat{\boldsymbol{n}}_2\, \boldsymbol{\sigma} \cdot \hat{\boldsymbol{n}}_3\right] + G_2 \left[\boldsymbol{T}^\dagger \cdot \hat{\boldsymbol{n}}_1\, \boldsymbol{\sigma} \cdot \hat{\boldsymbol{n}}_2 + \boldsymbol{T}^\dagger \cdot \hat{\boldsymbol{n}}_2\, \boldsymbol{\sigma} \cdot \hat{\boldsymbol{n}}_1\right] \\ + G_3\, \boldsymbol{T}^\dagger \cdot \hat{\boldsymbol{n}}_1 + G_4\, \boldsymbol{T}^\dagger \cdot \hat{\boldsymbol{n}}_3\end{aligned} \tag{2.14b}$$

for $J^P = \frac{3}{2}^-$. The coefficients F_i and G_i are expressed in terms of the partial-wave matrix elements as given in Appendix 2.4.1. They are also related to the corresponding coefficients F_i' and G_i' in Eq. (2.13) by

$$F_1' = \frac{1}{\sin\theta} F_1 \ , \qquad G_1' = \frac{1}{\sin\theta} G_1 - \frac{\cos\theta}{\sin^2\theta} G_2 \ , \tag{2.15a}$$

$$F_2' = \frac{1}{\sin^2\theta} F_2 \ , \qquad G_2' = \frac{1}{\sin^2\theta} G_2 \ , \tag{2.15b}$$

$$F_3' = \frac{1}{\sin\theta} F_3 - \frac{\cos\theta}{\sin^2\theta} F_2 \ , \qquad G_3' = \frac{1}{\sin\theta} G_3 \ , \tag{2.15c}$$

$$F_4' = F_4 + \frac{\cos^2\theta}{\sin^2\theta} F_2 - 2\frac{\cos\theta}{\sin\theta} F_3 \ , \qquad G_4' = G_4 - \frac{\cos\theta}{\sin\theta} G_3 \ . \tag{2.15d}$$

The polarization observables for this case will be discussed in the next section in terms of the SDM elements.

2.1.3 Spin-Density Matrix Formalism

As mentioned before, when dealing with higher-spin Ξ (i.e., spins higher than 1/2) in particular, it is more convenient to continue the analysis of the $\bar{K}N \to K\Xi$ reaction in terms of spin-density matrix (SDM) elements. A similar (but not identical) analysis to the present one based on the SDM formalism was performed in Ref. [88] for a general two-body reaction with unpolarized initial state. Also, the reaction $\bar{K}N \to \omega\Lambda$ was analyzed within the SDM approach in Ref. [89].

In Secs. 2.1.1 and 2.1.2, we have exploited the mirror (or reflection) symmetry about the reaction plane in our analysis, in particular, for the parity determination of the Ξ resonances. In fact, as long as the production process conserves total parity, the reaction amplitude should have this symmetry [84, 85]. This mirror operation is equivalent to doing a parity transformation followed by a subsequent rotation by 180° about the $\hat{\boldsymbol{n}}_2$-axis: $\hat{\mathcal{P}}_y = \hat{R}_y(180^\circ)\hat{\mathcal{P}}$. The resulting symmetry, in terms of the spin matrix element, is

$$\begin{aligned}\langle S_f\, m_f|\hat{M}|S_i\, m_i\rangle &= \langle S_f\, m_f|\hat{\mathcal{P}}_y^\dagger\mathcal{P}_y\hat{M}\mathcal{P}_y^\dagger\mathcal{P}_y|S_i\, m_i\rangle \\ &= \pi_f\pi_i\,(-1)^{(S_f-m_f)-(S_i-m_i)}\,\langle S_f - m_f|\hat{M}|S_i - m_i\rangle\ , \end{aligned} \tag{2.16}$$

and holds as long as the quantization axis is in the production plane. Here, $\pi_{i(f)}$ is the intrinsic parity of the initial (final) state.

Based on this symmetry, the $J^P = \frac{1}{2}^\pm$ Ξ production amplitude, $\hat{M}$ given by Eq. (2.4), is completely described by two complex helicity amplitudes, $\mathcal{H}_1$ and $\mathcal{H}_2$, given by the spin matrix elements,

$$\begin{aligned}\mathcal{H}_1 &\equiv \langle\lambda_\Xi = \tfrac{1}{2}|\,\hat{M}\,|\lambda_N = \tfrac{1}{2}\rangle \\ &= \pi_\Xi\,\langle\lambda_\Xi = -\tfrac{1}{2}|\,\hat{M}\,|\lambda_N = -\tfrac{1}{2}\rangle\ , \end{aligned} \tag{2.17a}$$

$$\begin{aligned}\mathcal{H}_2 &\equiv \langle\lambda_\Xi = \tfrac{1}{2}|\,\hat{M}\,|\lambda_N = -\tfrac{1}{2}\rangle \\ &= -\pi_\Xi\,\langle\lambda_\Xi = -\tfrac{1}{2}|\,\hat{M}\,|\lambda_N = \tfrac{1}{2}\rangle\ , \end{aligned} \tag{2.17b}$$

where λ_N and λ_Ξ denote the helicity of the initial nucleon and final Ξ, respectively. Here, reference

to the spin quantum numbers $S_\Xi = S_N = 1/2$ has been suppressed. The helicity amplitudes are related to the coefficient amplitudes in Eq. (2.4) by

$$\mathcal{H}_1 = M_0 \cos\frac{\theta}{2} + iM_2 \sin\frac{\theta}{2} \ , \tag{2.18a}$$

$$\mathcal{H}_2 = -iM_2 \cos\frac{\theta}{2} + M_0 \sin\frac{\theta}{2} \tag{2.18b}$$

for a positive parity Ξ, and by

$$\mathcal{H}_1 = M_3 \cos\frac{\theta}{2} + M_1 \sin\frac{\theta}{2} \ , \tag{2.19a}$$

$$\mathcal{H}_2 = M_1 \cos\frac{\theta}{2} - M_3 \sin\frac{\theta}{2} \tag{2.19b}$$

for a negative parity Ξ. Here, θ is the scattering angle, i.e., $\cos\theta \equiv \hat{\boldsymbol{p}} \cdot \hat{\boldsymbol{p}}'$.

Likewise, the production amplitude $\hat{M}$ for a Ξ with $J^P = \frac{3}{2}^\pm$ determined by Eq. (2.14) is completely described by four complex amplitudes given as

$$\begin{aligned}\mathcal{H}_1 &\equiv \langle \lambda_\Xi = \tfrac{3}{2} | \hat{M} | \lambda_N = \tfrac{1}{2} \rangle \\ &= \pi_\Xi \, \langle \lambda_\Xi = -\tfrac{3}{2} | \hat{M} | \lambda_N = -\tfrac{1}{2} \rangle \ ,\end{aligned} \tag{2.20a}$$

$$\begin{aligned}\mathcal{H}_2 &\equiv \langle \lambda_\Xi = \tfrac{3}{2} | \hat{M} | \lambda_N = -\tfrac{1}{2} \rangle \\ &= -\pi_\Xi \, \langle \lambda_\Xi = -\tfrac{3}{2} | \hat{M} | \lambda_N = \tfrac{1}{2} \rangle \ ,\end{aligned} \tag{2.20b}$$

$$\begin{aligned}\mathcal{H}_3 &\equiv \langle \lambda_\Xi = \tfrac{1}{2} | \hat{M} | \lambda_N = \tfrac{1}{2} \rangle \\ &= -\pi_\Xi \, \langle \lambda_\Xi = -\tfrac{1}{2} | \hat{M} | \lambda_N = -\tfrac{1}{2} \rangle \ ,\end{aligned} \tag{2.20c}$$

$$\begin{aligned}\mathcal{H}_4 &\equiv \langle \lambda_\Xi = \tfrac{1}{2} | \hat{M} | \lambda_N = -\tfrac{1}{2} \rangle \\ &= \pi_\Xi \, \langle \lambda_\Xi = -\tfrac{1}{2} | \hat{M} | \lambda_N = \tfrac{1}{2} \rangle \ .\end{aligned} \tag{2.20d}$$

These helicity amplitudes are related to the coefficient functions in Eq. (2.14) by

$$\mathcal{H}_1 = \frac{1}{\sqrt{2}}\left[i\cos\frac{\theta}{2}F_1 - \cos\theta\sin\frac{\theta}{2}F_2 - \cos\frac{3\theta}{2}F_3 + \sin\theta\cos\frac{\theta}{2}F_4\right], \tag{2.21a}$$

$$\mathcal{H}_2 = \frac{1}{\sqrt{2}}\left[i\sin\frac{\theta}{2}F_1 - \cos\theta\cos\frac{\theta}{2}F_2 + \sin\frac{3\theta}{2}F_3 - \sin\theta\sin\frac{\theta}{2}F_4\right], \tag{2.21b}$$

$$\mathcal{H}_3 = \frac{1}{\sqrt{6}}\left[-i\sin\frac{\theta}{2}F_1 + (2-3\cos\theta)\cos\frac{\theta}{2}F_2 + 3\sin\frac{3\theta}{2}F_3 - (1-3\cos\theta)\cos\frac{\theta}{2}F_4\right], \tag{2.21c}$$

$$\mathcal{H}_4 = \frac{1}{\sqrt{6}}\left[i\cos\frac{\theta}{2}F_1 + (2+3\cos\theta)\sin\frac{\theta}{2}F_2 + 3\cos\frac{3\theta}{2}F_3 - (1+3\cos\theta)\sin\frac{\theta}{2}F_4\right], \tag{2.21d}$$

for a positive-parity Ξ and by

$$\mathcal{H}_1 = \frac{1}{\sqrt{2}}\left[i\,(2-\cos\theta)\cos\frac{\theta}{2}G_1 + 2i\sin^3\frac{\theta}{2}G_2 - \cos\theta\cos\frac{\theta}{2}G_3 + \sin\theta\cos\frac{\theta}{2}G_4\right], \tag{2.22a}$$

$$\mathcal{H}_2 = \frac{1}{\sqrt{2}}\left[-i\,(2+\cos\theta)\sin\frac{\theta}{2}G_1 + 2i\cos^3\frac{\theta}{2}G_2 - \cos\theta\sin\frac{\theta}{2}G_3 + \sin\theta\sin\frac{\theta}{2}G_4\right], \tag{2.22b}$$

$$\mathcal{H}_3 = \frac{1}{\sqrt{6}}\left[3i\cos\theta\sin\frac{\theta}{2}G_1 + 3i\sin\theta\sin\frac{\theta}{2}G_2 + (2+3\cos\theta)\sin\frac{\theta}{2}G_3 + (3\cos\theta-1)\cos\frac{\theta}{2}G_4\right], \tag{2.22c}$$

$$\mathcal{H}_4 = \frac{1}{\sqrt{6}}\left[-3i\cos\theta\cos\frac{\theta}{2}G_1 - 3i\sin\theta\cos\frac{\theta}{2}G_2 + (2-3\cos\theta)\cos\frac{\theta}{2}G_3 + (3\cos\theta+1)\sin\frac{\theta}{2}G_4\right] \tag{2.22d}$$

for a negative-parity Ξ.

The SDM elements are defined by

$$\rho^{\Xi,i}_{\lambda\lambda'} \equiv \langle\lambda|\hat{\rho}^{N,i}|\lambda'\rangle = \frac{1}{2}\,\langle\lambda|\hat{M}\sigma_i\hat{M}^\dagger|\lambda'\rangle\,, \tag{2.23}$$

for $i = 0,\ldots,3$, where λ and λ' stand for the helicity of the produced Ξ baryon and $\sigma_0 = \mathbb{1}$ is the 2×2 unit matrix. For completeness, a relevant part of the SDM formalism for the present work is presented in Appendix 2.4.2. The SDM elements are related by

$$\rho^{\Xi,i}_{\lambda,\lambda'} = (-1)^{i+\lambda-\lambda'}\rho^{\Xi,i}_{-\lambda,-\lambda'}\,, \tag{2.24a}$$

$$\rho^{\Xi,i}_{\lambda,\lambda'} = \rho^{\Xi,i*}_{\lambda',\lambda} \tag{2.24b}$$

due to the symmetry of the spin matrix element (2.16) and the hermiticity of Eq. (2.23).

We now relate the SDM elements, $\rho^{\Xi,i}_{\lambda,\lambda'}$, to the helicity amplitudes $\mathcal{H}_j$ given by Eqs. (2.17) and (2.20) which determine the reaction amplitudes. The purpose is to find a set of SDM elements that fixes those helicity amplitudes completely.

Ξ of $J^P = \frac{1}{2}^{\pm}$

Starting with $J = \frac{1}{2}$, there are sixteen possible SDM elements $\rho^{\Xi,i}_{\lambda\lambda'}$. However, only four of them are independent for a given parity and they determine the amplitudes $\mathcal{H}_1$ and $\mathcal{H}_2$ apart from an irrelevant overall phase. Inserting Eq. (2.17) into Eq. (2.23), a set of four independent SDM elements can be determined as

$$2\rho^0_{\frac{1}{2},\frac{1}{2}} = 2i\pi_\Xi\,\rho^2_{\frac{1}{2},-\frac{1}{2}} = |\mathcal{H}_1|^2 + |\mathcal{H}_2|^2 \ , \tag{2.25a}$$

$$2\rho^3_{\frac{1}{2},\frac{1}{2}} = 2\pi_\Xi\,\rho^1_{\frac{1}{2},-\frac{1}{2}} = |\mathcal{H}_1|^2 - |\mathcal{H}_2|^2 \ , \tag{2.25b}$$

$$\rho^2_{\frac{1}{2},\frac{1}{2}} = i\pi_\Xi\,\rho^0_{\frac{1}{2},-\frac{1}{2}} = \mathrm{Im}\left[\mathcal{H}_1\mathcal{H}_2^*\right] \ , \tag{2.25c}$$

$$\rho^1_{\frac{1}{2},\frac{1}{2}} = -\pi_\Xi\,\rho^3_{\frac{1}{2},-\frac{1}{2}} = \mathrm{Re}\left[\mathcal{H}_1\mathcal{H}_2^*\right] \ , \tag{2.25d}$$

where the superindex Ξ in $\rho^{\Xi,i}_{\lambda\lambda'}$ was dropped for simplicity. A complete list of SDM elements $\rho^i_{\lambda,\lambda'}$ in terms of helicity amplitudes $\mathcal{H}_i$ is given in Appendix 2.4.3.

The SDM elements are directly related to the observables defined by Eq. (2.6). For example, from Eqs. (2.24) and (2.73d), we have

$$\frac{d\sigma}{d\Omega} = 2\rho^0_{\frac{1}{2},\frac{1}{2}} \ , \qquad \frac{d\sigma}{d\Omega}K_{yy'} = 2i\rho^2_{\frac{1}{2},-\frac{1}{2}} \ , \tag{2.26a}$$

$$\frac{d\sigma}{d\Omega}T_y = 2\rho^2_{\frac{1}{2},\frac{1}{2}} \ , \qquad \frac{d\sigma}{d\Omega}P_{y'} = 2i\rho^0_{\frac{1}{2},-\frac{1}{2}} \ , \tag{2.26b}$$

$$\frac{d\sigma}{d\Omega}K_{xx'} = 2\rho^1_{\frac{1}{2},-\frac{1}{2}} \ , \qquad \frac{d\sigma}{d\Omega}K_{zz'} = 2\rho^3_{\frac{1}{2},\frac{1}{2}} \ , \tag{2.26c}$$

$$\frac{d\sigma}{d\Omega}K_{xz'} = 2\rho^1_{\frac{1}{2},\frac{1}{2}} \ , \qquad \frac{d\sigma}{d\Omega}K_{zx'} = 2\rho^3_{\frac{1}{2},-\frac{1}{2}} \ , \tag{2.26d}$$

where the primed Cartesian components correspond to the rotated frame (see Fig. 2.1; note that $y' \equiv y$).

From Eqs. (2.10) and (2.26), we see, in particular, that

$$K_{yy'} = \frac{i\rho^2_{\frac{1}{2},-\frac{1}{2}}}{\rho^0_{\frac{1}{2},\frac{1}{2}}} = \pi_\Xi \ . \tag{2.27}$$

More generally, in terms of the SDM elements, one obtains

$$(-1)^{\frac{1}{2}-\lambda'} \frac{i\rho^2_{\lambda,-\lambda'}}{\rho^0_{\lambda,\lambda'}} = (-1)^{\frac{1}{2}-\lambda'} \frac{\rho^1_{\lambda,-\lambda'}}{\rho^3_{\lambda,\lambda'}} = \pi_\Xi \ . \tag{2.28}$$

This result reveals that one needs to measure two SDM elements to determine the parity of the Ξ baryon: either $\rho^0_{\lambda,\lambda'}$ with unpolarized target nucleon and $\rho^2_{\lambda,-\lambda'}$ with polarized target nucleon along the direction $\hat{\boldsymbol{n}}_2 \equiv \hat{\boldsymbol{n}}'_2$ perpendicular to the reaction plane, or $\rho^1_{\lambda,\lambda'}$ with transversally polarized target along $\hat{\boldsymbol{n}}_1$, and $\rho^3_{\lambda,-\lambda'}$ with longitudinally polarized target along $\hat{\boldsymbol{n}}_3 \equiv \hat{\boldsymbol{p}}$. Note that $\rho^0_{\lambda,\lambda'}$ is directly related to the cross section $d\sigma/d\Omega$ when $\lambda = \lambda'$.

Ξ of $J^P = \frac{3}{2}^{\pm}$

For $J = 3/2$, analogously to the $J = 1/2$ case, inserting Eq. (2.20) into Eq. (2.23), the SDM elements are related to the four amplitudes $\mathcal{H}_i$ $(i = 1, \ldots, 4)$ by

$$2\rho^0_{\frac{3}{2},\frac{3}{2}} = |\mathcal{H}_1|^2 + |\mathcal{H}_2|^2 \ , \tag{29a}$$

$$2\rho^1_{\frac{3}{2},-\frac{3}{2}} = \pi_\Xi \left(|\mathcal{H}_1|^2 - |\mathcal{H}_2|^2\right) \ , \tag{29b}$$

$$-i\rho^0_{\frac{3}{2},-\frac{3}{2}} = \pi_\Xi \, \mathrm{Im}\left[\mathcal{H}_2 \mathcal{H}_1^*\right] \ , \tag{29c}$$

$$\rho^1_{\frac{3}{2},\frac{3}{2}} = \mathrm{Re}\left[\mathcal{H}_2 \mathcal{H}_1^*\right] \ , \tag{29d}$$

$$2\rho^0_{\frac{1}{2},\frac{1}{2}} = |\mathcal{H}_3|^2 + |\mathcal{H}_4|^2 \ , \tag{30a}$$

$$2\rho^1_{\frac{1}{2},-\frac{1}{2}} = \pi_\Xi \left(|\mathcal{H}_4|^2 - |\mathcal{H}_3|^2\right) \ , \tag{30b}$$

$$-i\rho^0_{\frac{1}{2},-\frac{1}{2}} = \pi_\Xi \, \mathrm{Im}\left[\mathcal{H}_3 \mathcal{H}_4^*\right] \ , \tag{30c}$$

$$\rho^1_{\frac{1}{2},\frac{1}{2}} = \mathrm{Re}\left[\mathcal{H}_3 \mathcal{H}_4^*\right] \ , \tag{30d}$$

$$2\rho^1_{\frac{3}{2},-\frac{1}{2}} = \pi_\Xi \left(\mathcal{H}_2 \mathcal{H}_4^* - \mathcal{H}_1 \mathcal{H}_3^*\right) \ , \tag{31a}$$

$$2\rho^0_{\frac{3}{2},\frac{1}{2}} = \mathcal{H}_2 \mathcal{H}_4^* + \mathcal{H}_1 \mathcal{H}_3^* \ , \tag{31b}$$

$$2\rho^0_{\frac{3}{2},-\frac{1}{2}} = \pi_\Xi \left(\mathcal{H}_1 \mathcal{H}_4^* - \mathcal{H}_2 \mathcal{H}_3^*\right) \ , \tag{32a}$$

$$2\rho^1_{\frac{3}{2},\frac{1}{2}} = \mathcal{H}_1 \mathcal{H}_4^* + \mathcal{H}_2 \mathcal{H}_3^* \ . \tag{32b}$$

A complete list of SDM elements $\rho^{\Xi,i}_{\lambda,\lambda'}$ in terms of the helicity amplitudes $\mathcal{H}_i$ is given in Appendix 2.4.3.

As mentioned in the previous section, a set of eight independent SDM elements (e.g., $\rho^0_{\frac{1}{2},\frac{1}{2}}$, $\rho^0_{\frac{3}{2},\frac{3}{2}}$, $\mathrm{Re}[\rho^0_{\frac{3}{2},\frac{1}{2}}]$, $\mathrm{Im}[\rho^0_{\frac{3}{2},\frac{1}{2}}]$, $\mathrm{Re}[\rho^0_{\frac{3}{2},-\frac{1}{2}}]$, $\rho^1_{\frac{1}{2},-\frac{1}{2}}$, $\rho^1_{\frac{3}{2},-\frac{3}{2}}$, $\mathrm{Re}[\rho^1_{\frac{3}{2},\frac{1}{2}}]$) determines all four helicity amplitudes $\mathcal{H}_i$, $(i = 1, \ldots, 4)$, apart from an irrelevant overall phase. The analysis here is analogous to the one carried out in Ref. [90] for pion photoproduction.

Equations (2.24) and (2.76) can be used to calculate K_{yy} in terms of SDM elements involving

Ξ of spin-3/2. This leads to

$$K_{yy} = \frac{i\left(\rho^2_{\frac{3}{2},-\frac{3}{2}} - \rho^2_{\frac{1}{2},-\frac{1}{2}}\right)}{\rho^0_{\frac{3}{2},\frac{3}{2}} + \rho^0_{\frac{1}{2},\frac{1}{2}}} = \pi_\Xi \tag{2.33}$$

or, more generally,

$$(-1)^{\frac{3}{2}-\lambda'}\,\frac{i\rho^2_{\lambda,-\lambda'}}{\rho^0_{\lambda,\lambda'}} = (-1)^{\frac{3}{2}-\lambda'}\,\frac{\rho^1_{\lambda,-\lambda'}}{\rho^3_{\lambda,\lambda'}} = \pi_\Xi\ . \tag{2.34}$$

Equations (2.27), (2.28), (2.33), and (2.34) can be extended to an arbitrary spin J of the Ξ baryon, i.e.,

$$K_{yy} = \frac{i\sum_\lambda (-1)^{J-\lambda}\rho^2_{\lambda,-\lambda}}{\sum_\lambda \rho^0_{\lambda,\lambda}} = \pi_\Xi \tag{2.35}$$

and

$$(-1)^{J-\lambda'}\,\frac{i\rho^2_{\lambda,-\lambda'}}{\rho^0_{\lambda,\lambda'}} = (-1)^{J-\lambda'}\,\frac{\rho^1_{\lambda,-\lambda'}}{\rho^3_{\lambda,\lambda'}} = \pi_\Xi\ . \tag{2.36}$$

Note here that in the last expression two SDM elements are sufficient to determine the parity, whereas one needs a whole sum of SDM elements to achieve the same in terms of K_{yy}.

2.1.4 Decay Measurement and Spin-Parity Determination

To extract SDM elements from experiment, following Chung [91] and Biagi *et al.* [92], one may relate them to moments, H^i, and weak decay-asymmetry parameters. Their definitions and further full details are given in Appendix 2.4.4. Here, we only present some pertinent results.

For a spin-J Ξ undergoing a single weak decay process, one obtains the SDM element

$$\rho^{\Xi,i}_{\lambda_\Xi,\lambda'_\Xi} = \sum_L \frac{2L+1}{2J+1}\,\langle J\,\lambda'_\Xi\,L\,M|J\,\lambda_\Xi\rangle\ t^{J,i}_{LM}\ , \tag{2.37}$$

where $M = \lambda_\Xi - \lambda'_\Xi$. The coefficients $t^{J,i}_{LM}$ can be determined from the ratio of the moments,

$$\left(\frac{d\sigma}{d\Omega}\right)\frac{H^i(L,M)}{H^0(0,0)} = \zeta_L\,t^{J,i}_{LM}\ \langle J\,\tfrac{1}{2}\,L\,0|J\,\tfrac{1}{2}\rangle\ , \tag{2.38}$$

where $\zeta_L = 1$ for even L and $\zeta_L = \alpha_\Xi$ for odd L, with α_Ξ denoting the Ξ decay-asymmetry

parameter.

Note that since all moments vanish identically for $L > 2J$, Eq. (2.38) offers a way of determining the spin of the Ξ undergoing a single (weak) decay by measuring the moments as a function of L. In other words, the nonvanishing $H^i(L, M)$ with the largest L value for some i and M determines J as $J = L/2$. Experimentally, of course, this may be challenging since it is not a priori clear how small the measured values of the next higher moment $H^i(L + 1, M)$ would need to be for being compatible with zero. And, moreover, one would need to confirm that the smallness of this moment is not accidental.

Similar results are obtained for excited Ξ resonances, Ξ^*, undergoing a double decay process, as discussed in Appendix 2.4.4. In this case, we have,

$$\left(\frac{d\sigma}{d\Omega}\right) \frac{H^i(0,0,L,M)}{H^0(0,0,0,0)} = t_{LM}^{J,i} \, \langle J \, \tfrac{1}{2} \, L \, 0 | J \, \tfrac{1}{2} \rangle \tag{2.39a}$$

for even L and

$$\left(\frac{d\sigma}{d\Omega}\right) \frac{H^i(1,0,L,M)}{H^0(0,0,0,0)} = \frac{\alpha_\Lambda}{3} \, t_{LM}^{J,i} \, \langle J \, \tfrac{1}{2} \, L \, 0 | J \, \tfrac{1}{2} \rangle \tag{2.39b}$$

for odd L. Here, α_Λ denotes the Λ decay-asymmetry parameter for the decay chain $\Xi^* \to \Lambda + \bar{K}$ followed by $\Lambda \to N + \pi$. In the case of $\Xi^* \to \Xi + \pi$ followed by $\Xi \to \Lambda + \pi$ instead, α_Λ needs to be replaced by α_Ξ.

For Ξ resonances decaying along the double decay chain specified in Eq. (2.87), the result of the corresponding moments given by Eq. (2.106) leads to [92]

$$\frac{H^0(1,\pm 1,L,M)}{H^0(1,0,L,M)} = \pi_\Xi (-1)^{J+\frac{1}{2}} \frac{2J+1}{\sqrt{2L(L+1)}} \tag{2.40}$$

for an unpolarized target and for odd values of $L(\leq 2J)$. This offers a way of determining the spin and parity of the excited Ξ resonance simultaneously. A similar measurement was performed to determine the parity of $\Lambda(1405)$ in Ref. [93]

2.2 Model Calculation of $\bar{K} + N \to K + \Xi$

In this section, we present the results of our model for $\bar{K} + N \to K + \Xi$. There have already been attempts to analyse this data. To date, recent calculations are reported by Sharov *et al.* [94] and by Shyam *et al.* [95]. The former authors have considered both the total and differential cross sections as well as the recoil polarization data in their analysis, while the latter authors have considered only the total cross section data, although they too have predicted the differential cross sections, mentioning that they found it difficult to use the differential cross section data [76] for several reasons. Although the analyses of Refs. [94, 95] are both based on very similar effective Lagrangian approaches, the number of $S = -1$ hyperon resonances included in the intermediate state are different. While in Ref. [94] only the $\Sigma(1385)$ and $\Lambda(1520)$ are considered in addition to the above-threshold $\Sigma(2030)$ and $\Sigma(2250)$ resonances,[2] in Ref. [95] eight of the 3- and 4-star Λ and Σ resonances with masses up to 2.0 GeV have been considered. While the authors of Ref. [94] pointed out the significance of the above-threshold resonances, the authors of Ref. [95] have found the dominance of the sub-threshold $\Lambda(1520)$ resonance. The reaction (2.1) has been also considered quite recently by Magas *et al.* [41] within the coupled channels Unitarized Chiral Perturbation approach in connection to the issue of determining the parameters of the next-to-leading-order interactions. The authors of Ref. [41] have added the $\Sigma(2030)$ and $\Sigma(2250)$ resonances into their calculation to improve the fit quality to the total cross section data. Just recently, a calculation by the Argonne-Osaka group [96] within a Dynamical Coupled Channels approach to the $\bar{K}$-induced two-body reactions up to $W = 2.1$ GeV has been also reported.

In the present section, we perform a model-dependent analysis of the existing data based on the effective Lagrangian approach that includes a phenomenological contact amplitude which accounts for the rescattering contributions and/or unknown (short-range) dynamics that have not been included explicitly into the model.

It should be restated that the present study is our first step toward building a more complete reaction model capable of reliably extracting the properties of hyperons from the forthcoming experimental data, in addition to providing some guidance for planning future experiments. The

[2]The production threshold energy for the reaction of $\bar{K} + N \to K + \Xi$ is about 1813 MeV.

investigation of this reaction also impacts the study of Ξ hypernuclei, where the elementary process of $\bar{K} + N \to K + \Xi$ is an input to the models of hypernuclei productions [97–100]. As mentioned before, there is a proposed program at J-PARC and eventually at GSI-FAIR to obtain information about the spectroscopy of Ξ hypernuclei through the anti-kaon induced reactions on nuclear targets. Establishing the existence and properties of Ξ hypernuclei is of considerable importance for a number of reasons and the study of this reaction is an essential step to this end.

2.2.1 Effective Lagrangian Model Description

The reaction amplitude T describing the two-body process like the reaction (2.1) is, in general, given by the Bethe-Salpeter equation,

$$T = V + VGT\,, \tag{2.41}$$

where V stands for the (two-body) meson-baryon irreducible (Hermitian) driving amplitude and G the meson-baryon propagator. Note that the above equation represents, in principle, a coupled-channels equation in meson-baryon channel space. It can be recast into the pole and the non-pole parts as

$$T = T^{\rm P} + T^{\rm NP}\,, \tag{2.42}$$

where the non-pole part $T^{\rm NP}$ obeys

$$T^{\rm NP} = V^{\rm NP} + V^{\rm NP} G\, T^{\rm NP} \tag{2.43}$$

with

$$V^{\rm NP} \equiv V - V^{\rm P} \tag{2.44}$$

denoting the one-baryon irreducible (non-pole) part of the driving amplitude V. Here, $V^{\rm P}$ stands for the one-baryon reducible (pole) part of V in the form of

$$V^{\rm P} = \sum_r |F_{0r}\rangle\, S_{0r}\, \langle F_{0r}|\,, \tag{2.45}$$

where $|F_{0r}\rangle$ and $S_{0r} = (p_r^2 - m_{0r}^2 + i\eta)^{-1}$ stand for the so-called bare vertex and bare baryon propagator, respectively. The summation runs over the baryons in the intermediate state, each specified by the index r. The four-momentum and the bare mass of the propagating baryon are denoted by p_r and m_{0r}, respectively. It can be understood that $V^{\rm P}$ is nothing other than the sum of the s-channel Feynman diagrams corresponding to the bare baryon propagations in the intermediate state as can be seen in Fig. 2.2. The pole part of the reaction amplitude $T^{\rm P}$ in Eq. (2.42) is given by

$$T^{\rm P} = \sum_{r'r} |F_{r'}\rangle \, S_{r'r} \, \langle F_r| \, , \tag{2.46}$$

where the so-called dressed vertex reads

$$\begin{aligned} |F_{r'}\rangle &= \left(1 + T^{\rm NP} G\right) |F_{0r'}\rangle \, , \\ \langle F_r| &= \langle F_{0r}| \left(1 + G \, T^{\rm NP}\right) , \end{aligned} \tag{2.47}$$

and the dressed propagator $S_{r'r}$ is written as

$$S_{r'r}^{-1} = S_{0r}^{-1} \delta_{r'r} - \Sigma_{r'r} \, , \tag{2.48}$$

with

$$\Sigma_{r'r} = \langle F_{0r'}| \, G \, |F_r\rangle \tag{2.49}$$

denoting the self-energy.

In the present work we shall make the following approximations to the reaction amplitude in Eq. (2.42). First, we approximate the pole part of the reaction amplitude $T^{\rm P}$ by the s-channel Feynman amplitude, M_s, specified by effective Lagrangians and phenomenological Feynman propagators. Here, the dressed resonance coupling constants, dressed masses as well as the corresponding widths are parameters either fixed from independent sources or adjusted to reproduce the experimental data. The couplings of the resonances in the propagator are ignored in the pressnt work.

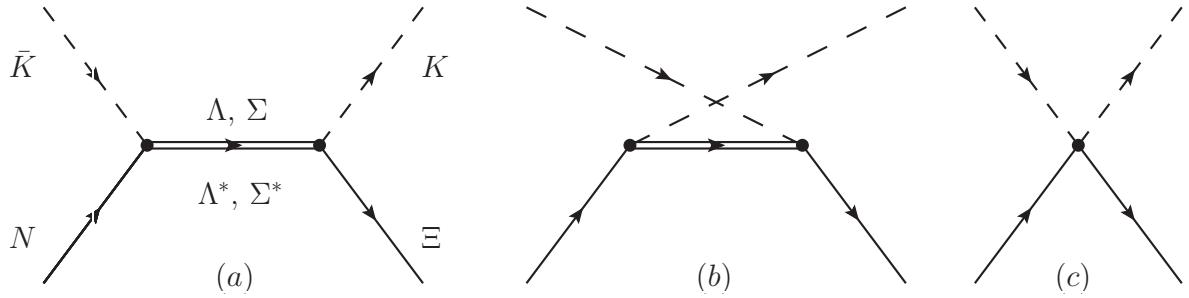

Figure 2.2: Diagrams included in the present calculation. (a) s-channel Λ and Σ hyperon exchange amplitude, M_s. (b) u-channel amplitude, M_u, including the same hyperon exchanges as in (a). (c) contact amplitude, M_c, as discussed in this section.

More explicitly, we have

$$
\begin{aligned}
|F_{r'}\rangle &\to \hat{\Gamma}^{\dagger}_{MBr'}\,, \\
\langle F_r| &\to \hat{\Gamma}_{MBr}\,, \\
S_{r'r} &\to \hat{S}_r \delta_{r'r}\,,
\end{aligned}
\tag{2.50}
$$

with the subscripts M and B denoting a meson and a baryon, respectively. The meson-baryon-baryon vertices of $MB \to r'$ and $r \to MB$ are denoted by $\Gamma^{\dagger}_{MBr'}$ and Γ_{MBr}, respectively, and can be obtained from the effective Lagrangians given in Appendix 2.4.5. The phenomenological Feynman propagators for dressed baryon $\hat{S}_r$ are also given in Appendix 2.4.5.

Second, the non-pole part of the reaction amplitude $T^{\rm NP}$ is approximated as follows.

(i) Since there is no meson-exchange t-channel process in the present reaction unless the exchanged meson is an exotic one with strangeness quantum number $S = 2$, $V^{\rm NP}$ of the reaction is approximated by the u-channel Feynman amplitude M_u constructed also from the same effective Lagrangians and Feynman propagators used to construct the s-channel Feynman amplitudes.

(ii) The rescattering term $V^{\rm NP} G\, T^{\rm NP}$ in $T^{\rm NP}$ of Eq. (2.43) and other effects not included explicitly in the present approach are accounted for by a phenomenological contact term, M_c, which is

specified below. This contact term will be discussed in more detail later.

With the approximations described above, the reaction amplitude in the present work is given by

$$T = M_s + M_u + M_c\,, \tag{2.51}$$

where M_s and M_u are the s- and u-channel Feynman diagrams with the ground state hyperons as well as some of the $S = -1$ hyperon resonances in the intermediate state. Figure 2.2 shows a diagrammatic representation of M_s, M_u, and M_c.

The contact amplitude M_c is decomposed in terms of the spin-flip and spin-non-flip amplitudes, each expanded in partial-waves. The spin amplitude for the reaction of Eq. (2.1) can be expanded in partial waves as[3]

$$\begin{aligned} M_{\frac{1}{2},\frac{1}{2}} &= M_{-\frac{1}{2},-\frac{1}{2}} \\ &= \frac{1}{4\pi}\sum_{LT}\Big[(L+1)\,M_{LL}^{TJ_+}(p',p) + L\,M_{LL}^{TJ_-}(p',p)\Big]\,P_L(\hat{\boldsymbol{p}}\cdot\hat{\boldsymbol{p}}')\,\hat{P}_T\,, \end{aligned} \tag{2.52a}$$

$$\begin{aligned} M_{\frac{1}{2},-\frac{1}{2}} &= -M_{-\frac{1}{2},\frac{1}{2}} \\ &= \frac{1}{4\pi}\sum_{LT}\Big[M_{LL}^{TJ_-}(p',p) - M_{LL}^{TJ_+}(p',p)\Big]\,P_L^1(\hat{\boldsymbol{p}}\cdot\hat{\boldsymbol{p}}')\,\hat{P}_T\,, \end{aligned} \tag{2.52b}$$

where the indices s' and (s) in $M_{s's}$ stands for the spin-projection quantum number of the final (initial) state and $J_\pm \equiv L \pm \frac{1}{2}$. The Legendre and associated Legendre functions are denoted by $P_L(x)$ and $P_L^1(x)$, respectively.[4] The total angular momentum, orbital angular momentum, and total isospin of the initial $\bar{K}N$ state are represented by J, L, and T, respectively. $\hat{P}_T$ stands for the isospin projection operator onto the total isospin 0 or 1 as $T = 0$ or $T = 1$, respectively. Explicitly, $\hat{P}_{T=0} = (3 + \boldsymbol{\tau}_1\cdot\boldsymbol{\tau}_2)/4$ and $\hat{P}_{T=1} = (1 - \boldsymbol{\tau}_1\cdot\boldsymbol{\tau}_2)/4$.

Following the essential idea of Ref. [83] for the phenomenological contact term, M_c, the spin

[3]There are in total four spin matrix elements to describe the reaction (2.1). However, only two of them, corresponding to the spin-non-flip and spin-flip processes, are independent due to the reflection symmetry about the reaction plane for parity conserving processes. See Ref. [101] for more detailed discussions.

[4]Here, the phase convention for the associated Legendre function is such that $P_1^1(x) = -\sin(x)$.

amplitudes in the above equation corresponding to M_c are parametrized as

$$\begin{aligned} M_{c\,\frac{1}{2}\frac{1}{2}} &= M_{c\,-\frac{1}{2}-\frac{1}{2}} \\ &= \sum_{LT} g_1^{LT} \left(\frac{p'}{\Lambda_S}\right)^L \exp\left[-\alpha_L^T \frac{p'^2}{\Lambda_S^2}\right] P_L(\theta)\hat{P}_T\,, \\ M_{c\,\frac{1}{2}-\frac{1}{2}} &= -M_{c\,-\frac{1}{2}\frac{1}{2}} \\ &= \sum_{LT} g_2^{LT} \left(\frac{p'}{\Lambda_S}\right)^L \exp\left[-\beta_L^T \frac{p'^2}{\Lambda_S^2}\right] P_L^1(\theta)\hat{P}_T \end{aligned} \tag{2.53}$$

with $g_1^{LT} \equiv a_L^T \exp\left(i\{\phi_a\}_L^T\right)$, $g_2^{LT} \equiv b_L^T \exp\left(i\{\phi_b\}_L^T\right)$, and α_L^T, β_L^T being constants to be fitted. Λ_S is a typical scale parameter of the reaction at hand. The momentum dependence of the partial-wave matrix elements given above is suited for hard processes, where one has a large momentum transfer for, in those processes, the amplitude is expected to be independent of energy and nearly constant apart from the centrifugal barrier effect. The reaction (2.1) is not a very hard process.[5] Nonetheless, the p'^L-dependence captures the essence of the behavior of the amplitude at low momentum in the final state. We refer the details to Ref. [83]. The exponential factor in Eq. (2.53) is simply a damping factor to suppress the high momentum behavior introduced by p'^L.

It should be noted that our phenomenological contact term M_c can only account for effects that give rise to a smooth energy dependence. Effects such as due to dynamically generated resonances and/or channel couplings [102–105] that give rise to a strong variation of the amplitude as a function of energy cannot be taken into account by the contact term.

Before closing this section, we comment on a feature encountered in describing the reaction (2.1) within a standard effective Lagrangian approach, like that in Refs. [94, 95], where only the (tree-level) s-, u- and t-channel diagrams are included without the phenomenological contact term. The existing data show backward peeking differential cross sections (see Sec. 2.2.2), which may indicate a considerable contribution from the u-channel amplitude M_u. In fact, there are a number of Λ and Σ resonances as can be seen in Table 2.1 that contribute, in principle, to this reaction. However, it happens that the u-channel resonance contributions, especially, from many of those sub-threshold

[5] For example, the momentum transfer of this reaction at threshold is about 200 MeV.

Table 2.1: The Λ and Σ hyperons listed by the Particle Data Group [6] (PDG) as three- or four-star states. The decay widths and branching ratios of higher-mass resonances ($m_r > 1.6$ GeV) are in a broad range, and the coupling constants are determined from their centroid values. In the present work, the masses (m_r) and widths (Γ_r) of the hyperons as given in this table have been used, except for the $\Sigma(2250)$ resonance. For the latter resonance, see the text.

Λ states					Σ states				
State	m_r (MeV)	Γ_r (MeV)	Rating	$\lvert g_{N\Lambda K}\rvert$	State	m_r (MeV)	Γ_r (MeV)	Rating	$\lvert g_{N\Sigma K}\rvert$
$\Lambda(1116)\ 1/2^+$	1115.7		****		$\Sigma(1193)\ 1/2^+$	1193		****	
$\Lambda(1405)\ 1/2^-$	1406	50	****		$\Sigma(1385)\ 3/2^+$	1385	37	****	
$\Lambda(1520)\ 3/2^-$	1520	16	****						
$\Lambda(1600)\ 1/2^+$	1600	150	***	4.2	$\Sigma(1660)\ 1/2^+$	1660	100	***	2.5
$\Lambda(1670)\ 1/2^-$	1670	35	****	0.3	$\Sigma(1670)\ 3/2^-$	1670	60	****	2.8
$\Lambda(1690)\ 3/2^-$	1690	60	****	4.0	$\Sigma(1750)\ 1/2^-$	1750	90	***	0.5
$\Lambda(1800)\ 1/2^-$	1800	300	***	1.0	$\Sigma(1775)\ 5/2^-$	1775	120	****	
$\Lambda(1810)\ 1/2^+$	1810	150	***	2.8	$\Sigma(1915)\ 5/2^+$	1915	120	****	
$\Lambda(1820)\ 5/2^+$	1820	80	****		$\Sigma(1940)\ 3/2^-$	1940	220	***	< 2.8
$\Lambda(1830)\ 5/2^-$	1830	95	****		$\Sigma(2030)\ 7/2^+$	2030	180	****	
$\Lambda(1890)\ 3/2^+$	1890	100	****	0.8	$\Sigma(2250)\ ?^?$	2250	100	***	
$\Lambda(2100)\ 7/2^-$	2100	200	****						
$\Lambda(2110)\ 5/2^+$	2110	200	***						
$\Lambda(2350)\ 9/2^+$	2350	150	***						

resonances, also give rise to a total cross section which keeps increasing with energy, a feature that is not supported by the data which reaches a peak and then falls off as a function of energy. Indeed, our model calculation, when those hyperon resonances are considered but without the contact term, exhibits exactly this feature owing to the increasing contribution of the u-channel diagrams with energy. This means that the rescattering term ($V^{\rm NP}GT^{\rm NP}$) in the non-pole T-matrix $T^{\rm NP}$ should somehow cancel the increasing contribution from the u-channel resonance amplitudes. Or, perhaps, one needs to consider the u-channel Regge trajectories instead of individual resonances. In the present work, we do not attempt the difficult task of extracting the contributions of these many sub-threshold resonances but, instead, we account for their combined effects with the phenomenological contact term. In any case, it seems that the problem has two scales, one corresponding to the long-range and the other to the short-range dynamics. The latter is, of course, sensitive to the form factors used at the meson-baryon coupling vertices to account for the composite nature of the hadrons and we somehow account for it through the phenomenological contact terms. Problems with two scales have been addressed in the past, where some authors have introduced two form factors, one soft and other hard, to account for such effects [106]. Also, in effective field theories the unknown short-range dynamics is accounted for by contact terms.

We note that the recent calculations by other authors reported in Refs. [94, 95] within usual effective Lagrangian approaches, have dealt with this problem by suppressing the high-energy u-channel contributions. In Ref. [94], this is done by introducing an ad-hoc energy-dependent damping factor in the u-channel resonance diagrams. In Ref. [95] (see, also Ref. [107]) the form factor used in the u-channel diagrams is not an off-shell form factor in that it is not a function of the "off-shellness" $(p_r^2 - m_r^2)$ of the propagating hyperon. Moreover, by using a different form of the form factor in the u-channel as compared to that in the s-channel amplitudes, it violates the crossing symmetry already at the tree-level.

2.2.2 Results

In this section, we present our results for the reaction $\bar{K} + N \to K + \Xi$ in different isospin channels. More specifically, we investigate the reactions $K^- + p \to K^+ + \Xi^-$, $K^- + p \to K^0 + \Xi^0$, and $K^- + n \to K^0 + \Xi^-$ considering all the available data on the total and differential cross sections as well as recoil polarization asymmetries.

Before we present our results, we briefly remark on the experimental data considered in this work on total cross sections, differential cross sections, and recoil polarization asymmetries. These data come from different sources of Refs. [70–76, 82] and are available in various forms. Some of them are not in the tabular (numerical) form that can be readily used but are given only in graphical form or as parametrization in terms of the Legendre polynomial expansions. In Ref. [94], Sharov *et al.* have carefully considered the data extraction from these papers. We have checked that the extracted data are consistent with those in the original papers within the permitted accuracy of the check. In the present work, we use these data and no cross sections resulting from the expansion coefficients are considered here.

As mentioned before, there are a number of 3- and 4-star Λ and Σ resonances, including those low-mass sub-threshold ones that contribute, in principle, to the reaction (2.1). A list for these hyperon resonances and some of their properties is shown in Table 2.1. However, apart from the ground state $\Lambda(1116)$ and $\Sigma(1193)$, for most of these resonances, the required information on the resonance parameters such as the coupling strength (including their signs) to Ξ and/or N are

largely unknown. Therefore, the strategy adopted in this work is to consider these parameters as fit parameters and consider the minimum number of resonances required to reproduce the existing data. In particular, we have considered only those resonances that give rise to a considerable contribution to the cross section within a physically reasonable range of the resonance parameter values. More specifically, during the fitting procedure, resonances were added one by one to the model and the quality of fit was checked. It should be mentioned that we have also checked the influence of various combinations of resonances at a time (and not just one by one) to the fit quality. The resonances kept in the presented calculation were those that increased the quality of the fit by a noticeable amount with the variation in χ^2 per data points N, namely, $\delta\chi^2/N > 0.1$. An example of this procedure is shown in Table 2.2 where the results of adding one more resonance to the current model, as specified later, is shown. We see that some of these resonances improve somewhat the fit quality of the total cross section but not much the other observables or even worsen the fit quality slightly. We have not included these resonances into our model because the total cross sections suffer from a relatively large uncertainties.

Table 2.2: Variation in χ^2 per data point N, $\delta\chi^2/N$, obtained when adding one more resonance to the current model (specified in Table. 2.3). A negative $\delta\chi^2/N$ corresponds to an improvement in the result. The quantity $\delta\chi^2_i/N_i$ corresponds to $\delta\chi^2/N$ evaluated for a given type of observable specified by index i: $i = \sigma$(total cross section), $= d\sigma$(differential cross section) and, $= P$(recoil asymmetry). $N = N_\sigma + N_{d\sigma} + N_P$ denotes the total number of data points. Furthermore, $\delta\chi^2_i/N_i$ is given for the charged Ξ^- ($\delta\chi^2_-/N_-$) and neutral Ξ^0 ($\delta\chi^2_0/N_0$) production processes, separately. The last column corresponds to $\delta\chi^2/N$ of the global fit considering all the data of both reaction processes. The last row corresponds to χ^2_i/N_i of the current model.

	$K^- + p \to K^+ + \Xi^-$				$K^- + p \to K^0 + \Xi^0$				
Y added	$\delta\chi^2_\sigma/N_\sigma$	$\delta\chi^2_{d\sigma}/N_{d\sigma}$	$\delta\chi^2_P/N_P$	$\delta\chi^2_-/N_-$	$\delta\chi^2_\sigma/N_\sigma$	$\delta\chi^2_{d\sigma}/N_{d\sigma}$	$\delta\chi^2_P/N_P$	$\delta\chi^2_0/N_0$	$\delta\chi^2/N$
$\Lambda(1405)$	-0.01	0.03	0.00	-0.01	0.03	0.00	0.02	0.01	0.00
$\Lambda(1600)$	-0.02	0.00	-0.01	-0.01	0.02	0.00	0.02	0.01	0.00
$\Lambda(1670)$	-0.01	0.00	0.00	0.00	0.02	0.00	0.02	0.01	0.00
$\Lambda(1800)$	0.00	0.01	0.00	0.00	-0.01	0.00	0.01	0.00	0.00
$\Lambda(1810)$	-0.01	-0.01	0.00	-0.01	0.02	0.00	0.02	0.01	0.00
$\Lambda(1520)$	-0.06	0.02	0.00	0.00	-0.05	-0.01	0.00	-0.02	0.00
$\Lambda(1690)$	0.00	0.00	0.00	0.00	0.00	0.00	0.00	0.00	0.00
$\Lambda(1820)$	-0.08	0.01	0.01	0.00	-0.07	0.00	-0.02	-0.02	-0.01
$\Lambda(1830)$	-0.05	0.01	0.01	0.00	0.00	0.02	0.02	0.01	0.00
$\Lambda(2110)$	-0.02	0.02	0.01	0.01	-0.03	-0.01	-0.03	-0.02	0.00
$\Lambda(2100)$	-0.08	0.04	0.03	0.02	-0.04	-0.02	-0.01	-0.03	0.01
$\Sigma(1660)$	-0.02	0.00	0.00	0.00	-0.01	0.01	0.00	0.01	0.00
$\Sigma(1750)$	-0.01	0.01	0.00	0.00	-0.01	0.01	0.00	0.00	0.00
$\Sigma(1670)$	-0.01	0.00	-0.01	0.00	0.02	0.01	0.01	0.01	0.00
$\Sigma(1940)$	0.02	0.00	0.01	0.00	0.01	-0.01	0.01	-0.01	0.00
$\Sigma(1775)$	-0.01	0.01	0.04	0.01	-0.02	0.00	-0.02	-0.01	0.00
$\Sigma(1915)$	0.01	-0.01	0.00	-0.01	-0.03	0.00	0.00	-0.01	-0.01
	χ^2_σ/N_σ	$\chi^2_{d\sigma}/N_{d\sigma}$	χ^2_P/N_P	χ^2_-/N_-	χ^2_σ/N_σ	$\chi^2_{d\sigma}/N_{d\sigma}$	χ^2_P/N_P	χ^2_0/N_0	χ^2/N
	1.53	1.64	1.85	1.64	0.88	1.06	1.73	1.10	1.49

Whenever appropriate, for each resonance considered in this work, the corresponding coupling constants g_{KYN} and $g_{KY\Xi}$ were constrained in such way that the sum of the branching ratios $\beta_{Y\to KN} + \beta_{Y\to K\Xi}$ not to exceed unit. Because, within our model, the data are sensitive only to the product of the coupling constants $g_{KYN}g_{KY\Xi}$, setting $|g_{KYN}| = |g_{KY\Xi}|$ for the purpose of estimating the individual branching ratios, and only for this purpose, is a simple way of keeping our coupling constant values within a physically acceptable range. Admittedly, the currently existing data are limited and suffer from large uncertainties, thus an accurate determination of the resonance parameters are not possible at this stage. For this, one needs to wait for new more precise data, possibly including more spin polarization data. In this regard, the multi-strangeness baryon spectroscopy program using the anti-kaon beam at J-PARC will be of particular relevance. For the ground states $\Lambda(1116)$ and $\Sigma(1193)$, the corresponding coupling constants are estimated based on the flavor SU(3) symmetry relations [53].

The phenomenological contact amplitude M_c contains two sets of free parameters, $\{g_1^{LT}, \alpha_L^T\}$ and $\{g_2^{LT}, \beta_L^T\}$, to be fixed by adjusting to reproduce the experimental data, for a given set of $\{L, T\}$ as shown in Eq. (2.53). In order to reduce the number of free parameters, we have assumed the parameter α_L^T to be equal to β_L^T and independent on T and L, i.e., $\alpha_L^T = \beta_L^T = \alpha$. The scale parameter Λ_S has been fixed as $\Lambda_S = 1$ GeV. Note that the phenomenological contact amplitude can and should be complex in principle, since it accounts for the rescattering contribution ($V^{\rm NP}GT^{\rm NP}$) of the non-pole T-matrix which is complex in general. Accordingly, the coupling strength parameters g_1^{LT} and g_2^{LT} are complex quantities. In order to reduce the number of free parameters, we take their phases to be independent on L and T, so that, $\{\phi_a\}_L^T = \phi_a$ and $\{\phi_b\}_L^T = \phi_b$ for all the sets $\{L, T\}$. Also, in the present calculation, we find that it suffices to consider partial waves up to $L = 2$ in the contact amplitude to reproduce the existing data.

The resonances included in the present model calculations and the corresponding resonance parameters are displayed in Table 2.3 as well as the parameters of the phenomenological contact term M_c. We do not give the associated uncertainties here because they are not well constrained. In the present calculation, resonances with $J \leq 7/2$ were considered. The masses and the total widths of the resonances are taken to be those quoted in PDG [6] and are given in Table 2.1, except

Table 2.3: Fitted parameter values of the current model. For the details of the resonance parameters, see Appendix 2.4.5. For the contact amplitude, see Eq. (2.53). The entries in boldface are taken from Ref. [53] and they are not fit parameters. Here, it is assumed that $\{\phi_a\}_L^T = \phi_a$ and $\{\phi_b\}_L^T = \phi_b$, in addition to $\alpha_L^T = \beta_L^T = \alpha$.

Y	$g_{N\Lambda K}$	$\lambda_{N\Lambda K}$	$g_{\Xi\Lambda K}$	$\lambda_{\Xi\Lambda K}$	Λ (MeV)
$\Lambda(1116)\frac{1}{2}^+$	**−13.24**	**1.0**	**3.52**	**1.0**	900
$\Sigma(1193)\frac{1}{2}^+$	**3.58**	**1.0**	**−13.26**	**1.0**	900

	$g_{N\Lambda K}g_{\Xi\Lambda K}$	$\lambda_{N\Lambda K}$	–	$\lambda_{\Xi\Lambda K}$	Λ (MeV)	L	a_L^0	a_L^1	b_L^0	b_L^1	ϕ_a	ϕ_b
$\Lambda(1890)\frac{3}{2}^-$	-0.11				900	0	0.28	−1.18				
$\Sigma(1385)\frac{3}{2}^+$	18.76	**1.0**		**1.0**	900	1	3.22	−4.84	3.40	−0.60		
$\Sigma(2030)\frac{7}{2}^+$	0.49				900	2	3.06	21.08	−9.40	2.28		
$\Sigma(2250)\frac{5}{2}^-$	−0.033				900			$\Lambda_S = 1$ GeV		$\alpha = 3.62$	0.22	-0.16

for the mass of the $\Sigma(2250)$ resonance. Currently, the $\Sigma(2250)$ resonance is not well established and have a three-star status [6]. In fact, the PDG doesn't even assign the spin-parity quantum numbers for this resonance. The analyses of Ref. [78], actually show as two possible resonances, one with $J^P = 5/2^-$ at about 2270 ± 50 MeV and another with $J^P = 9/2^-$ at about 2210 ± 30 MeV. In the present work we have assumed $\Sigma(2250)$ to have $J^P = 5/2^-$ with the mass of 2265 MeV. This is motivated by the fact that the total cross section in $K^- + p \to K^+ + \Xi^-$ shows a small bump structure at around 2300 MeV, which is well reproduced in our model with the mass of $\Sigma(2250)$ adjusted to be at 2265 MeV. For the corresponding width, we have adopted the value quoted in PDG as shown in Table 2.1.

All the parameters of the present model calculation are determined as described above and we now present the results obtained in our model. The overall fit quality is quite good with $\chi^2/N = 1.49$ as displayed in Table 2.2. There we also show the partial χ_i^2/N_i evaluated for a given type of observable specified by the index i as explained in the caption of Table 2.2. In Fig. 2.3 we show the results for the total cross section in the charged Ξ production reaction from the proton target, i.e., $K^- + p \to K^- + \Xi^-$, for the center-of-mass energies up to $W = 3$ GeV. Figure 2.3(a) displays the total contribution which reproduces the data rather well. The dynamical content of the present model is also shown in the same figure. We find that the contact term rises quickly from threshold peaking at around 2.1 GeV and falls off more slowly as energy increases. It dominates largely the cross section except for energies very close to threshold and above ~ 2.7 GeV, where the hyperon resonance contributions are comparable. The Λ hyperons contribution is strongest

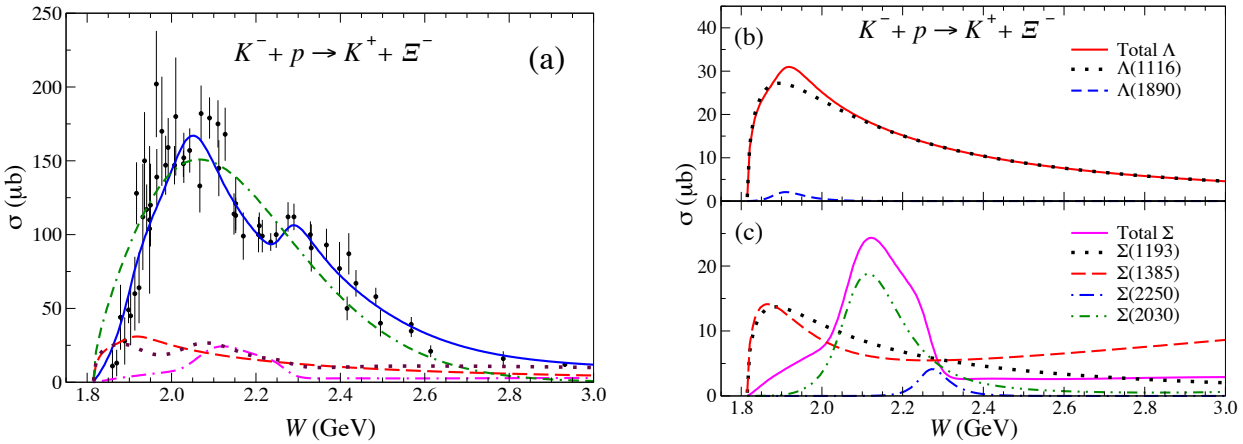

Figure 2.3: (Color online) Total cross section for the $K^- + p \to K^+ + \Xi^-$ reaction. (a) The solid blue line represents the result of the full calculation of the present model. The red dashed line shows the combined Λ hyperons contribution. The magenta dash-dotted line shows the combined Σ hyperons contribution. The brown dotted line shows the combined Λ and Σ hyperons contribution. The green dash-dash-dotted line corresponds to the contact term. (b) The solid red line represents the combined Λ hyperons contribution that is the same as the red dashed line in (a). The dotted and dashed lines show the $\Lambda(1116)$ and $\Lambda(1890)$ contributions, respectively. (c) The solid magenta line represents the combined Σ hyperons contribution that is the same as the magenta dash-dotted line in (a). The dotted, dashed, dot-dashed, and dot-dot-dashed lines show the contributions from the $\Sigma(1193)$, $\Sigma(1385)$, $\Sigma(2250)$, and $\Sigma(2030)$, respectively. The experimental data (black circles) are the digitized version as quoted in Ref. [94] from the original work of Refs. [69–81].

near threshold and dies off very slowly as energy increases. The Σ contribution is relatively small over the entire energy range considered, except in the interval of 2.0–2.3 GeV, where it becomes comparable to the Λ contribution. Near threshold, there is a strong destructive interference between the contact term and (mainly) the Λ hyperons contribution. At higher energies, the data indicates an existence of a bump structure at $W \sim 2.3$ GeV. Our model reproduces this feature due to a delicate destructive and constructive interference of the contact term and the hyperon resonance contributions as the energy increases. We also mention that we have explored the possibility of a much smaller contact amplitude contribution than shown in Fig. 2.3(a) considering various different sets of hyperon resonances from Table 2.1; however, we were unable to find a solution with a comparable fit quality to that of Fig. 2.3(a).

Figure 2.3(b) displays the individual Λ hyperon contributions. We see that the ground state

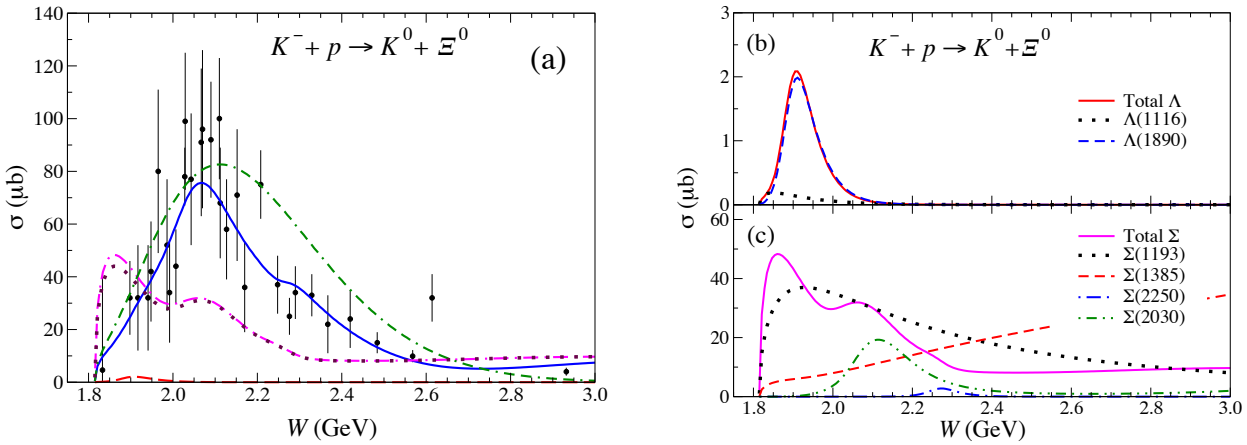

Figure 2.4: (Color online) Same as Fig. 2.3 for the $K^- + p \to K^0 + \Xi^0$ reaction. The experimental data (black circles) are the digitized version as quoted in Ref. [94] from the original work of Refs. [70, 76–78, 81, 82].

$\Lambda(1116)$ is, by far, the dominant contribution which is due to the tail of the corresponding u-channel process. Analogously, the individual Σ hyperon contributions are shown in Fig. 2.3(c). Here, the relatively small cross section near threshold is due to the destructive interference between the $\Sigma(1192)$ and $\Sigma(1385)$. The enhancement of the cross section in the energy interval of 2.0–2.3 GeV is basically due to the $\Sigma(2030)$ resonance. The $\Sigma(2250)$ leads to a little shoulder in the total Σ contribution. We note that any non-negligible contribution from the hyperons for energies above ~ 2.3 GeV is due to the u-channel processes.

In Fig. 2.4 we show the total cross section results for the neutral Ξ production process, $K^- + p \to K^0 + \Xi^0$. Here, the data are of such poor quality that they impose much less constraint on the model parameters than the corresponding data in the charged Ξ^- production. Here, the resulting dynamical content shown in Fig. 2.4(a) is similar to that for the charged Ξ^- production discussed above, i.e., it is largely dominated by the contact term. However, we see a quite different feature in the Λ and Σ resonance contributions as compared to that for the charged Ξ^- production [cf. Fig. 2.3(a)]. One notable difference between the charged and neutral Ξ production reactions considered here is that the u-channel Λ hyperon contribution is absent in the Ξ^0 production case. Also, the relative contribution of the Σ hyperons is much larger in the neutral Ξ^0 production than

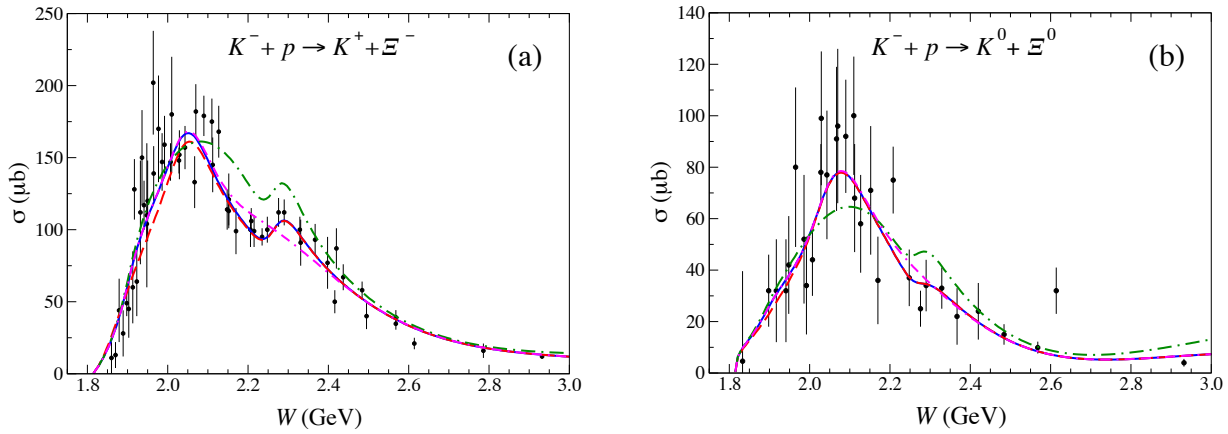

Figure 2.5: (Color online) Total cross section results with individual resonances switched off (a) for $K^- + p \to K^+ + \Xi^-$ and (b) for $K^- + p \to K^0 + \Xi^0$. The blue lines represent the full result shown in Figs. 2.3 and 2.4. The red dashed lines, which almost coincide with the blue lines represent the result with $\Lambda(1890)$ switched off. The green dash-dotted lines represent the result with $\Sigma(2030)$ switched off and the magenta dash-dash-dotted lines represent the result with $\Sigma(2250)5/2^-$ switched off.

in the charged Ξ^- production, especially, in the near threshold region.

Figures 2.4(b) and 2.4(c) show the individual hyperon contributions. As mentioned before, due to the absence of the u-channel Λ exchange in the neutral Ξ^0 production, the $\Lambda(1116)$ contribution is insignificant, leading to a negligible contribution of the Λ hyperons. Due to the isospin factors, here, the $\Sigma(1192)$ and $\Sigma(1385)$ hyperons interfere constructively, especially, near the threshold. Recall that, for charged Ξ^- production, these hyperons interfere destructively [cf. Fig. 2.3(c)].

In Fig. 2.5 we illustrate the amount of the above-threshold resonance contributions of the present model to the total cross sections by switching them off one by one with respect to the full results shown in Figs. 2.3(a) and 2.4(a). We see in Fig. 2.5(a) that the $\Sigma(2030)$ affects most the cross sections in the range of $W \sim 2.0$ to 2.4 GeV. This resonance is clearly needed in our model to reproduce the data. It also affects the recoil polarization as will be discussed later. It should be mentioned that this resonance also helps to reproduce the measured $K^+\Xi^-$ invariant mass distribution in $\gamma p \to K^+K^+\Xi^-$ [54], by filling in the valley in the otherwise double-bump structured invariant mass distribution, a feature that is not observed in the data [108]. The $\Lambda(1890)$ affects the total cross section in the range of $W \sim 1.9$ to 2.1 GeV and the $\Sigma(2250)5/2^-$ around

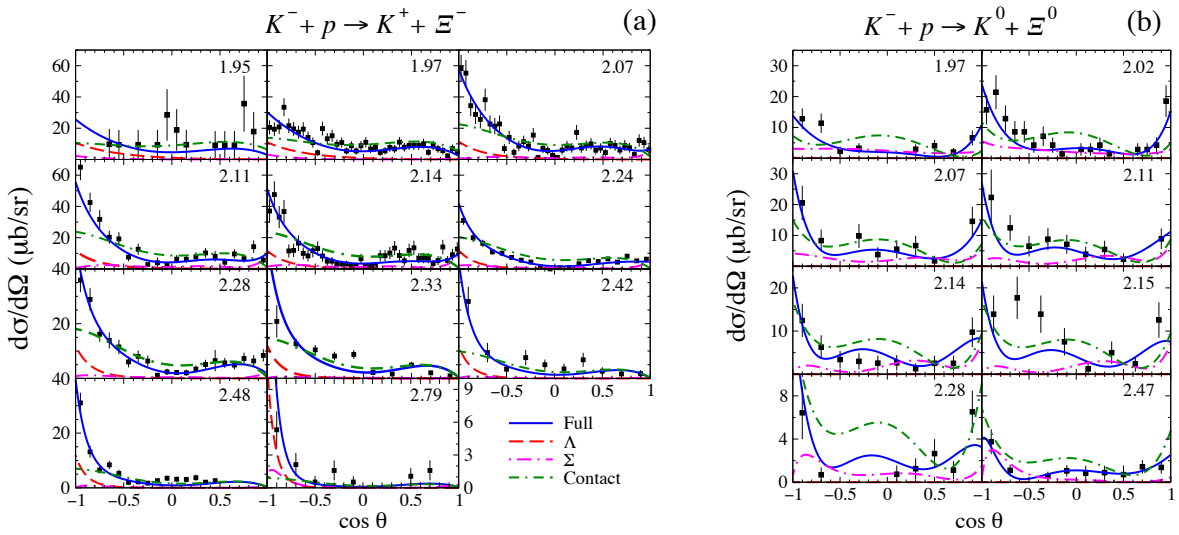

Figure 2.6: Kaon angular distributions in the center-of-mass frame (a) for $K^- + p \to K^+ + \Xi^-$ and (b) for $K^- + p \to K^0 + \Xi^0$. The blue lines represent the full model results. The red dashed lines show the combined Λ hyperons contribution. The magenta dash-dotted lines show the combined Σ hyperons contribution. The green dash-dash-dotted line corresponds to the contact term. The numbers in the upper right corners correspond to the centroid total energy of the system W. Note the different scales used. The experimental data (black circles) are the digitized version as quoted in Ref. [94] from the original work of Refs. [71–76] for the $K^- + p \to K^+ + \Xi^-$ reaction and of Ref. [70, 74, 76, 82] for the $K^- + p \to K^0 + \Xi^0$ reaction.

$W \sim 2.2$ GeV to reproduce the observed bump structure. A more accurate data set is clearly needed for a more definitive answer about the role of the $\Lambda(1890)$ and $\Sigma(2250)$ resonances. Figure 2.5(b) for the neutral Ξ^0 production shows also a similar feature observed in the Ξ^- case for the $\Sigma(2030)$ resonance. Here, the influence of the $\Sigma(2250)5/2^-$ is smaller and that of the $\Lambda(1890)$ is hardly seen. Recall that there is no u-channel Λ contribution in the neutral Ξ^0 production.

The results for differential cross sections in both $K^- + p \to K^+ + \Xi^-$ and $K^- + p \to K^0 + \Xi^0$ are shown in Figs. 2.6(a) and 2.6(b), respectively, in the energy domain up to $W = 2.8$ GeV for the former and up to $W = 2.5$ GeV for the latter reaction. Overall, the model reproduces the data quite well. There seem to be some discrepancies for energies $W = 2.33$ to 2.48 GeV in the charged Ξ^- production. Our model underpredicts the yield around $\cos\theta = 0$. As in the total cross sections, the data for the neutral Ξ^0 production are fewer and less accurate than for the charged

Ξ^- production. In particular, the Ξ^0 production data at $W = 2.15$ GeV seems incompatible with those at nearby lower energies and that the present model is unable to reproduce the observed shape at backward angles. It is clear from Figs. 2.6(a) and 2.6(b) that the charged channel shows a backward peaked angular distributions, while the neutral channel shows enhancement for both backward and forward scattering angles (more symmetric around $\cos\theta = 0$) for all but perhaps the highest energies. In the charged Ξ^- production, both the resonance and contact amplitude contributions are backward angle peaked and, as the energy increases, they get smaller and smaller at forward angles. In Ξ^0 production, both the Σ resonance and contact amplitude contributions also exhibit an enhancement for forward angles. Note that the Λ resonance contribution here is negligible due to the absence of the u-channel process. The interference pattern in the forward angular region depends on energy. At lower energies the interfere is constructive and it becomes destructive at higher energies. The behavior of the angular distributions in terms of the partial waves will be discussed later in connection to the results of Figs. 2.7(b) and 2.9(b).

The partial-wave content in the cross sections for the charged Ξ^- production process arising from the present model is shown in Figs. 2.7(a) and 2.7(b). As can be seen in Fig. 2.7(a), the total cross section is dominated by the P and D waves in almost the entire range of energy considered, even at energies very close to threshold where one sees a strongly raising P-wave contribution. The S-wave contribution is very small. This peculiar feature is caused by the ground state $\Lambda(1116)$, whose contribution cancels to a large extent the otherwise dominant S-wave contribution close to threshold, in addition to enhancing the P-wave contribution. One way of probing the S-wave content close to threshold in a model-independent manner is to look at the quantity σ/p' as a function of p'^2, where p' is the relative momentum of the final $K\Xi$ state. The reason to look at this quantity is that, for hard processes, the partial wave reaction amplitude goes basically with p'^L for a given orbital angular momentum L as mentioned in Sec. 2.2.1. This leads to

$$\frac{\sigma}{p'} = c_0 + c_1 p'^2 + c_2 p'^4 + \dots , \tag{2.54}$$

where c_L's are constants. Figure 2.8 illustrates this point. Although the existing experimental data are of poor quality, they reveal the general features just mentioned. In particular, for the

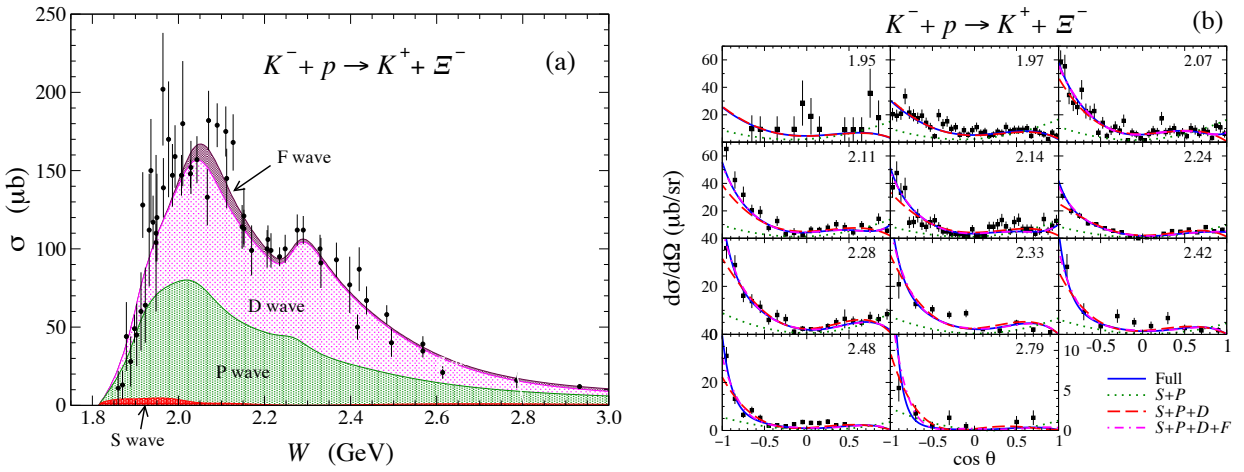

Figure 2.7: Partial wave decomposition of the total cross section and the angular distribution for $K^- + p \to K^+ + \Xi^-$. (a) Total cross section sectioned by contributions from each partial wave L. The red shaded area indicates the S-wave contribution, while the green area corresponds to the P-wave. Magenta indicates the D-wave and maroon the F-wave. (b) K^+ angular distribution: the solid blue lines are the full results, while the dotted green lines represent the sum of $S + P$ waves, the red dashed lines represent the $S + P + D$ waves and the dash-dotted magenta lines represent the $S + P + D + F$ waves. For lower energies, the $S + P + D$ waves already saturate the full cross section results so that the F- and higher-wave contributions cannot be distinguished from the full result.

charged Ξ^- production process, the data indicate a linear dependence of σ/p' close to threshold implying a strong P-wave contribution. The present model result is consistent with this behavior. The corresponding results for the neutral Ξ^0 production are also shown in Fig. 2.8. There, the data are scattered around but are consistent with the S-wave dominance and our model just shows this feature [see also Fig. 2.9(a)]. In Fig. 2.7(a) we also see a small F-wave contribution above $W \sim 2.0$ GeV and practically saturates the total cross section for energies considered. Note that since our contact term includes the partial waves through the D waves only, the F-wave contribution is entirely due to the hyperon resonances. The enhancement of the D-wave contribution around $W = 2.3$ GeV as well as the little shoulder in the P-wave contribution are due to the $\Sigma(2250)$ hyperon. Of course, the partial wave contributions are constrained dominantly by the differential cross section and they are shown in Fig. 2.7(b). As mentioned before, the shape of the angular distribution is backward-angle peaked and that the cross section is very small at forward angles.

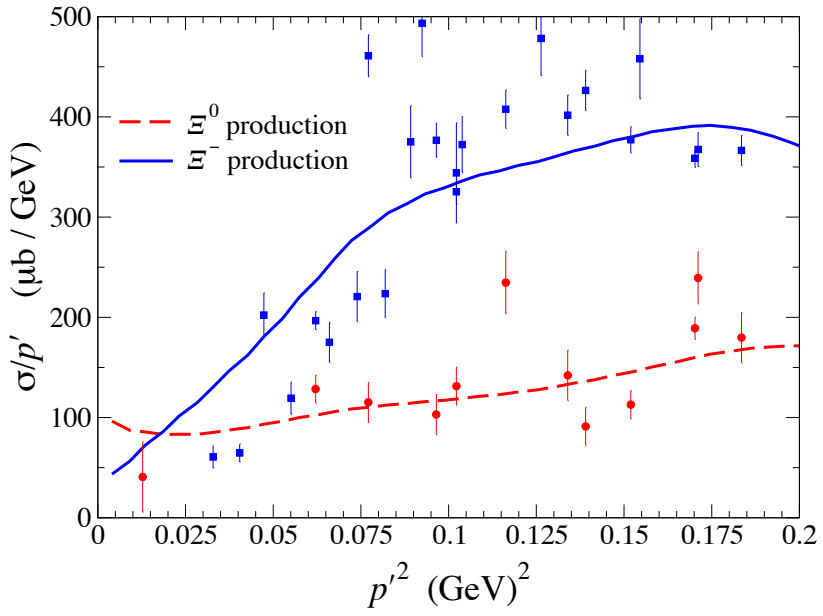

Figure 2.8: Ratio of the measured total cross section σ and the final state $K\Xi$ relative momentum p' as a function of p'^2. The blue square data correspond to $K^- + p \to K^+ + \Xi^-$, while the red circle data to $K^- + p \to K^0 + \Xi^0$. The blue solid and red dashed curves are the present model results corresponding to $K^- + p \to K^+ + \Xi^-$ and $K^- + p \to K^0 + \Xi^0$, respectively.

This behavior is a direct consequence of the very significant interference between the P and D waves. This can be seen by expanding the cross section in partial waves. Considering the partial waves through $L = 2$ and following Ref. [101] and Appendix 2.4.1, the differential cross section may be expressed as

$$\frac{d\sigma}{d\Omega} = \left[|\alpha_{02}|^2 + \left(|\alpha_1|^2 + \alpha_{02}\alpha_2^*\right)\cos^2\theta + |\alpha_2|^2\cos^4\theta + \left(|\beta_1|^2 + \left|\tilde{\beta}_2\right|^2\cos^2\theta\right)\sin^2\theta\right] + 2\,\mathrm{Re}\left[\alpha_{02}\alpha_1^* + \alpha_1\alpha_2^*\cos^2\theta + \beta_1\tilde{\beta}_2^*\sin^2\theta\right]\cos\theta\,, \tag{2.55}$$

where the coefficients α_L (β_L) denotes a linear combination of the partial-wave matrix elements corresponding to the spin-non-flip (spin flip) process with a given orbital angular momentum L [see Eq. (2.52)]. Here, $\alpha_{02} \equiv \alpha_0 - \frac{1}{3}\alpha_2$ and $\tilde{\beta}_2 \equiv 2\beta_2$. In the above equation, the last term on the right hand side which involves an interference between the P and D waves is an odd function in $\cos\theta$,

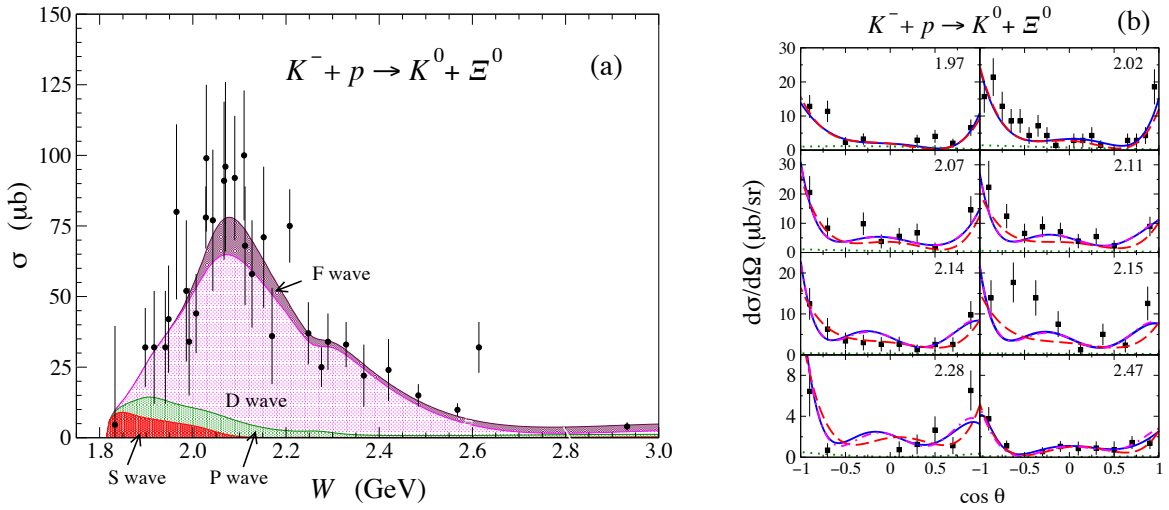

Figure 2.9: Same as in Fig. 2.7 but for $K^- + p \to K^0 + \Xi^0$.

while the other term (in big brackets) is an even function. These two terms cancel each other to a large extent at forward angles while at backward angles they add up. Note that these partial waves are comparable in strength as shown in Fig. 2.7(a) so that their interference term leading to an odd function part can largely cancel the even term at forward angles.

Figures 2.9(a) and 2.9(b) display the partial wave content in the cross sections for the neutral Ξ^0 production process. In contrast to the charged Ξ^- production, here one sees that the largest contribution to the total cross section is the D-wave and that the P-wave is largely suppressed, which is a direct consequence of the shape of the observed angular distribution whose partial wave contributions are shown in Fig. 2.9(b). There, compared to that for charged Ξ^-, one sees a more symmetric angular shape about $\cos\theta = 0$ that is dominated by the D-wave. The present model reproduces the observed behavior of the K^0 angular distribution by suppressing the P-wave contribution as can be easily understood from Eq. (2.55). The rather drastic suppression of the P wave can be better seen in Fig. 2.9(a). For energies very close to threshold, the cross section is dominated by the S-wave as seen also in Fig. 2.9(a).

The results for the recoil polarization asymmetry multiplied by the cross section are shown in Fig. 2.10 in the energy interval of $W = 2.1$ to 2.5 GeV. Overall, we reproduce the data reasonably

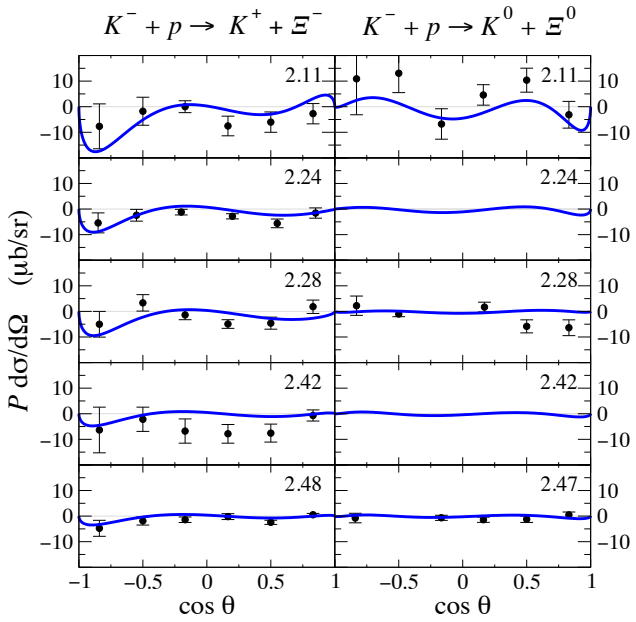

Figure 2.10: The recoil asymmetry $\frac{d\sigma}{d\Omega}P$ for both the $K^- + p \to K^+ + \Xi^-$ and $K^- + p \to K^0 + \Xi^0$ reactions. The blue solid lines represent the full results of the current model. Data are from Refs. [73, 76].

well. We also find that the results shown at $W = 2.11$ GeV are still significantly affected by $\Sigma(2030)$. This corroborates the findings of Ref. [94]. We recall that the recoil asymmetry is proportional to the imaginary part of the product of the non-spin-flip matrix element (M_{ss}) with the complex conjugate of the spin-flip matrix element ($M_{s's}$ with $s' \neq s$) [101], so that it vanishes identically unless these matrix elements are complex with non-vanishing real and imaginary parts. We can therefore expect the recoil polarization to be sensitive to the complex nature of the reaction amplitude, in particular, to the phenomenological contact amplitude M_c introduced in the present model. Indeed, if one forces the coupling strength parameters g_1^{LT} and g_2^{LT} in Eq. (2.53) to be purely real during the fitting procedure, the χ^2_P/N_P deteriorates, e.g., from 1.85 to 2.25 for the $K^- + p \to K^+ + \Xi^-$ reaction, although the quality of fit for cross sections is nearly unchanged.

In Fig. 2.11 we show the present model predictions for the target-beam asymmetries K_{xx} and K_{xz} multiplied by the unpolarized cross section, i.e., $\frac{d\sigma}{d\Omega}K_{xx}$ and $\frac{d\sigma}{d\Omega}K_{xz}$ for both the charged Ξ^- and neutral Ξ^0 production processes. Note that these target-recoil asymmetries, together

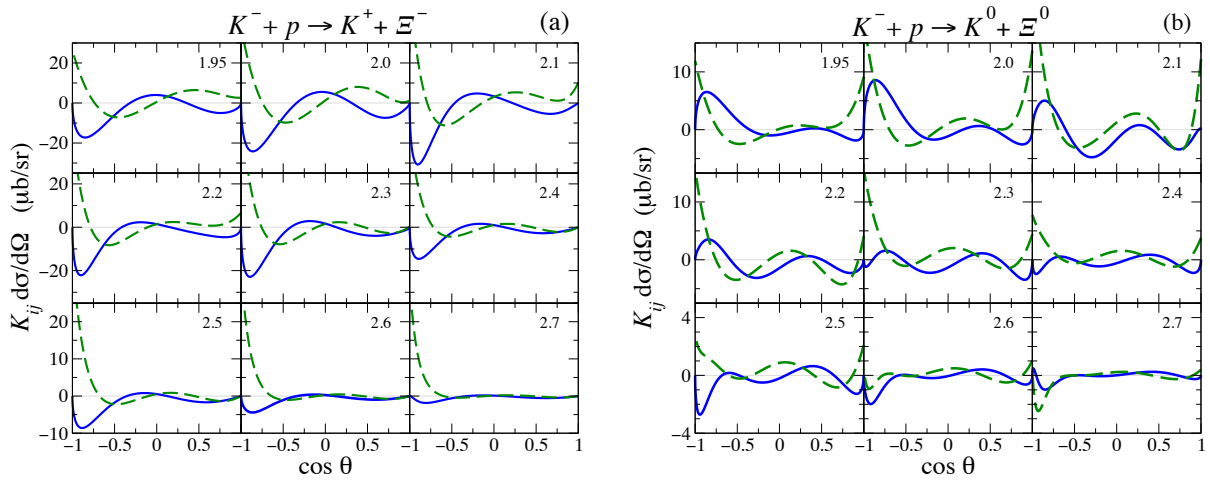

Figure 2.11: Target-recoil asymmetries K_{xx} (green dashed curves) and K_{xz} (blue solid curves) as defined in Ref. [101] for the reactions (a) $K^- + p \to K^+ + \Xi^-$ and (b) $K^- + p \to K^0 + \Xi^0$. The numbers in the upper right corners represent the total energy of the system W in units of GeV.

with K_{yy}, are the only three independent double-spin observables in the reaction of Eq. (2.1) as discussed in Ref. [101] and Section 2.1. Indeed, the only two other non-vanishing target-recoil asymmetries are related by $K_{zz} = K_{xx}$ and $K_{zx} = -K_{xz}$.[6] We mention that $\frac{d\sigma}{d\Omega}K_{xx}$ is proportional to the difference of the magnitude squared of the spin-non-flip and spin-flip matrix elements, while $\frac{d\sigma}{d\Omega}K_{xz}$ is proportional to the real part of the product of the spin-non-flip matrix element with the complex conjugate of the spin-flip matrix element. Therefore, unlike the recoil asymmetry, these spin observables do not vanish even if the reaction amplitude is purely real or purely imaginary. This means that they are, like the cross section, much less sensitive to the complex nature of the phenomenological contact amplitude.

To gain some insight into the angular dependence exhibited by these target-recoil asymmetries

[6]Note that the symmetry of the reaction leads to $K_{yy} = \pi_\Xi$ independent on the scattering angle θ [87, 101]. Here, π_Ξ stands for the parity of the produced Ξ which is taken to be $\pi_\Xi = +1$ for the ground state Ξ. Also, $K_{xx} = K_{zz}\big|_{\cos\theta=\pm1} = \pi_\Xi$. The target asymmetry is identical to the recoil asymmetry in the present reaction. Therefore, we exhaust all the *independent* observables available in the reaction processes considered here.

in Fig. 2.11, we express them in terms of partial waves with $L \leq 2$. We have

$$\frac{d\sigma}{d\Omega}K_{xx} = \left[|\alpha_{02}|^2 + \left(|\alpha_1|^2 + \alpha_{02}\alpha_2^*\right)\cos^2\theta + |\alpha_2|^2\cos^4\theta - \left(|\beta_1|^2 + \left|\tilde{\beta}_2\right|^2\cos^2\theta\right)\sin^2\theta\right] + 2\,\mathrm{Re}\left[\alpha_{02}\alpha_1^* + \alpha_1\alpha_2^*\cos^2\theta - \beta_1\tilde{\beta}_2^*\sin^2\theta\right]\cos\theta\,, \tag{2.56a}$$

$$\frac{d\sigma}{d\Omega}K_{xz} = 2\,\mathrm{Re}\left[\alpha_{02}\beta_1^* + \left(\alpha_1\tilde{\beta}_2^* + \alpha_2\beta_1^*\right)\cos^2\theta + \left(\alpha_{02}\tilde{\beta}_2^* + \alpha_1\beta_1^*\right)\cos\theta + \alpha_2\tilde{\beta}_2^*\cos^3\theta\right]\sin\theta\,. \tag{2.56b}$$

Note that the only difference between $\frac{d\sigma}{d\Omega}K_{xx}$ given above and differential cross section given by Eq. (2.55) is the sign change of the terms involving β_L. These terms are, however, proportional to $\sin^2\theta$. Therefore, this spin observable behaves like the differential cross section at very forward and backward angles, where $\sin^2\theta \ll 1$. At $\cos\theta = 0$, the difference is due to the term of $\pm|\beta_1|^2$ which is a P-wave contribution in the spin-flip amplitude. Now, if we ignore the P-wave contribution — which is relatively very small in the neutral Ξ^0 production over the nearly entire energy region considered as seen in Fig. 2.9(a) — it is immediate to see that Eq. (2.56a) involves only terms that are symmetric about $\cos\theta = 0$. We see in Fig. 2.11(b) that $\frac{d\sigma}{d\Omega}K_{xx}$ exhibits roughly this symmetry.

For $\frac{d\sigma}{d\Omega}K_{xz}$, Eq. (2.56b) reveals a rather complicated angular dependence in general, and no particular feature is apparent in the results shown in Fig. 2.11, especially for the charged Ξ^- production process. Neglecting the P-wave contribution, Eq. (2.56b) reduces to $\frac{d\sigma}{d\Omega}K_{xz} = \mathrm{Re}\left[\left(\alpha_{02} + \alpha_2\cos^2\theta\right)\tilde{\beta}_2^*\right]\sin 2\theta$, which is roughly the angular dependence exhibited in Fig. 2.11(b).

The present model predictions for the $K^- + n \to K^0 + \Xi^-$ reaction are shown in Fig. 2.12. Here, the experimental data are extremely scarce and they were not included in the present fitting procedure. Nevertheless, the current model is seen to predict those few data quite reasonably. Both the total and differential cross sections exhibit a very similar feature to those of the $K^- + p \to K^+ + \Xi^-$ reaction with a noticeable small enhancement in the differential cross sections as seen in Fig. 2.12(b) for forward angles near $\cos\theta = 0$ in $K^- + n \to K^0 + \Xi^-$. We see, however, some bigger differences in the individual amplitude contributions, more clearly seen in the total cross sections that are given in Fig. 2.12(a). There, the Σ hyperon contribution is larger than the Λ contribution over the entire energy region up to $W \sim 2.3$ GeV, in particular, at low energies near threshold.

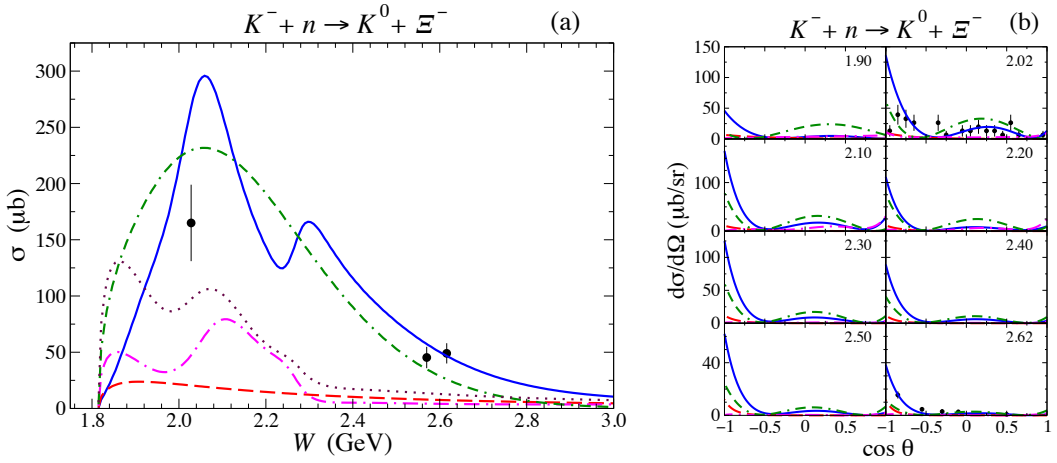

Figure 2.12: Same as Figs. 2.3(a) and 2.6 for the $K^- + n \to K^- + \Xi^0$ reaction. The experimental data are from Refs. [70, 77].

This is due to the absence of the strong destructive interference between the $\Sigma(1385)$ and $\Sigma(1192)$ (not shown), since the latter hyperon contribution is suppressed to a large extent compared to the case of $K^- + p \to K^+ + \Xi^-$. Moreover, there is a constructive interference with the Λ hyperon, which makes the sum of the hyperons contribution relatively large in the low energy region.

2.3 Chapter Summary

A model-independent analysis of the $\bar{K} + N \to K + \Xi$ reaction has been performed. Following the method of Ref. [83], the most general spin structure of the reaction amplitude, consistent with basic symmetries, for Ξ baryons of $J^P = \frac{1}{2}^{\pm}$ and $\frac{3}{2}^{\pm}$ has been derived. The coefficients multiplying each spin structure have been presented in partial-wave-decomposed form, thus permitting partial-wave analyses, once sufficient data become available for these reactions. The method of Ref. [83] is general, and can be applied, in principle, to derive the structure of the reaction amplitude involving higher-spin Ξ production.

Furthermore, a minimal set of independent observables required to determine completely the reaction amplitude has been identified. In addition to the unpolarized cross sections, one also needs single- and double-spin observables, which poses a formidable experimental challenge, in particular,

since one needs to measure the polarization of the outgoing Ξ. Note that, for the Ξ of spin-1/2, there are two complex amplitudes to be determined, whereas for the Ξ of spin-3/2, there are four complex amplitudes. We then formulated the problem using the SDM approach and expressed the spin observables in terms of the SDM elements. Following Ref. [91, 92], it was shown that the latter can be extracted from the moments associated with the Ξ decay processes in conjunction with the self-analyzing nature of the hyperon (Λ or Ξ) resulting from the subsequent decay of the Ξ produced in the primary reaction. The moments, in turn, can be extracted from the measurement of the angular distribution of the decay products.

Since the determination of the spin and parity quantum numbers is a fundamental part of any spectroscopy study, reflection symmetry about the reaction plane has been exploited, in particular, to show that, apart from the spin-transfer coefficient K_{yy}, the ratio of the SDM elements given by Eq. (2.36) determines the parity of a Ξ resonance with an arbitrary spin. Furthermore, the moments given by Eq. (2.40) determine the spin and parity of the Ξ resonance simultaneously [92].

We also mention that the present analysis applies as given only to Ξ resonances that are sufficiently narrow to permit them being treated like on-shell particles. For broad resonances, a partial-wave analysis would be required to extract them from experimental data.

In summary, the present analysis provides the model-independent framework for developing reliable reaction theories of Ξ production to help in the planning of future experimental efforts in Ξ baryon spectroscopy. This will also help in analyzing the data to understand the production mechanisms of Ξ baryons.

We have also presented our analysis on the reaction of $K^- + N \to K + \Xi$ within an effective Lagrangian approach that includes a phenomenological contact term to account for the rescattering contribution of the non-pole part of the reaction amplitude in the Bethe-Salpeter equation and for other possible (short-range) dynamics that are not taken into account explicitly in the model. By introducing the phenomenological contact term, we avoid the problem of a strong u-channel hyperon contribution which keeps growing as a function of energy leading to ever increasing cross sections, a common feature of the effective Lagrangian approaches. The present model also includes the $\Lambda(1890)$, $\Sigma(1385)$, $\Sigma(2030)$, and $\Sigma(2250)$ resonance contributions apart from the ground states

$\Lambda(1116)$ and $\Sigma(1193)$.

The available total and differential cross sections, as well as the recoil asymmetry data, in both the $K^- + p \to K^+ + \Xi^-$ and $K^- + p \to K^0 + \Xi^0$ processes are well reproduced by the present model. We have found that the above-threshold resonances $\Lambda(1890)$, $\Sigma(2030)$, and $\Sigma(2250)$ are required to achieve a good fit quality of the data. Among them, the $\Sigma(2030)$ resonance is the most critical one. This resonance affects not only the cross sections but also the recoil asymmetry. In addition, it also brings a model calculation of Ref. [54] into an agreement with the observed $K^+\Xi^-$ invariant mass distribution in Ξ photoproduction [108]. The $\Lambda(1890)$ is also required to improve the fit quality in the present model, especially in the energy dependence of the total cross sections of the charged Ξ^- production around $W = 1.9$ GeV. The total cross section data in the charged Ξ^- production seems to indicate a bump structure at around $W = 2.3$ GeV, which is accounted for by the $\Sigma(2250)$ resonance with $J^P = 5/2-$ and a mass of 2265 MeV in the present model. More accurate data are required before a more definitive answer can be provided for the role of these two resonances. In this regard, the multi-strangess hyperon production programs using an intense anti-Kaon beam at J-PARC is of particular relevance in providing the much needed higher-precision data for the present reaction.

Apart from the recoil asymmetry, we have also predicted the target-recoil asymmetries for which there are no experimental data currently. In contrast to the recoil polarization — which are small —- these observables are quite sizable and may help impose more stringent constraints on the model parameters. In principle, one requires four independent observables to model-independently determine the reaction amplitude for spin-1/2 Ξ production [101]. As said before, measurements of these spin observables are challenging experimentally by any standard, but one can exploit the self-analyzing nature of the produced hyperon to extract these observables [101, 124]. Of course, for the target-recoil asymmetry measurements, one requires a polarized target in addition o spin measurements of the produced Ξ. The measurement of the spin of the cascade is possible by exploiting the self-analyzing nature of the cascade as mentioned before. The polarized targets are nowadays available at some of the major laboratories worldwide. Combined with the availability of intense beams, measuring these spin observables is no longer out of reach. In fact, various single-

and double-polarization observables in photoproduction reactions are currently being measured at the major facilities such as JLab, ELSA, and MAMI, aiming at the so-called complete experiments in order to model-independently determine the photoproduction amplitudes.

There is some controversy about the role of particular resonances among the recent calculations of the $K^- + N \to K + \Xi$ reaction, in particular, those based on effective Lagrangians as mentioned in the Introduction [94,95] and now including the present work. The common feature among these calculations, including that based on the Unitarized Chiral Perturbation approach [41], is that some $S = -1$ hyperon resonances seem to be required to reproduce the existing data. To pin down the role of a particular resonance among them requires more precise and complete data, in addition to a more complete theoretical model. Anyway, the present reaction is very suited for studying $S = -1$ hyperon resonances.

Finally, the present work is our first step toward building a more complete reaction theory in a DCC approach to help analyze the data and extract the properties of Ξ resonances in future experimental efforts in Ξ baryon spectroscopy.

2.4 Appendixes

2.4.1 Appendix A: Expansion of $\bar{K} + N \to K + \Xi$ Spin Coefficients

In this Appendix, we give the partial wave decomposition of the coefficients multiplying each spin structure of the reaction amplitudes in Eqs. (2.4) and (2.14) for Ξ with spin-parity $J^P = \frac{1}{2}^{\pm}$ and $\frac{3}{2}^{\pm}$. The partial-wave expansion of the (plane-wave) matrix element $\hat{M}$ in Eqs. (2.4) and (2.14) is

$$\langle S' M_{S'} | \hat{M}(\boldsymbol{p}', \boldsymbol{p}) | S M_S \rangle = \sum i^{L-L'} \langle S\, M_S\, L\, M_L | J\, M_J \rangle \langle S'\, M_{S'}\, L'\, M_{L'} | J\, M_J \rangle \times M^{TJ}_{L'L}(p', p) Y_{L' M_{L'}}(\hat{\boldsymbol{p}}') Y^*_{L M_L}(\hat{\boldsymbol{p}})\, \hat{P}_T \ , \tag{2.57}$$

where S, L, J, T stand for the total spin, orbital angular momentum, total angular momentum, and the total isospin, respectively, of the initial $\bar{K}N$ state. The corresponding projection quantum numbers are denoted by M_S, M_L, and M_J. The primed quantities represent the corresponding quantum numbers of the final $K\Xi$ state. The summation runs over all quantum numbers not specified in the left-hand side of Eq. (3.33). The relative momenta of the initial $\bar{K}N$ and final $K\Xi$ states are denoted by $\boldsymbol{p}$ and $\boldsymbol{p}'$, respectively, and $p = |\boldsymbol{p}|$, $p' = |\boldsymbol{p}'|$. In the following, without loss of generality, we choose $\hat{\boldsymbol{n}}_3$ along the momentum $\boldsymbol{p}$ of the nucleon in the CM system, i.e., $\hat{\boldsymbol{n}}_3 \equiv \hat{\boldsymbol{p}}$ as specified in Fig. 2.1. In Eq. (3.33), $\hat{P}_T$ stands for the total isospin projection operator onto the isospin singlet ($T = 0$) and isospin triplet ($T = 1$) states,

$$\hat{P}_0 = \frac{1}{4}(1 - \boldsymbol{\tau}_1 \cdot \boldsymbol{\tau}_2) \quad \text{and} \quad \hat{P}_1 = \frac{1}{4}(3 + \boldsymbol{\tau}_1 \cdot \boldsymbol{\tau}_2) \ , \tag{2.58}$$

where the $\boldsymbol{\tau}_i$ $(i = 1, 2)$ are the usual vectors made out of isospin Pauli matrices.

For a Ξ of $J^P = \frac{1}{2}^{\pm}$, following Ref. [83], the coefficients M_i in Eq. (2.4) are given by

$$M_0 = \frac{1}{4\pi} \sum_{L',T} \Big[(L'+1)\, M^{TJ_+}_{L'L'}(p',p) + L'\, M^{TJ_-}_{L'L'}(p',p) \Big] P_{L'}(\hat{\boldsymbol{p}} \cdot \hat{\boldsymbol{p}}')\, \hat{P}_T \ , \tag{2.59a}$$

$$M_2 = \frac{i}{4\pi} \sum_{L',T} \Big[M^{TJ_-}_{L'L'}(p',p) - M^{TJ_+}_{L'L'}(p',p) \Big] P^1_{L'}(\hat{\boldsymbol{p}} \cdot \hat{\boldsymbol{p}}')\, \hat{P}_T \ , \tag{2.59b}$$

$$M_1 = \frac{i}{4\pi} \sum_{L',T} \Big[M^{TJ_-}_{L'\,L'-1}(p',p) + M^{TJ_+}_{L'\,L'+1}(p',p) \Big] P^1_{L'}(\hat{\boldsymbol{p}} \cdot \hat{\boldsymbol{p}}')\, \hat{P}_T \ , \tag{2.59c}$$

$$M_3 = \frac{i}{4\pi} \sum_{L',T} \Big[(L'+1)\, M^{TJ_+}_{L'\,L'+1}(p',p) - L'\, M^{TJ_-}_{L'\,L'-1}(p',p) \Big] P_{L'}(\hat{\boldsymbol{p}} \cdot \hat{\boldsymbol{p}}')\, \hat{P}_T \ , \tag{2.59d}$$

where $J_\pm \equiv L' \pm \frac{1}{2}$, and $P_{L'}(x)$ and $P^1_{L'}(x)$ denote the Legendre and associated Legendre functions, respectively.[7] The amplitudes M_i here are operators in isospin space whose actions are specified by the projectors $\hat{P}_T$ defined in Eq. (2.58).

Likewise, for a Ξ of $J^P = \frac{3}{2}^{\pm}$, following Ref. [83], the coefficients F_i and G_i in Eq. (2.14) are given by

$$F_1 = i\frac{3}{8\pi} \sum_{J,L',T} (-1)^{L'+J+\frac{3}{2}} [J]^2 \frac{[L']}{\sqrt{L'(L'+1)}} \begin{Bmatrix} \frac{1}{2} & L' & J \\ L' & \frac{3}{2} & 1 \end{Bmatrix} M^{JT}_{L'L'}(p',p) P^1_{L'}(\hat{\boldsymbol{p}}' \cdot \hat{\boldsymbol{p}})\, \hat{P}_T \ , \tag{2.60a}$$

$$F_2 = \frac{1}{\sqrt{2}} \sum_{J,L',L,T} i^{L-L'} (-1)^{J+\frac{1}{2}} [J]^2 \begin{Bmatrix} \frac{1}{2} & L & J \\ L' & \frac{3}{2} & 2 \end{Bmatrix} M^{JT}_{L'L}(p',p)\, a_{L'L}\, \hat{P}_T \ , \tag{2.60b}$$

$$F_3 = \frac{1}{2\sqrt{2}} \sum_{J,L',L,T} i^{L-L'} (-1)^{J+\frac{1}{2}} [J]^2 \begin{Bmatrix} \frac{1}{2} & L & J \\ L' & \frac{3}{2} & 2 \end{Bmatrix} M^{JT}_{L'L}(p',p)\, b_{L'L}\, \hat{P}_T \ , \tag{2.60c}$$

$$F_4 = \frac{1}{\sqrt{2}} \sum_{J,L',L,T} i^{L-L'} (-1)^{J+\frac{1}{2}} [J]^2 \begin{Bmatrix} \frac{1}{2} & L & J \\ L' & \frac{3}{2} & 2 \end{Bmatrix} M^{JT}_{L'L}(p',p)\, c_{L'L}\, \hat{P}_T \ , \tag{2.60d}$$

[7] Here, the phase convention for the associated Legendre function is such that $P^1_1(x) = +\sin(x)$.

and

$$G_1 = \frac{1}{2\sqrt{2}} \sum_{J,L',L,T} i^{L-L'} (-1)^{J+\frac{1}{2}} [J]^2 \begin{Bmatrix} \frac{1}{2} & L & J \\ L' & \frac{3}{2} & 2 \end{Bmatrix} M^{JT}_{L'L}(p',p)\, a'_{L'L}\, \hat{P}_T \ , \tag{2.61a}$$

$$G_2 = \frac{1}{2\sqrt{2}} \sum_{J,L',L,T} i^{L-L'} (-1)^{J+\frac{1}{2}} [J]^2 \begin{Bmatrix} \frac{1}{2} & L & J \\ L' & \frac{3}{2} & 2 \end{Bmatrix} M^{JT}_{L'L}(p',p)\, b'_{L'L}\, \hat{P}_T \ , \tag{2.61b}$$

$$G_3 = \sqrt{\frac{3}{2}} \frac{1}{4\pi} \sum_{J,L',L,T} i^{L-L'} (-1)^{J+\frac{1}{2}} [J]^2 \frac{[LL']}{\sqrt{L'(L'+1)}} \langle L\,0\,L'1\,|1\,1\rangle \begin{Bmatrix} \frac{1}{2} & L & J \\ L' & \frac{3}{2} & 1 \end{Bmatrix}$$
$$\times\, M^{JT}_{L'L}(p',p) P^1_{L'}(\hat{\boldsymbol{p}}' \cdot \hat{\boldsymbol{p}})\, \hat{P}_T \ , \tag{2.61c}$$

$$G_4 = \frac{\sqrt{3}}{8\pi} \sum_{J,L',L,T} i^{L-L'} (-1)^{J+\frac{3}{2}} [J]^2 [LL']\, \langle L\,0\,L'\,0|1\,0\rangle \begin{Bmatrix} \frac{1}{2} & L & J \\ L' & \frac{3}{2} & 1 \end{Bmatrix} M^{JT}_{L'L}(p',p) P_{L'}(\hat{\boldsymbol{p}}' \cdot \hat{\boldsymbol{p}})\, \hat{P}_T \ , \tag{2.61d}$$

where we introduced the notation $[J] \equiv \sqrt{2J+1}$ and $[j_1 j_2] \equiv [j_1]\,[j_2]$. The summations extend over all the quantum numbers J, L', L and T. Note that total parity conservation imposes the condition $(-1)^{L'+L} = \pm 1$ as the parity of the Ξ baryon is $\pi_\Xi = \pm 1$. The coefficients $a_{L'L}$, $b_{L'L}$, etc, are given by

$$a_{L',L} = 2\frac{[LL']}{4\pi} \langle L\,0\,L'\,2 \mid 2\,2\rangle \sqrt{\frac{(L'-2)!}{(L'+2)!}}\, P^2_{L'}(\hat{\boldsymbol{p}}' \cdot \hat{\boldsymbol{p}}) \ , \tag{2.62a}$$

$$b_{L',L} = 2\frac{[LL']}{4\pi} \langle L\,0\,L'\,1 \mid 2\,1\rangle \sqrt{\frac{(L'-1)!}{(L'+1)!}}\, P^1_{L'}(\hat{\boldsymbol{p}}' \cdot \hat{\boldsymbol{p}}) \ , \tag{2.62b}$$

$$c_{L',L} = \frac{[LL']}{4\pi} \left[\langle L\,0\,L'\,2 \mid 2\,2\rangle \sqrt{\frac{(L'-2)!}{(L'+2)!}}\, P^2_{L'}(\hat{\boldsymbol{p}}' \cdot \hat{\boldsymbol{p}}) + \sqrt{\frac{3}{2}} \langle L\,0\,L'\,0 \mid 2\,0\rangle\, P_{L'}(\hat{\boldsymbol{p}}' \cdot \hat{\boldsymbol{p}}) \right] \ , \tag{2.62c}$$

$$a'_{L',L} = i b_{L',L} \ , \tag{2.62d}$$

$$b'_{L',L} = -i a_{L',L} \ . \tag{2.62e}$$

The $\boldsymbol{T}^\dagger$ matrices take the form

$$T_1^\dagger = \frac{1}{\sqrt{2}} \begin{pmatrix} -1 & 0 \\ 0 & -\frac{1}{\sqrt{3}} \\ \frac{1}{\sqrt{3}} & 0 \\ 0 & 1 \end{pmatrix} , \qquad T_2^\dagger = \frac{i}{\sqrt{2}} \begin{pmatrix} 1 & 0 \\ 0 & \frac{1}{\sqrt{3}} \\ \frac{1}{\sqrt{3}} & 0 \\ 0 & 1 \end{pmatrix} , \qquad T_3^\dagger = \sqrt{\frac{2}{3}} \begin{pmatrix} 0 & 0 \\ 1 & 0 \\ 0 & 1 \\ 0 & 0 \end{pmatrix} . \quad (2.63)$$

2.4.2 Appendix B: Details of the SDM Formalism

A density operator can be used to describe an ensemble of quantum states. It is defined as

$$\hat{\rho} \equiv \sum_{\psi} I_\psi \left|\psi\right\rangle \left\langle\psi\right| \ , \tag{2.64}$$

where I_ψ denotes the probability of finding an element of the ensemble in the state ψ, subject to the condition $\sum_\psi I_\psi = 1$. For the present application, the states $|\psi\rangle$ are the spin states of the initial state, N, or the final state, Ξ. For the initial nucleon state, the spin-density operator reads

$$\begin{aligned} \hat{\rho} \to \hat{\rho}^N &\equiv \sum_{\psi_N} I_{\psi_N} \left|\psi_N\right\rangle \left\langle\psi_N\right| \\ &= \frac{1}{2} \left(\mathbb{1} + \boldsymbol{P}\cdot\boldsymbol{\sigma}\right) \ , \end{aligned} \tag{2.65}$$

where $\boldsymbol{\sigma} = (\sigma_1, \sigma_2, \sigma_3)$ denotes the vector formed of Pauli spin matrices and $\boldsymbol{P}$ is the polarization vector of the nucleon which is the difference between the probability of finding the nucleon in the $m_N = +\frac{1}{2}$ spin state and the probability of finding the nucleon in the $m_N = -\frac{1}{2}$ state (m_N is the spin projection quantum number along the $\boldsymbol{P}$ direction) or symbolically $|I_{\psi_+} - I_{\psi_-}| = |\boldsymbol{P}|$.

An unpolarized ensemble has $\boldsymbol{P} = 0$. The trace of this spin-$\frac{1}{2}$ density matrix is normalized to 1. By introducing the notation $\sigma_0 \equiv \mathbb{1}$ and $P_0 \equiv 1$, the nucleon SDM in Eq. (2.65) can be rewritten as

$$\hat{\rho}^N = \frac{\mathbb{1} + \boldsymbol{P}\cdot\boldsymbol{\sigma}}{2} = \sum_{i=0}^{3} P_i \, \hat{\rho}^{N,i} \tag{2.66}$$

with

$$\hat{\rho}^{N,i} \equiv \frac{1}{2}\sigma_i \tag{2.67}$$

for $i = 0, \ldots, 3$.

The spin-density operator for a produced Ξ particle, $\hat{\rho}^{\Xi}$, can be expressed in terms of the production amplitude $\hat{M}$ which is an operator that maps the initial nucleon spin state ψ_N into a spin-state of the Ξ. In the helicity basis for the produced Ξ, the corresponding spin-density matrix elements read

$$\rho^{\Xi}_{\lambda\lambda'}(\psi_N) \equiv \langle\lambda|\, \hat{M}\, |\psi_N\rangle \, \langle\psi_N|\, \hat{M}^{\dagger}\, |\lambda'\rangle \,, \tag{2.68}$$

where λ and λ' enumerate the Ξ's helicities.

When the beam of anti-Kaons scatters off an ensemble of nucleons, one needs to average over all nucleon spin states with their appropriate probability weights, i.e.,

$$\begin{aligned}
\rho^{\Xi}_{\lambda,\lambda'} &\equiv \sum_{\psi_N} I_{\psi_N} \rho^{\Xi}_{\lambda\lambda'}(\psi_N) \\
&= \sum_{\psi_N} I_{\psi_N} \, \langle\lambda|\, \hat{M}\, |\psi_N\rangle \, \langle\psi_N|\, \hat{M}^{\dagger}\, |\lambda'\rangle \\
&= \langle\lambda|\, \hat{M} \hat{\rho}^{N} \hat{M}^{\dagger}\, |\lambda'\rangle \\
&= \langle\lambda|\, \hat{\rho}^{\Xi}\, |\lambda'\rangle \ ,
\end{aligned} \tag{2.69}$$

where Eq. (2.64) was used to show that the Ξ spin-density operator is given by [109]

$$\hat{\rho}^{\Xi} = \hat{M} \hat{\rho}^{N} \hat{M}^{\dagger} \ . \tag{2.70}$$

Using Eq. (2.66), we may write

$$\hat{\rho}^{\Xi} = \sum_{i=0}^{3} P_i \, \hat{\rho}^{\Xi,i} \ , \tag{2.71}$$

where

$$\hat{\rho}^{\Xi,i} \equiv \frac{1}{2} \hat{M} \sigma_i \hat{M}^{\dagger} \ , \tag{2.72}$$

for $i = 0, \ldots, 3$. Here, $\hat{\rho}^{\Xi,0}$ and $\hat{\rho}^{\Xi,j}$ $(j = 1, 2, 3)$ provide the respective contributions for unpolarized

and polarized initial nucleons.

For a Ξ baryon of spin-1/2, comparing Eqs. (2.7) and (2.72) gives

$$\frac{d\sigma}{d\Omega} = \frac{1}{2}\,\mathrm{Tr}\left[\hat{M}\hat{M}^\dagger\right] = \mathrm{Tr}\left[\hat{\rho}^{\Xi,0}\right] \ , \tag{2.73a}$$

$$\frac{d\sigma}{d\Omega}T_i = \frac{1}{2}\,\mathrm{Tr}\left[\hat{M}\sigma_i\hat{M}^\dagger\right] = \mathrm{Tr}\left[\hat{\rho}^{\Xi,i}\right] \ , \tag{2.73b}$$

$$\frac{d\sigma}{d\Omega}P_i = \frac{1}{2}\,\mathrm{Tr}\left[\hat{M}\hat{M}^\dagger\sigma_i\right] = \mathrm{Tr}\left[\hat{\rho}^{\Xi,0}\sigma_i\right] \ , \tag{2.73c}$$

$$\frac{d\sigma}{d\Omega}K_{ij} = \frac{1}{2}\,\mathrm{Tr}\left[\hat{M}\sigma_i\hat{M}^\dagger\sigma_j\right] = \mathrm{Tr}\left[\hat{\rho}^{\Xi,i}\sigma_j\right] \ . \tag{2.73d}$$

When a Ξ baryon of spin-3/2 (or higher-spin) is involved, there will be many more possible degrees of polarization than the spin-1/2 case. For the particular case of the spin-transfer coefficient, K_{ij}, discussed in connection to the parity of Ξ, its definition given in Eq. (2.6d) has to be generalized. For this purpose, we first introduce the operator $\Omega(\boldsymbol{J}\cdot\hat{\boldsymbol{n}})$ as

$$\Omega(\boldsymbol{J}\cdot\hat{\boldsymbol{n}}) \equiv \sum_{M=-J}^{+J} (-1)^{\frac{1}{2}-M}\ \mathsf{P}^{J,M}_{\hat{\boldsymbol{n}}}, \tag{2.74}$$

where $\mathsf{P}^{J,M}_{\hat{\boldsymbol{n}}}$ denotes the spin-projection operator onto an arbitrary direction $\hat{\boldsymbol{n}}$ for an arbitrary half-integer spin J. It can be explicitly calculated as

$$\mathsf{P}^{J,M}_{\hat{\boldsymbol{n}}} = \prod_{m=-J}^{+J}{}' \ \frac{m-\boldsymbol{J}\cdot\hat{\boldsymbol{n}}}{m-M} \ , \tag{2.75}$$

where the prime indicates that the factor with $m = M$ is omitted. Here, $\boldsymbol{J} \equiv (J_1, J_2, J_3)$ stands for the generator of spin-J rotation. This expression provides a rotationally invariant polynomial of order $2J$ in $\boldsymbol{J}\cdot\hat{\boldsymbol{n}}$ that is a generalization to arbitrary spin of the usual $(1 \pm \boldsymbol{\sigma}\cdot\hat{\boldsymbol{n}})/2$ projectors for spin-1/2.

With the spin-projection operator defined above, the spin-transfer coefficient involving a Ξ baryon with an arbitrary spin J is now generalized to

$$\frac{d\sigma}{d\Omega}K_{ba} = \frac{1}{2}\,\mathrm{Tr}\left[\hat{M}\,\boldsymbol{\sigma}\cdot\hat{\boldsymbol{b}}\,\hat{M}^\dagger\,\Omega(\boldsymbol{J}\cdot\hat{\boldsymbol{a}})\right] \ , \tag{2.76}$$

where $\hat{\boldsymbol{b}}$ and $\hat{\boldsymbol{a}}$ are the spin directions. For $J = 1/2$, in view of $\Omega(\boldsymbol{J}\cdot\hat{\boldsymbol{a}}) \to \boldsymbol{\sigma}\cdot\hat{\boldsymbol{a}}$, this reduces to the familiar expression (2.6d), of course. For Cartesian directions $\hat{\boldsymbol{b}} = \hat{\boldsymbol{n}}_i$ and $\hat{\boldsymbol{a}} = \hat{\boldsymbol{n}}'_j$, in particular, Eq. (2.76) may be written as

$$\frac{d\sigma}{d\Omega}K_{ij'} = \mathrm{Tr}\left[\hat{\rho}^{\Xi,i}\Omega^J_{j'}\right], \tag{2.77}$$

where $\Omega^J_{j'} \equiv \Omega(\boldsymbol{J}\cdot\hat{\boldsymbol{n}}'_j)$.

For the Cartesian frame $\{\hat{\boldsymbol{n}}'_1, \hat{\boldsymbol{n}}'_2 \equiv \hat{\boldsymbol{n}}_2, \hat{\boldsymbol{n}}'_3 \equiv \hat{\boldsymbol{p}}'\}$ aligned with the momentum $\boldsymbol{p}'$ of the outgoing Ξ (see Fig. 2.1), explicit expressions for $\Omega^J_{j'}$ are found as

$$\Omega^{\frac{3}{2}}_{x'} = \begin{pmatrix} 0 & 0 & 0 & -1 \\ 0 & 0 & -1 & 0 \\ 0 & -1 & 0 & 0 \\ -1 & 0 & 0 & 0 \end{pmatrix}, \quad \Omega^{\frac{3}{2}}_{y'} = \begin{pmatrix} 0 & 0 & 0 & -i \\ 0 & 0 & i & 0 \\ 0 & -i & 0 & 0 \\ i & 0 & 0 & 0 \end{pmatrix}, \quad \Omega^{\frac{3}{2}}_{z'} = \begin{pmatrix} -1 & 0 & 0 & 0 \\ 0 & 1 & 0 & 0 \\ 0 & 0 & -1 & 0 \\ 0 & 0 & 0 & 1 \end{pmatrix}, \tag{2.78a}$$

which were derived with the help of the spin-3/2 generators in their spinor representation,

$$J_1 = \begin{pmatrix} 0 & \frac{\sqrt{3}}{2} & 0 & 0 \\ \frac{\sqrt{3}}{2} & 0 & 1 & 0 \\ 0 & 1 & 0 & \frac{\sqrt{3}}{2} \\ 0 & 0 & \frac{\sqrt{3}}{2} & 0 \end{pmatrix}, \quad J_2 = i\frac{\sqrt{3}}{2}\begin{pmatrix} 0 & -1 & 0 & 0 \\ 1 & 0 & \frac{-2}{\sqrt{3}} & 0 \\ 0 & \frac{2}{\sqrt{3}} & 0 & -1 \\ 0 & 0 & 1 & 0 \end{pmatrix}, \quad J_3 = \frac{1}{2}\begin{pmatrix} 3 & 0 & 0 & 0 \\ 0 & 1 & 0 & 0 \\ 0 & 0 & -1 & 0 \\ 0 & 0 & 0 & -3 \end{pmatrix}. \tag{2.79a}$$

For arbitrary spin of Ξ, K_{ba} of Eq. (2.76) becomes

$$K_{ba} = \frac{\Sigma^{\mathrm{even}}_{ba} - \Sigma^{\mathrm{odd}}_{ba}}{\Sigma^{\mathrm{even}}_{ba} + \Sigma^{\mathrm{odd}}_{ba}}, \tag{2.80}$$

where

$$\Sigma^{\mathrm{even/odd}}_{ba} = \sum_{m_a,m_b} \frac{d\sigma_{m_b,m_a}}{d\Omega}, \quad m_a - m_b = \text{even/odd}, \tag{2.81}$$

denotes the sum of all polarized differential cross sections such that the differences of all possible combinations of initial and final spin projections m_a and m_b along $\hat{\boldsymbol{a}}$ and $\hat{\boldsymbol{b}}$, respectively, are an

even or odd number.

2.4.3 Appendix C: Explicit form of the SDM's

In this section, we list the SDM elements of each ρ^i $(i = 0, \ldots, 3)$ in terms of the helicity amplitudes, $\mathcal{H}_i$. The Hermitian ρ^i matrices are arranged according to

$$\hat{\rho}^i = \begin{pmatrix} \rho^i_{J,J} & \rho^i_{J,J-1} & \cdots & \rho^i_{J,-J} \\ \rho^i_{J-1,J} & \rho^i_{J-1,J-1} & \cdots & \rho^i_{J-1,-J} \\ \vdots & \vdots & \ddots & \vdots \\ \rho^i_{-J,J} & \rho^i_{-J,J-1} & \cdots & \rho^i_{-J,-J} \end{pmatrix} . \tag{2.82}$$

For $J = \frac{1}{2}$, the matrices read explicitly

$$\hat{\rho}^0 = \frac{1}{2} \begin{pmatrix} |\mathcal{H}_1|^2 + |\mathcal{H}_2|^2 & 2i\pi_\Xi \operatorname{Im}[\mathcal{H}_2 \mathcal{H}_1^*] \\ -2i\pi_\Xi \operatorname{Im}[\mathcal{H}_2 \mathcal{H}_1^*] & |\mathcal{H}_1|^2 + |\mathcal{H}_2|^2 \end{pmatrix} , \tag{2.83a}$$

$$\hat{\rho}^1 = \frac{1}{2} \begin{pmatrix} 2\operatorname{Re}[\mathcal{H}_2 \mathcal{H}_1^*] & \pi_\Xi \left(|\mathcal{H}_1|^2 - |\mathcal{H}_2|^2 \right) \\ \pi_\Xi \left(|\mathcal{H}_1|^2 - |\mathcal{H}_2|^2 \right) & -2\operatorname{Re}[\mathcal{H}_2 \mathcal{H}_1^*] \end{pmatrix} , \tag{2.83b}$$

$$\hat{\rho}^2 = \frac{1}{2} \begin{pmatrix} -2\operatorname{Im}[\mathcal{H}_2 \mathcal{H}_1^*] & -i\pi_\Xi (|\mathcal{H}_1|^2 + |\mathcal{H}_2|^2) \\ i\pi_\Xi (|\mathcal{H}_1|^2 + |\mathcal{H}_2|^2) & -2\operatorname{Im}[\mathcal{H}_2 \mathcal{H}_1^*] \end{pmatrix} , \tag{2.83c}$$

$$\hat{\rho}^3 = \frac{1}{2} \begin{pmatrix} |\mathcal{H}_1|^2 - |\mathcal{H}_2|^2 & -2\pi_\Xi \operatorname{Re}[\mathcal{H}_2 \mathcal{H}_1^*] \\ -2\pi_\Xi \operatorname{Re}[\mathcal{H}_2 \mathcal{H}_1^*] & -|\mathcal{H}_1|^2 + |\mathcal{H}_2|^2 \end{pmatrix} , \tag{2.83d}$$

where π_Ξ is the parity of the Ξ.

For a $J = \frac{3}{2}$ resonance,

$$\hat{\rho}^0 = \frac{1}{2}\begin{pmatrix} |\mathcal{H}_2|^2 + |\mathcal{H}_1|^2 & \mathcal{H}_2\mathcal{H}_4{}^* + \mathcal{H}_1\mathcal{H}_3{}^* & \pi_\Xi\left(\mathcal{H}_1\mathcal{H}_4{}^* - \mathcal{H}_2\mathcal{H}_3{}^*\right) & 2i\pi_\Xi \operatorname{Im}\left[\mathcal{H}_2\mathcal{H}_1{}^*\right] \\ \mathcal{H}_4\mathcal{H}_2{}^* + \mathcal{H}_3\mathcal{H}_1{}^* & |\mathcal{H}_4|^2 + |\mathcal{H}_3|^2 & 2i\pi_\Xi \operatorname{Im}\left[\mathcal{H}_3\mathcal{H}_4{}^*\right] & \pi_\Xi\left(-\mathcal{H}_3\mathcal{H}_2{}^* + \mathcal{H}_4\mathcal{H}_1{}^*\right) \\ \pi_\Xi\left(\mathcal{H}_4\mathcal{H}_1{}^* - \mathcal{H}_3\mathcal{H}_2{}^*\right) & -2i\pi_\Xi \operatorname{Im}\left[\mathcal{H}_3\mathcal{H}_4{}^*\right] & |\mathcal{H}_4|^2 + |\mathcal{H}_3|^2 & -\mathcal{H}_4\mathcal{H}_2{}^* - \mathcal{H}_3\mathcal{H}_1{}^* \\ -2i\pi_\Xi \operatorname{Im}\left[\mathcal{H}_2\mathcal{H}_1{}^*\right] & \pi_\Xi\left(-\mathcal{H}_2\mathcal{H}_3{}^* + \mathcal{H}_1\mathcal{H}_4{}^*\right) & -\mathcal{H}_2\mathcal{H}_4{}^* - \mathcal{H}_1\mathcal{H}_3{}^* & |\mathcal{H}_2|^2 + |\mathcal{H}_1|^2 \end{pmatrix}, \tag{2.84a}$$

$$\hat{\rho}^1 = \frac{1}{2}\begin{pmatrix} 2\operatorname{Re}\left[\mathcal{H}_2\mathcal{H}_1{}^*\right] & \mathcal{H}_1\mathcal{H}_4{}^* + \mathcal{H}_2\mathcal{H}_3{}^* & \pi_\Xi\left(\mathcal{H}_2\mathcal{H}_4{}^* - \mathcal{H}_1\mathcal{H}_3{}^*\right) & \pi_\Xi\left(-|\mathcal{H}_2|^2 + |\mathcal{H}_1|^2\right) \\ \mathcal{H}_4\mathcal{H}_1{}^* + \mathcal{H}_3\mathcal{H}_2{}^* & 2\operatorname{Re}\left[\mathcal{H}_4\mathcal{H}_3{}^*\right] & \pi_\Xi\left(|\mathcal{H}_4|^2 - |\mathcal{H}_3|^2\right) & \pi_\Xi\left(-\mathcal{H}_4\mathcal{H}_2{}^* + \mathcal{H}_3\mathcal{H}_1{}^*\right) \\ \pi_\Xi\left(\mathcal{H}_4\mathcal{H}_2{}^* - \mathcal{H}_3\mathcal{H}_1{}^*\right) & \pi_\Xi\left(|\mathcal{H}_4|^2 - |\mathcal{H}_3|^2\right) & -2\operatorname{Re}\left[\mathcal{H}_4\mathcal{H}_3{}^*\right] & \mathcal{H}_3\mathcal{H}_2{}^* + \mathcal{H}_4\mathcal{H}_1{}^* \\ \pi_\Xi\left(-|\mathcal{H}_2|^2 + |\mathcal{H}_1|^2\right) & \pi_\Xi\left(-\mathcal{H}_2\mathcal{H}_4{}^* + \mathcal{H}_1\mathcal{H}_3{}^*\right) & \mathcal{H}_2\mathcal{H}_3{}^* + \mathcal{H}_1\mathcal{H}_4{}^* & -2\operatorname{Re}\left[\mathcal{H}_2\mathcal{H}_1{}^*\right] \end{pmatrix}, \tag{2.84b}$$

$$\hat{\rho}^2 = \frac{1}{2}\begin{pmatrix} 2\operatorname{Im}\left[\mathcal{H}_1\mathcal{H}_2{}^*\right] & i\left(-\mathcal{H}_1\mathcal{H}_4{}^* + \mathcal{H}_2\mathcal{H}_3{}^*\right) & i\pi_\Xi\left(\mathcal{H}_2\mathcal{H}_4{}^* + \mathcal{H}_1\mathcal{H}_3{}^*\right) & -i\pi_\Xi\left(|\mathcal{H}_2|^2 + |\mathcal{H}_1|^2\right) \\ i\left(\mathcal{H}_4\mathcal{H}_1{}^* - \mathcal{H}_3\mathcal{H}_2{}^*\right) & 2\operatorname{Im}\left[\mathcal{H}_3\mathcal{H}_4{}^*\right] & i\pi_\Xi\left(|\mathcal{H}_4|^2 + |\mathcal{H}_3|^2\right) & -i\pi_\Xi\left(\mathcal{H}_4\mathcal{H}_2{}^* + \mathcal{H}_3\mathcal{H}_1{}^*\right) \\ -i\pi_\Xi\left(\mathcal{H}_4\mathcal{H}_2{}^* + \mathcal{H}_3\mathcal{H}_1{}^*\right) & -i\pi_\Xi\left(|\mathcal{H}_4|^2 + |\mathcal{H}_3|^2\right) & 2\operatorname{Im}\left[\mathcal{H}_3\mathcal{H}_4{}^*\right] & i\left(\mathcal{H}_3\mathcal{H}_2{}^* - \mathcal{H}_4\mathcal{H}_1{}^*\right) \\ i\pi_\Xi\left(|\mathcal{H}_2|^2 + |\mathcal{H}_1|^2\right) & i\pi_\Xi\left(\mathcal{H}_2\mathcal{H}_4{}^* + \mathcal{H}_1\mathcal{H}_3{}^*\right) & i\left(-\mathcal{H}_2\mathcal{H}_3{}^* + \mathcal{H}_1\mathcal{H}_4{}^*\right) & 2\operatorname{Im}\left[\mathcal{H}_1\mathcal{H}_2{}^*\right] \end{pmatrix}, \tag{2.84c}$$

$$\hat{\rho}^3 = \frac{1}{2}\begin{pmatrix} -|\mathcal{H}_2|^2 + |\mathcal{H}_1|^2 & -\mathcal{H}_2\mathcal{H}_4{}^* + \mathcal{H}_1\mathcal{H}_3{}^* & \pi_\Xi\left(\mathcal{H}_1\mathcal{H}_4{}^* + \mathcal{H}_2\mathcal{H}_3{}^*\right) & -2\pi_\Xi \operatorname{Re}\left[\mathcal{H}_2\mathcal{H}_1{}^*\right] \\ -\mathcal{H}_4\mathcal{H}_2{}^* + \mathcal{H}_3\mathcal{H}_1{}^* & -|\mathcal{H}_4|^2 + |\mathcal{H}_3|^2 & 2\pi_\Xi \operatorname{Re}\left[\mathcal{H}_4\mathcal{H}_3{}^*\right] & \pi_\Xi\left(-\mathcal{H}_3\mathcal{H}_2{}^* - \mathcal{H}_4\mathcal{H}_1{}^*\right) \\ \pi_\Xi\left(\mathcal{H}_4\mathcal{H}_1{}^* + \mathcal{H}_3\mathcal{H}_2{}^*\right) & 2\pi_\Xi \operatorname{Re}\left[\mathcal{H}_4\mathcal{H}_3{}^*\right] & |\mathcal{H}_4|^2 - |\mathcal{H}_3|^2 & -\mathcal{H}_4\mathcal{H}_2{}^* + \mathcal{H}_3\mathcal{H}_1{}^* \\ -2\pi_\Xi \operatorname{Re}\left[\mathcal{H}_2\mathcal{H}_1{}^*\right] & \pi_\Xi\left(-\mathcal{H}_2\mathcal{H}_3{}^* - \mathcal{H}_1\mathcal{H}_4{}^*\right) & -\mathcal{H}_2\mathcal{H}_4{}^* + \mathcal{H}_1\mathcal{H}_3{}^* & |\mathcal{H}_2|^2 - |\mathcal{H}_1|^2 \end{pmatrix}. \tag{2.84d}$$

2.4.4 Appendix D: Measuring the SDM Elements

In Sec. 2.1.3, we identified a set of SDM elements that determines the reaction amplitude completely. A standard way of measuring the SDM elements is via the subsequent decay of the produced particle in a primary reaction by exploiting the self-analyzing property of the decay-product particle.

In the present work, the reaction in Eq. (2.1) is the primary (or production) reaction, where the Ξ baryon is produced. If the produced Ξ is a ground state Ξ, then, it decays via a single weak decay process into

$$\Xi \to \Lambda + \pi, \tag{2.85}$$

whose associated Ξ decay-asymmetry parameters, α_{Ξ}, are known to be [46]

$$\alpha_{\Xi^0} = -0.406 \pm 0.013 \ , \tag{2.86a}$$

$$\alpha_{\Xi^-} = -0.458 \pm 0.012 \ . \tag{2.86b}$$

An excited Ξ resonance, Ξ^*, on the other hand, may undergo a double-decay process

$$\begin{array}{lll} \Xi^* \to \Xi + \pi & \text{or} & \Xi^* \to \Lambda + \bar{K} \\ \quad \hookrightarrow \Lambda + \pi \ , & & \quad \hookrightarrow N + \pi \ . \end{array} \tag{2.87a}$$

The associated Λ decay-asymmetry parameter for the second-step process $\Lambda \to N + \pi$ is [46]

$$\begin{aligned} \alpha_{\Lambda-} &= +0.642 \pm 0.013 \qquad (\Lambda^0 \to p + \pi^-) \ , \\ \alpha_{\Lambda 0} &= +0.650 \pm 0.015 \qquad (\Lambda^0 \to n + \pi^0) \ . \end{aligned} \tag{2.88}$$

The Ξ production process (2.1) is described in the CM frame of the reaction. The Ξ decay processes of Eqs. (2.85) and (2.87), on the other hand, are described in the rest frame of the produced Ξ, whose right-handed Cartesian coordinate system $\{\hat{\boldsymbol{n}}'_1, \hat{\boldsymbol{n}}'_2 \equiv \hat{\boldsymbol{n}}_2, \hat{\boldsymbol{n}}'_3 \equiv \hat{\boldsymbol{p}}'\}$ is fully specified in Fig. 2.1.

In the double-decay processes (2.87), the subsequent Λ decay process is described in the rest

frame of the decaying Λ denoted by $\{\hat{\boldsymbol{n}}_1'', \hat{\boldsymbol{n}}_2'', \hat{\boldsymbol{n}}_3''\}$, with $\hat{\boldsymbol{n}}_3'' \equiv \hat{\boldsymbol{p}}_\Lambda$, where $\boldsymbol{p}_\Lambda$ describes the direction of the Λ's momentum in the $\{\hat{\boldsymbol{n}}_1', \hat{\boldsymbol{n}}_2', \hat{\boldsymbol{n}}_3'\}$ frame (see Fig. 2.1); the other two axes are given by $\hat{\boldsymbol{n}}_2'' = (\hat{\boldsymbol{n}}_3' \times \hat{\boldsymbol{p}}_\Lambda)/|\hat{\boldsymbol{n}}_3' \times \hat{\boldsymbol{p}}_\Lambda|$ and $\hat{\boldsymbol{n}}_1'' = \hat{\boldsymbol{n}}_2'' \times \hat{\boldsymbol{n}}_3''$.

Single-decay process: Ground state Ξ

The ground-state Ξ decays weakly almost entirely into $\Lambda + \pi$. We define the amplitude describing the Ξ production process $\bar{K} + N \to K + \Xi$, followed by the subsequent weak decay of the produced Ξ, $\Xi \to \Lambda + \pi$, as [91, 92]

$$\begin{aligned} A &\equiv A(\Omega_\Xi, \Omega_\Lambda, \lambda_\Xi, \lambda_\Lambda, \lambda_N) \\ &= \langle \Omega_\Lambda, \lambda_\Lambda | \, \hat{M}_D \, | \lambda_\Xi \rangle \, \langle \Omega_\Xi, \lambda_\Xi | \, \hat{M} \, | \lambda_N \rangle \end{aligned} \tag{2.89}$$

with $\langle \Omega_\Xi, \lambda_\Xi | \, \hat{M} \, | \lambda_N \rangle$ denoting the production reaction amplitude (in the corresponding CM frame) and

$$\langle \Omega_\Lambda, \lambda_\Lambda | \, \hat{M}_D \, | \lambda_\Xi \rangle \equiv \sqrt{\frac{2J+1}{4\pi}} F^\Xi_{\lambda_\Lambda} D^{J*}_{\lambda_\Xi, \lambda_\Lambda}(\Omega_\Lambda), \tag{2.90}$$

denoting the subsequent Ξ decay amplitude (in the rest frame of Ξ). Here, Ω_Ξ and Ω_Λ are shorthand notations, respectively, for the polar and azimuthal angles of the produced Ξ in the CM frame of the production, $\Omega_\Xi = (\theta, \phi = 0)$, and for the polar and azimuthal angles of the Λ in the rest frame of the produced Ξ, $\Omega_\Lambda = (\theta_\Lambda, \phi_\Lambda)$. $\lambda_\Xi(\lambda_\Lambda)$ is the helicity of the $\Xi(\Lambda)$ in the respective frame, while J denotes the spin of the decaying Ξ. $F^\Xi_{\lambda_\Lambda}$ stands for the helicity Ξ-decay amplitude and $D^J_{\lambda_\Xi, \lambda_\Lambda}(\Omega_\Lambda)$ is the usual Wigner rotation matrix. Here, the argument Ω_Λ in $D^J_{\lambda_\Xi, \lambda_\Lambda}(\Omega_\Lambda)$ is to be understood as the set of Euler angles $\{\alpha, \beta, \gamma\}$, such that, $D^J_{\lambda_\Xi, \lambda_\Lambda}(\Omega_\Lambda) \equiv D^J_{\lambda_\Xi, \lambda_\Lambda}(\alpha = \phi_\Lambda, \beta = \theta_\Lambda, \gamma = 0)$ in the conventions defined in Ref. [110].

The angular distribution of the Λ hyperon, $I(\Omega_\Lambda)$, in the $\Xi \to \Lambda + \pi$ decay (for fixed Ξ angle Ω_Ξ) is given by

$$I(\Omega_\Lambda) = \sum_{i=0}^{3} P_i \, I^i(\Omega_\Lambda) \ , \tag{2.91}$$

where

$$
\begin{aligned}
I^i(\Omega_\Lambda) &\equiv \sum_{\text{all } \lambda' \text{s}} A(\Omega_\Xi, \Omega_\Lambda, \lambda_\Xi, \lambda_\Lambda, \lambda_N)\, \rho^{N,i}_{\lambda_N, \lambda'_N} A^*(\Omega_\Xi, \Omega_\Lambda, \lambda'_\Xi, \lambda_\Lambda, \lambda'_N) \\
&= \frac{(2J+1)}{4\pi} \sum_{\text{all } \lambda' \text{s}} F^\Xi_{\lambda_\Lambda} F^{\Xi *}_{\lambda_\Lambda}\, M_{\lambda_\Xi, \lambda_N}\, \rho^{N,i}_{\lambda_N, \lambda'_N}\, M^*_{\lambda'_\Xi, \lambda'_N} D^{J*}_{\lambda_\Xi, \lambda_\Lambda}(\Omega_\Lambda) D^J_{\lambda'_\Xi, \lambda'_\Lambda}(\Omega_\Lambda) \\
&= \frac{(2J+1)}{4\pi} \sum_{\text{all } \lambda' \text{s}} F^\Xi_{\lambda_\Lambda} F^{\Xi *}_{\lambda_\Lambda}\, \rho^{\Xi,i}_{\lambda_\Xi, \lambda'_\Xi}\, D^{J*}_{\lambda_\Xi, \lambda_\Lambda}(\Omega_\Lambda) D^J_{\lambda'_\Xi, \lambda'_\Lambda}(\Omega_\Lambda),
\end{aligned}
\tag{2.92}
$$

Here, $\rho^{N,i}_{\lambda_N, \lambda'_N} = \langle \lambda_N | \hat{\rho}^{N,i} | \lambda'_N \rangle$ denotes the target nucleon SDM element with $\hat{\rho}^{N,i}$ given by Eq. (2.66), and Eq. (2.70) was used in the last step. Also, we note that the explicit reference to the Ω_Ξ dependence of the angular distribution I^i in Eqs. (2.91) and (2.92) has been suppressed for the sake of simplicity of notation. The same holds for the angular distribution in Eqs. (2.103) and (3.46) in the next subsection.

We now define the moments, $H^i(L, M)$, of this distribution as

$$
\begin{aligned}
H^i(L, M) &\equiv \int d\Omega_\Lambda\, I^i(\Omega_\Lambda) D^L_{M,0}(\Omega_\Lambda) \\
&= t^{J,i}_{LM} \sum_{\lambda_\Lambda} F^\Xi_{\lambda_\Lambda} F^{\Xi *}_{\lambda_\Lambda} \langle J\, \lambda_\Lambda\, L\, 0 | J\, \lambda_\Lambda \rangle\,,
\end{aligned}
\tag{2.93}
$$

where $d\Omega_\Lambda \equiv \sin\theta_\Lambda\, d\theta_\Lambda\, d\phi_\Lambda$. The quantity $t^{J,i}_{LM}$ here is related to the SDM elements of the Ξ by [91]

$$
t^{J,i}_{LM} \equiv \sum_{\lambda_\Xi, \lambda'_\Xi} \rho^{\Xi,i}_{\lambda_\Xi, \lambda'_\Xi} \langle J\, \lambda'_\Xi\, L\, M | J\, \lambda_\Xi \rangle\ , \tag{2.94}
$$

whose inversion produces

$$
\rho^{\Xi,i}_{\lambda_\Xi, \lambda'_\Xi} = \sum_L \frac{2L+1}{2J+1} \langle J\, \lambda'_\Xi\, L\, M | J\, \lambda_\Xi \rangle\, t^{J,i}_{LM}\ , \tag{2.95}
$$

where $M = \lambda_\Xi - \lambda'_\Xi$.

Introducing further the quantities

$$
g^\Xi_\pm \equiv F^\Xi_{\pm\frac{1}{2}} F^{\Xi *}_{\pm\frac{1}{2}}\ , \tag{2.96}
$$

we can re-express the moments in Eq. (2.93) as

$$H^i(L,M) = t^{J,i}_{LM}\ \langle J\,\tfrac{1}{2}\,L\,0|J\,\tfrac{1}{2}\rangle\,\left[g^{\Xi}_{+} + (-1)^L g^{\Xi}_{-}\right]\ . \tag{2.97}$$

We note that $g^{\Xi}_{\pm}$ introduced in Eq. (2.96) are related to the Ξ decay-asymmetry parameter, α_{Ξ}, given in Eq. (2.86) by [111, 112]

$$\frac{g^{\Xi}_{+} - g^{\Xi}_{-}}{g^{\Xi}_{+} + g^{\Xi}_{-}} = \alpha_{\Xi}\ . \tag{2.98}$$

Then, taking the ratio of the moments $H^i(L,M)$ $(i = 1,2,3)$ and $H^0(0,0)$, we obtain

$$\frac{H^i(L,M)}{H^0(0,0)} = \zeta_L\,\frac{t^{J,i}_{LM}}{t^{J,0}_{00}}\,\langle J\,\tfrac{1}{2}\,L\,0|J\,\tfrac{1}{2}\rangle\ , \tag{2.99}$$

where $\zeta_L = 1$ for even L and $\zeta_L = \alpha_{\Xi}$ for odd L.

Now, from Eq. (2.94) and the definition of $\hat{\rho}^{\Xi,0}$ in Eq. (2.72), we get

$$t^{J,0}_{00} = \mathrm{Tr}\left[\hat{\rho}^{\Xi,0}\right] = \frac{d\sigma}{d\Omega}\ . \tag{2.100}$$

One can now use Eq. (2.99) to extract $t^{J,i}_{LM}$. Once $t^{J,i}_{LM}$ is known, the SDM elements $\rho^{\Xi,i}_{\lambda_\Xi,\lambda'_\Xi}$ are obtained by making use of Eq. (2.95). Note that the non-vanishing moments $H^i(LM)$ are restricted to $L \le 2J$ and $|M| \le L$.

Double-decay process: Excited Ξ resonance

The double-decay processes shown in Eq. (2.87) are treated analogously to the single-decay process of the previous subsection. Here, we discuss the decay chain with the subsequent decay of the Λ hyperon, $\Lambda \to p + \pi^-$, but the results apply to any decay chain that is a strong decay followed by a weak decay and containing a single pseudoscalar meson at each step of the decay.

As for the single-decay process case discussed in the previous subsection, we begin by defining the amplitude describing the Ξ^* production process $\bar{K} + N \to K + \Xi^*$, followed by the strong decay

of the produced Ξ^*, $\Xi^* \to \Lambda + K$, and the subsequent weak decay of Λ, $\Lambda \to N + \pi$, as [91, 92]

$$\begin{aligned} A &\equiv A(\Omega_\Xi, \Omega_\Lambda, \Omega_p, \lambda_N, \lambda_\Xi, \lambda_\Lambda, \lambda_p) \\ &= \langle \Omega_p, \lambda_p | \hat{M}'_D | \lambda_\Lambda \rangle \, \langle \Omega_\Lambda, \lambda_\Lambda | \hat{M}_D | \lambda_\Xi \rangle \, \langle \Omega_\Xi, \lambda_\Xi | \hat{M} | \lambda_N \rangle \ , \end{aligned} \tag{2.101}$$

where $\langle \Omega_\Xi, \lambda_\Xi | \, \hat{M} \, | \lambda_N \rangle$ stands for the Ξ^* production amplitude and

$$\langle \Omega_\Lambda, \lambda_\Lambda | \, \hat{M}_D \, | \lambda_\Xi \rangle \equiv \sqrt{\frac{2J+1}{4\pi}} \, F^\Xi_{\lambda_\Lambda} D^{J*}_{\lambda_\Xi, \lambda_\Lambda}(\Omega_\Lambda) \ , \tag{2.102a}$$

$$\langle \Omega_p, \lambda_p | \, \hat{M}'_D \, | \lambda_\Lambda \rangle \equiv \sqrt{\frac{2}{4\pi}} \, F^\Lambda_{\lambda_p} D^{\frac{1}{2}*}_{\lambda_\Lambda, \lambda_p}(\Omega_p) \ , \tag{2.102b}$$

denote the subsequent Ξ^* strong-decay and Λ weak-decay amplitudes, respectively. We note that the Ξ production and decay amplitudes are calculated in the CM frame of the production reaction and the rest frame of the produced Ξ, respectively, exactly in the same way as for the single-decay case discussed in the previous subsection. The subsequent Λ-decay amplitude, $\langle \Omega_p, \lambda_p | \, \hat{M}'_D \, | \lambda_\Lambda \rangle$, is calculated in the rest frame of the decaying Λ denoted by $\{\hat{\boldsymbol{n}}''_1, \hat{\boldsymbol{n}}''_2, \hat{\boldsymbol{n}}''_3\}$ [cf. the second paragraph just below Eq. (2.88)], where $\Omega_p = (\theta_p, \phi_p)$ is a short-hand notation for the polar and azimuthal angles θ_p and ϕ_p, respectively, of the decay-product proton measured in the Λ rest frame.

The angular distribution of the entire double decay process (for fixed Ξ production angle Ω_Ξ) is given as

$$I(\Omega_\Lambda, \Omega_p) = \sum_{i=0}^{3} P_i I^i(\Omega_\Lambda, \Omega_p) \ , \tag{2.103}$$

where

$$\begin{aligned} I^i\,(\Omega_\Lambda, \Omega_p) &\equiv \sum_{\text{all } \lambda' \text{s}} A(\Omega_\Xi, \Omega_\Lambda, \Omega_p, \lambda_N, \Lambda_\Xi, \lambda_\Lambda, \lambda_p) \, \rho^{N,i}_{\lambda_N, \lambda'_N} A^*(\Omega_\Xi, \Omega_\Lambda, \Omega_p, \lambda'_N, \lambda'_\Xi, \lambda'_\Lambda, \lambda_p) \\ &= \frac{2(2J+1)}{16\pi^2} \sum_{\text{all } \lambda' \text{s}} \rho^{\Xi,i}_{\lambda_\Xi, \lambda'_\Xi} \, g^\Lambda_{\lambda_p} \, g^\Xi_{\lambda_\Lambda, \lambda'_\Lambda} D^{\frac{1}{2}*}_{\lambda_\Lambda, \lambda_p}(\Omega_p) D^{\frac{1}{2}}_{\lambda'_\Lambda, \lambda_p}(\Omega_p) D^{\mathrm{J}*}_{\lambda_\Xi, \lambda_\Lambda}(\Omega_\Lambda) D^{\mathrm{J}}_{\lambda'_\Xi, \lambda'_\Lambda}(\Omega_\Lambda) \ , \end{aligned} \tag{2.104}$$

with

$$g^\Lambda_{\lambda_p} \equiv F^\Lambda_{\lambda_p} \, F^{\Lambda*}_{\lambda_p} \quad \text{and} \quad g^\Xi_{\lambda_\Lambda, \lambda'_\Lambda} \equiv F^\Xi_{\lambda_\Lambda} \, F^{\Xi*}_{\lambda'_\Lambda} \ . \tag{2.105}$$

To arrive at the last equality in Eq. (3.46), we have made use of Eq. (2.70).

We now define the moments $H^i(l,m,L,M)$ as

$$H^i(l,m,L,M) \equiv \int d\Omega_\Lambda d\Omega_p I^i(\Omega_\Lambda,\Omega_p)\, D^L_{M,m}(\Omega_\Lambda) D^l_{m,0}(\Omega_p)$$
$$= t^{\mathrm{J},i}_{LM} \sum_{\lambda_\Lambda,\lambda'_\Lambda} g^\Xi_{\lambda_\Lambda,\lambda'_\Lambda} \langle J\,\lambda'_\Lambda\, L\, m|J\,\lambda_\Lambda\rangle \langle \tfrac{1}{2}\,\lambda'_\Lambda\, l\, m|\tfrac{1}{2}\,\lambda_\Lambda\rangle \sum_{\lambda_p} g^\Lambda_{\lambda_p} \langle \tfrac{1}{2}\,\lambda_p\, l\, 0|\tfrac{1}{2}\,\lambda_p\rangle \ , \quad (2.106)$$

with $t^{J,i}_{LM}$ given by Eq. (2.94).

The different $g^\Xi_{\lambda_\Lambda,\lambda'_\Lambda}$ are related to each other by

$$g^\Xi_{--} = g^\Xi_{++} \ , \quad (2.107a)$$
$$g^\Xi_{+-} = g^\Xi_{-+} = \pi_\Xi\,(-1)^{J+\frac{1}{2}}\, g^\Xi_{++} \ . \quad (2.107b)$$

The $g^\Lambda_{\lambda_p}$ terms can be related to the Λ decay asymmetry parameter, α_Λ, by [111, 112]

$$\frac{g^\Lambda_+ - g^\Lambda_-}{g^\Lambda_+ + g^\Lambda_-} = \alpha_\Lambda \ . \quad (2.108)$$

Note that the non-vanishing moments $H^i(l,m,L,M)$ are restricted to $|m| \le l$, $l \le 1$, $|M| \le L$ and $L \le 2J$, as can be read off from Eq. (2.106). The moments $H^i(0,0,L,M)$ and $H^i(1,m,L,M)$ vanish identically for odd and even L, respectively, due to Eqs. (2.106) and (2.107). Analogously to the single-decay case, the ratios of the moments

$$\frac{H^i(0,0,L,M)}{H^0(0,0,0,0)} = \frac{t^{J,i}_{LM}}{t^{J,0}_{00}}\ \langle J\,\tfrac{1}{2}\,L\,0|J\,\tfrac{1}{2}\rangle \quad (2.109a)$$

for even L and

$$\frac{H^i(1,0,L,M)}{H^0(0,0,0,0)} = \frac{\alpha_\Lambda}{3}\,\frac{t^{J,i}_{LM}}{t^{J,0}_{00}}\ \langle J\,\tfrac{1}{2}\,L\,0|J\,\tfrac{1}{2}\rangle \quad (2.109b)$$

for odd L allow us to determine $t^{J,i}_{LM}$. Since $t^{J,0}_{00} = d\sigma/d\Omega$, once $t^{J,i}_{LM}$ is extracted, the SDM elements $\rho^{\Xi,i}_{\lambda_\Xi,\lambda'_\Xi}$ can be determined via Eq. (2.95).

2.4.5 Appendix E: Lagrangians, Propagators

In this Appendix, we give the effective Lagrangians and phenomenological dressed baryon propagators from which the s- and u-channel amplitudes M_s and M_u discussed in Sec. 2.2.1 are constructed. We follow Refs. [53, 54, 113–115] and consider not only the spin-1/2 ground state Λ and Σ but also their respective excited states with spin up to 7/2. In the following we use the notations for the iso-doublet fields

$$N = \begin{pmatrix} p \\ n \end{pmatrix}, \qquad \Xi = \begin{pmatrix} \Xi^0 \\ -\Xi^- \end{pmatrix}, \qquad K = \begin{pmatrix} K^+ \\ K^0 \end{pmatrix}, \qquad K_c = \begin{pmatrix} \bar{K}^0 \\ -K^- \end{pmatrix}, \tag{2.110}$$

and for the iso-triplet fields

$$\mathbf{\Sigma} = \begin{pmatrix} \Sigma^+ \\ \Sigma^0 \\ \Sigma^- \end{pmatrix}. \tag{2.111}$$

We also introduce the auxiliary operators in Dirac space

$$D^{1/2(\pm)}_{B'BM} \equiv -\Gamma^{(\pm)} \left[\pm i\lambda + \frac{1-\lambda}{m_{B'} \pm m_B} \not{\partial} \right], \tag{2.112a}$$

$$D^{3/2(\pm)}_{\nu} \equiv \Gamma^{(\mp)} \partial_\nu \,, \tag{2.112b}$$

$$D^{5/2(\pm)}_{\mu\nu} \equiv -i\Gamma^{(\pm)} \partial_\mu \partial_\nu \,, \tag{2.112c}$$

$$D^{7/2(\pm)}_{\mu\nu\rho} \equiv -\Gamma^{(\mp)} \partial_\mu \partial_\nu \partial_\rho \,, \tag{2.112d}$$

where $\Gamma^{(+)} \equiv \gamma_5$ and $\Gamma^{(-)} \equiv 1$. Here, m_B stands for the mass of the baryon B. The parameter λ has been introduced to interpolate between the pseudovector ($\lambda = 0$) and the pseudoscalar ($\lambda = 1$) couplings. Note that in the above equation the order of the subscript indices in $D^{1/2(\pm)}_{B'BM}$ is important, i.e., $D^{1/2(\pm)}_{B'BM} \neq D^{1/2(\pm)}_{BB'M}$.

The effective Lagrangians for spin-1/2 hyperons Λ and Σ (or their resonances) are, then, given

by

$$\mathcal{L}^{1/2(\pm)}_{\Lambda NK} = g_{\Lambda NK}\,\bar{\Lambda}\left\{D^{1/2(\pm)}_{\Lambda NK}\bar{K}\right\}N + \text{H.c.}\,, \tag{2.113a}$$

$$\mathcal{L}^{1/2(\pm)}_{\Sigma NK} = g_{\Sigma NK}\,\bar{\boldsymbol{\Sigma}}\cdot\left\{D^{1/2(\pm)}_{\Sigma NK}\bar{K}\right\}\boldsymbol{\tau}N + \text{H.c.}\,, \tag{2.113b}$$

$$\mathcal{L}^{1/2(\pm)}_{\Xi\Lambda K_c} = g_{\Xi\Lambda K_c}\,\bar{\Xi}\left\{D^{1/2(\pm)}_{\Xi\Lambda K}K_c\right\}\Lambda + \text{H.c.}\,, \tag{2.113c}$$

$$\mathcal{L}^{1/2(\pm)}_{\Xi\Sigma K_c} = g_{\Xi\Sigma K_c}\,\bar{\Xi}\boldsymbol{\tau}\left\{D^{1/2(\pm)}_{\Xi\Sigma K}K_c\right\}\cdot\boldsymbol{\Sigma} + \text{H.c.}\,, \tag{2.113d}$$

where the superscripts $\pm$ refer to the positive $(+)$ and negative $(-)$ relative parity of the baryons. Flavor SU(3) symmetry relates the coupling constants among the members of the octet $J^P = 1/2^+$ ground state baryons and $J^P = 0^-$ pseudoscalar mesons and we have

$$g_{\Lambda NK} = -g_8\frac{1+2\alpha}{\sqrt{3}}\,, \tag{2.114a}$$

$$g_{\Sigma NK} = g_8(1-2\alpha)\,, \tag{2.114b}$$

$$g_{\Xi\Lambda K_c} = -g_8\frac{1-4\alpha}{\sqrt{3}}\,, \tag{2.114c}$$

$$g_{\Xi\Sigma K_c} = -g_8\,, \tag{2.114d}$$

where $g_8 = g_{NN\pi} = 13.45$ empirically and the D/F mixing parameter $\alpha = 2/5$ from SU(6) considerations.

For spin-3/2 hyperons, we have

$$\mathcal{L}^{3/2(\pm)}_{\Lambda NK} = \frac{g_{\Lambda NK}}{m_K}\,\bar{\Lambda}^{\nu}\left\{D^{3/2(\pm)}_{\nu}\bar{K}\right\}N + \text{H.c.}\,, \tag{2.115a}$$

$$\mathcal{L}^{3/2(\pm)}_{\Sigma NK} = \frac{g_{\Sigma NK}}{m_K}\,\bar{\boldsymbol{\Sigma}}^{\nu}\cdot\left\{D^{3/2(\pm)}_{\nu}\bar{K}\right\}\boldsymbol{\tau}N + \text{H.c.}\,, \tag{2.115b}$$

$$\mathcal{L}^{3/2(\pm)}_{\Xi\Lambda K_c} = \frac{g_{\Xi\Lambda K_c}}{m_K}\,\bar{\Xi}\left\{D^{3/2(\pm)}_{\nu}K_c\right\}\Lambda^{\nu} + \text{H.c.}\,, \tag{2.115c}$$

$$\mathcal{L}^{3/2(\pm)}_{\Xi\Sigma K_c} = \frac{g_{\Xi\Sigma K_c}}{m_K}\,\bar{\Xi}\boldsymbol{\tau}\left\{D^{3/2(\pm)}_{\nu}K_c\right\}\cdot\boldsymbol{\Sigma}^{\nu} + \text{H.c.}\,, \tag{2.115d}$$

where m_K denotes the kaon mass. For spin-5/2 hyperons [54, 116],

$$\mathcal{L}^{5/2(\pm)}_{\Lambda NK} = \frac{g_{\Lambda NK}}{m_K^2}\,\bar{\Lambda}^{\mu\nu}\left\{D^{5/2(\pm)}_{\mu\nu}\bar{K}\right\}N + \text{H.c.}\,, \tag{2.116a}$$

$$\mathcal{L}^{5/2(\pm)}_{\Sigma NK} = \frac{g_{\Sigma NK}}{m_K^2}\,\bar{\boldsymbol{\Sigma}}^{\mu\nu}\cdot\left\{D^{5/2(\pm)}_{\mu\nu}\bar{K}\right\}\boldsymbol{\tau}N + \text{H.c.}\,, \tag{2.116b}$$

$$\mathcal{L}^{5/2(\pm)}_{\Xi\Lambda K_c} = \frac{g_{\Xi\Lambda K_c}}{m_K^2}\,\bar{\Xi}\left\{D^{5/2(\pm)}_{\mu\nu}K_c\right\}\Lambda^{\mu\nu} + \text{H.c.}\,, \tag{2.116c}$$

$$\mathcal{L}^{5/2(\pm)}_{\Xi\Sigma K_c} = \frac{g_{\Xi\Sigma K_c}}{m_K^2}\,\bar{\Xi}\boldsymbol{\tau}\left\{D^{5/2(\pm)}_{\mu\nu}K_c\right\}\cdot\boldsymbol{\Sigma}^{\mu\nu} + \text{H.c.}\,. \tag{2.116d}$$

And for spin-7/2 hyperons we have [54, 116]

$$\mathcal{L}^{7/2(\pm)}_{\Lambda NK} = \frac{g_{\Lambda NK}}{m_K^3}\,\bar{\Lambda}^{\mu\nu\rho}\left\{D^{7/2(\pm)}_{\mu\nu\rho}\bar{K}\right\}N + \text{H.c.}\,, \tag{2.117a}$$

$$\mathcal{L}^{7/2(\pm)}_{\Sigma NK} = \frac{g_{\Sigma NK}}{m_K^3}\,\bar{\boldsymbol{\Sigma}}^{\mu\nu\rho}\cdot\left\{D^{7/2(\pm)}_{\mu\nu\rho}\bar{K}\right\}\boldsymbol{\tau}N + \text{H.c.}\,, \tag{2.117b}$$

$$\mathcal{L}^{7/2(\pm)}_{\Xi\Lambda K_c} = \frac{g_{\Xi\Lambda K_c}}{m_K^3}\,\bar{\Xi}\left\{D^{7/2(\pm)}_{\mu\nu\rho}K_c\right\}\Lambda^{\mu\nu\rho} + \text{H.c.}\,, \tag{2.117c}$$

$$\mathcal{L}^{7/2(\pm)}_{\Xi\Sigma K_c} = \frac{g_{\Xi\Sigma K_c}}{m_K^3}\,\bar{\Xi}\boldsymbol{\tau}\left\{D^{7/2(\pm)}_{\mu\nu\rho}K_c\right\}\cdot\boldsymbol{\Sigma}^{\mu\nu\rho} + \text{H.c.}\,. \tag{2.117d}$$

The coupling constants in the above Lagrangians corresponding to Λ and Σ resonances are free parameters adjusted to reproduce the existing data. For those resonances considered in the present work, they are given in Table 2.3.

The MBr vertices $\hat{\Gamma}^{\dagger}_{MBr}(\hat{\Gamma}_{MBr})$ in Eq. (2.50) are obtained from the above Lagrangians. In addition, each MBr vertex is multiplied by an off-shell form factor given by

$$f(p_r^2, m_r, \Lambda_r) = \left(\frac{n\Lambda_r^4}{n\Lambda_r^4 + (p_r^2 - m_r^2)^2}\right)^n, \tag{2.118}$$

where p_r^2 and m_r are the square of the 4-momentum and mass of the exchanged hyperon, respectively. The cutoff parameter Λ_r is chosen to have a common value $\Lambda_r \equiv \Lambda = 900$ MeV for all the MBr vertices in order to keep the number of free parameters to a minimum. Also, we choose $n = 1$.

For the propagators of the dressed hyperons in Eq. (2.50), we could in principle adopt the

forms used in our previous work [54,113–115]. However, in view of the limited amount of currently available data for the present reaction and the rather poor quality of these data, here we adopt the simpler forms as given in the following. For a spin-1/2 baryon propagator, we use

$$\hat{S}_r^{1/2}(p_r) = \frac{1}{\not{p}_r - m_r + i\frac{\Gamma_r}{2}}\,, \tag{2.119}$$

where Γ_r is the baryon width assumed to be constant, independent of energy. For a stable (ground state) baryon, $\Gamma_r \to \epsilon$ with ϵ being positive infinitesimal.

For spin-3/2, the dressed propagator reads in a schematic matrix notation

$$\hat{S}_r^{3/2}(p_r) = \frac{1}{\not{p}_r - m_r + i\frac{\Gamma_r}{2}}\Delta\,, \tag{2.120}$$

where Δ is the Rarita-Schwinger tensor given by

$$\Delta \equiv \Delta^{\mu\nu} = -g^{\mu\nu} + \frac{1}{3}\gamma^\mu\gamma^\nu + \frac{2p^\mu p^\nu}{3m_r^2} + \frac{\gamma^\mu p^\nu - p^\mu\gamma^\nu}{3m_r}\,. \tag{2.121}$$

Similarly, the propagator for a spin-5/2 resonance is given by

$$\hat{S}_r^{5/2}(p_r) = \frac{1}{\not{p}_r - m_r + i\frac{\Gamma_r}{2}}\Delta\,, \tag{2.122}$$

where [116]

$$\begin{aligned}
\Delta &\equiv \Delta^{\beta_1\beta_2}_{\alpha_1\alpha_2} \\
&= \frac{1}{2}\left(\bar{g}^{\beta_1}_{\alpha_1}\bar{g}^{\beta_2}_{\alpha_2} + \bar{g}^{\beta_2}_{\alpha_1}\bar{g}^{\beta_1}_{\alpha_2}\right) - \frac{1}{5}\bar{g}_{\alpha_1\alpha_2}\bar{g}^{\beta_1\beta_2} \\
&\quad - \frac{1}{10}\left(\bar{\gamma}_{\alpha_1}\bar{\gamma}^{\beta_1}\bar{g}^{\beta_2}_{\alpha_2} + \bar{\gamma}_{\alpha_1}\bar{\gamma}^{\beta_2}\bar{g}^{\beta_1}_{\alpha_2} + \bar{\gamma}_{\alpha_2}\bar{\gamma}^{\beta_1}\bar{g}^{\beta_2}_{\alpha_1} + \bar{\gamma}_{\alpha_2}\bar{\gamma}^{\beta_2}\bar{g}^{\beta_1}_{\alpha_1}\right)
\end{aligned} \tag{2.123}$$

with

$$\bar{g}^{\mu\nu} \equiv g^{\mu\nu} - \frac{p^\mu p^\nu}{m_r^2}\,, \qquad \bar{\gamma}^\mu \equiv \gamma^\mu - \frac{p^\mu \not{p}}{m_r^2}\,. \tag{2.124}$$

The propagator for a spin-7/2 resonance is given by

$$\hat{S}_r^{7/2}(p_r) = \frac{1}{\not{p}_r - m_r + i\frac{\Gamma_r}{2}}\Delta\,, \tag{2.125}$$

where [116]

$$\begin{aligned}\Delta &\equiv \Delta^{\beta_1\beta_2\beta_3}_{\alpha_1\alpha_2\alpha_3} \\ &= \frac{1}{36}\sum_{P(\alpha),P(\beta)}\left\{\bar{g}^{\beta_1}_{\alpha_1}\bar{g}^{\beta_2}_{\alpha_2}\bar{g}^{\beta_3}_{\alpha_3} - \frac{3}{7}\bar{g}^{\beta_1}_{\alpha_1}\bar{g}_{\alpha_2\alpha_3}\bar{g}^{\beta_2\beta_3} - \frac{3}{7}\bar{\gamma}_{\alpha_1}\bar{\gamma}^{\beta_1}\bar{g}^{\beta_2}_{\alpha_2}\bar{g}^{\beta_3}_{\alpha_3} + \frac{3}{35}\bar{\gamma}_{\alpha_1}\bar{\gamma}^{\beta_1}\bar{g}_{\alpha_2\alpha_3}\bar{g}^{\beta_2\beta_3}\right\},\end{aligned} \tag{2.126}$$

and the summation runs over all possible permutations of $\{\alpha_1, \alpha_2, \alpha_3\}$ and of $\{\beta_1, \beta_2, \beta_3\}$.

Chapter 3

$\gamma + N \rightarrow K + K + \Xi$

Because resonances couple differently to different channels, studying the Ξ, Ξ^*, and Y^* mass spectra requires measurements involving different reaction processes. Different reaction channels also expand our experimental reach to different kinematic regions. Indeed, studying $\gamma + N \rightarrow K + K + \Xi$ alone may lead to erroneous conclusions concerning the contribution from the hyperon resonances, Y^*, due to the large kinematic region surveyed and the more complicated description required to explain a 3-body process. For example, at tree level, K resonances and K^* exchanges contribute to the $\gamma + N \rightarrow K + K + \Xi$ amplitude. Disentangling these 'background' amplitudes from Y^* contributions can become very difficult. Only when we study different production processes, for Ξ in this work, using a consistent approach, can we begin to gain confidence that we are truly understanding the reaction mechanisms that are responsible for the observed results.

The photoproduction reaction may not be the most ideal place to produce Ξ because of the lack of strangeness in the initial state. But because of advancements in detection techniques and the availability of machines capable of delivering intense beams, this reaction has been measured and new experiments are planned for the very near future. Currently available data include total and differential cross sections, as well as KK and $K\Xi$ invariant mass distributions, for the $\gamma + p \rightarrow K^+ + K^+ + \Xi^-$ channel [47]. New data for some spin observables was recently released as well [50,51]. In addition to studying Ξ and Ξ^* these new experiments plan to study exclusive Ω^- photoproduction for the first time [52].

In this chapter we first show how to build a gauge invariant amplitude, M^μ, for $\gamma + N \to K + K + \Xi$ from the $N \to K + K + \Xi$ amplitude. Gauge-invariance requires M^μ to satisfy the Ward-Takahashi Identity (WTI) [117,118]. In our formulation, we employ full local gauge-invariance as demanded by generalized WTI, in contrast to the global gauge-invariance used by many authors. This procedure is shown in Section 3.1. In Section 3.2, the most general spin-structure is derived and the issue of parity determination of the Ξ via photoproduction is explored. Our model for $\gamma + N \to K + K + \Xi$ is derived in Section 3.3. Such an approach will provide a consistent model which to study both the $\bar{K}$- and photon-induced reactions. Cross section formulas in terms of the amplitude M^μ above are derived in Appendix 3.5.5.

3.1 Gauge-Invariant Photoproduction Amplitude

To obtain the amplitude for the photoproduction reaction $\gamma(k) + N(p) \to K(q_1) + K(q_2) + \Xi(p')$, we attach the photon everywhere in the amplitude $\bar{T}$ of the $N \to K + K + \Xi$ process. This is done by means of gauge derivative technique introduced in Ref. [119]. Using the notation G_i for the propagator of the particle i, we have

$$\begin{aligned} M^\mu &\equiv \sum_i \Big(- G_i^{-1}\{G_i \bar{T} G_N\}^\mu G_N^{-1}\Big) \\ &= \sum_i \left(-G_i^{-1}\{G_i\}^\mu \bar{T}\right) - \bar{T}\{G_N\}^\mu G_N^{-1} - \{\bar{T}\}^\mu \\ &= \sum_i \left[-G_i^{-1}\{G_i\}^\mu G_i^{-1}\right] G_i\ \bar{T} + \bar{T} G_N \left[-G_N^{-1}\{G_N\}^\mu S_N^{-1}\right] - \{\bar{T}\}^\mu \\ &= \Gamma^\mu_{\Xi\Xi\gamma} G_\Xi \bar{T} + \Gamma^\mu_{K_1K_1\gamma} G_{K_1} \bar{T} + \Gamma^\mu_{K_2K_2\gamma} G_{K_2} \bar{T} + \bar{T} G_N \Gamma^\mu_{NN\gamma} + \bar{T}^\mu\ , \end{aligned} \tag{3.1}$$

where $\Gamma^\mu_{ii\gamma} \equiv -G_i^{-1}\{G_i\}^\mu G_i^{-1}$ denotes the $ii\gamma$ vertex ($i = N, \Xi, K$). Note that the first four terms on the right-hand-side of the above equation correspond to the photon attaching to the external four legs of $\bar{T}$. $\bar{T}^\mu \equiv -\{T\}^\mu$ is the interaction current where the photon is attached to the internal structure of $\bar{T}$. Each term on the right-hand-side of Eq. (3.1) is represented diagrammatically in Fig. 3.1.

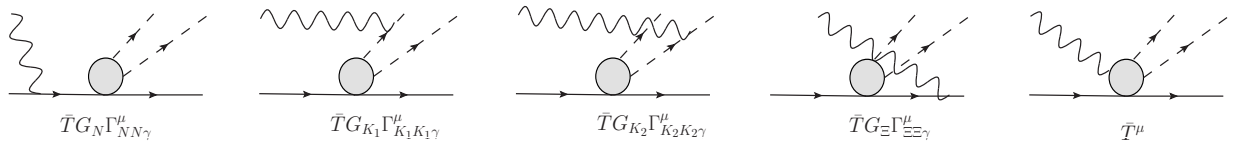

Figure 3.1: Diagrammatic representation of each term on the r.h.s. of Eq. (3.36). The blob represents the interaction $\bar{T} = \bar{T}_r + \bar{T}_c$ of Eq. (3.32). Symmetrization of the two kaons is implied.

Now, the gauge invariance condition of the two-meson photoproduction amplitude is given by the generalized Ward-Takahashi identity

$$k_\mu M^\mu = G_\Xi^{-1}\hat{Q}_\Xi G_\Xi \bar{T} + G_{K_1}^{-1}\hat{Q}_{K_1}G_{K_1}\bar{T} + G_{K_2}^{-1}\hat{Q}_{K_2}G_{K_2}\bar{T} - \bar{T}G_N\hat{Q}_N G_N^{-1} \ , \tag{3.2}$$

where $\hat{Q}_i$ stands for the charge operator of particle i and, at the same time, changes the momentum argument of the propagator G_i and of $\bar{T}$ to its left by $+k$. For G_i and $\bar{T}$ appearing on its right, the charge operator changes their momentum arguments by $-k$.

Taking the four-divergence of the photoproduction amplitude given by Eq. (3.1), we have

$$\begin{aligned}
k_\mu M^\mu &= k_\mu \Gamma^\mu_{\Xi\Xi\gamma} G_\Xi \bar{T} + k_\mu \Gamma^\mu_{K_1K_1\gamma} G_{K_1}\bar{T} + k_\mu \Gamma^\mu_{K_2K_2\gamma} G_{K_2}\bar{T} + \bar{T}G_N k_\mu \Gamma^\mu_{NN\gamma} + k_\mu \bar{T}^\mu \\
&= \Big\{ [G_\Xi^{-1}\hat{Q}_\Xi - \hat{Q}_\Xi G_\Xi^{-1}] G_\Xi \bar{T} + [G_{K_1}^{-1}\hat{Q}_{K_1} - \hat{Q}_{K_1}G_{K_1}^{-1}]G_{K_1}\bar{T} + [G_{K_2}^{-1}\hat{Q}_{K_2} - \hat{Q}_{K_2}G_{K_2}^{-1}]G_{K_2}\bar{T} \\
&\quad + \bar{T}G_N[G_N^{-1}\hat{Q}_N - \hat{Q}_N G_N^{-1}] \Big\} + k_\mu \bar{T}^\mu \\
&= \Big\{ G_\Xi^{-1}\hat{Q}_\Xi G_\Xi \bar{T} + G_{K_1}^{-1}\hat{Q}_{K_1}G_{K_1}\bar{T} + G_{K_2}^{-1}\hat{Q}_{K_2}G_{K_2}\bar{T} - \bar{T}G_N\hat{Q}_N G_N^{-1} \Big\} \\
&\quad - \Big\{ \hat{Q}_\Xi \bar{T} + \hat{Q}_{K_1}\bar{T} + \hat{Q}_{K_2}\bar{T} - \bar{T}\hat{Q}_N \Big\} + k_\mu \bar{T}^\mu \ ,
\end{aligned} \tag{3.3}$$

where we have made use of the Ward-Takahashi identity for the three-point vertex

$$k_\mu \Gamma^\mu_{ii\gamma} = G_i^{-1}\hat{Q}_i - \hat{Q}_i G_i^{-1} \ . \tag{3.4}$$

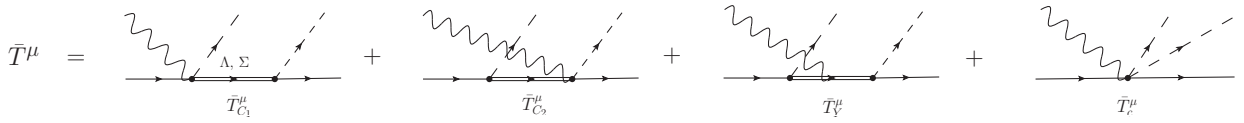

Figure 3.2: Details of the interaction current $\bar{T}^\mu$ (last diagram in Fig. 3.1). The first three terms comprise the interaction current arising from $\bar{T}_r$. $\bar{T}^\mu_{C_1}$ and $\bar{T}^\mu_{C_2}$ are the generalized four-point contact currents due to the presence of hadronic form factors in $\bar{T}_r$; they also include the usual Kroll-Ruderman contact currents. $\bar{T}^\mu_Y$ is the intermediate-state hyperon resonance current. The last term is the five-point contact current arising from $\bar{T}_c$. Symmetrization of the two kaons is implied.

Comparing Eqs. (3.2,3.3), we see that the interaction current $\bar{T}^\mu$ should obey

$$k_\mu \bar{T}^\mu = \hat{Q}_\Xi \bar{T} + \hat{Q}_{K_1} \bar{T} + \hat{Q}_{K_2} \bar{T} - \bar{T} \hat{Q}_N \ . \tag{3.5}$$

The major difficulty in deriving a full two-meson photo production amplitude, M^μ, lays on the derivation of the interaction current $\bar{T}^\mu$ for its determination requires the knowledge of the underlying microscopic structure of the amplitude $\bar{T}$. Note that the reaction $N \to K + K + \Xi$ involves three bodies in the final states and as such, it should obey the (three-body) Faddeev equation. An exact determination of the interaction current, $\bar{T}^\mu$, is therefore impractical and one needs to resort for some approximation(s) to determine it [120, 121].

In this work, we derive the interaction current, $\bar{T}^\mu$, consistently with our model presented in Section 2.2.1 for the reaction $\bar{K} + N \to K + \Xi$. This is done in Section 3.3.

3.2 Spin structure

In this section we derive the most general structure of the reaction amplitude for two scalar meson production in the photon-induced reaction,

$$\gamma + N \to M + M' + B \, . \tag{3.6}$$

We consider B to be a J=1/2 baryon and do distinguish the two mesons, M and M'. We use this notation to emphasis that this is a general procedure but this calculation will be applied to a $K + K + \Xi$ final state. With those considerations, there are four reaction channels to consider, $\gamma + p \to K^+ + K^+ + \Xi^-$, $\gamma + p \to K^+ + K^0 + \Xi^0$, $\gamma + n \to K^0 + K^0 + \Xi^0$, and $\gamma + n \to K^+ + K^0 + \Xi^-$, and two of them have identical Kaons in the final state, $K = K' = K^+$ or K^0. Symmetrization of the two Kaons is required for these cases .

Here, we follow Ref. [83] closely. We start by making a partial-wave expansion of the reaction amplitude

$$\langle S' M_{S'} | \hat{M}(\vec{q}, \vec{p}\,'; \vec{k}) | S M_S \rangle = \sum i^{L-L'-l} M^{S'J'SJ}_{lL'L}(q, p'; k) Y_{lm_l}(\hat{q}) Y_{L'M_{L'}}(\hat{p}') Y^*_{LM_L}(\hat{k}) \times (SM_S LM_L | JM_J)(S'M_{S'} L'M_{L'} | J'M_{J'})(J'M_{J'} lm_l | JM_J) \ , \quad (3.7)$$

where S, L, J stand for the total spin, total orbital angular momentum and the total angular momentum, respectively, of the initial γN state. M_S, M_L and M_J denote the corresponding projection quantum numbers. The primed quantities stand for the corresponding quantum numbers of the final $MM'B$ state. l and m_l denote the orbital angular momentum of one of the emitted mesons, M, and its projection, respectively, relative to the center-of-mass of the other meson and baryon ($M'B$) subsystem. The summation runs over all quantum numbers not specified in the l.h.s. of Eq.(3.7). $\vec{k}$ and $\vec{p}\,'$ denote the relative momenta of the γN and $M'B$ in the initial and final states, respectively. $\vec{q}$ denotes the momentum of the other emitted meson (M) with respect to the center-of-mass of $M'B$ in the final state. We note that, in Eq.(3.7), apart from the restrictions on the quantum numbers encoded in the geometrical factors, total parity conservation imposes that $(-)^{l+L+L'} = -1$ in the case of a positive parity baryon B and $(-)^{l+L+L'} = +1$ in the case of a negative parity B if the mesons M and M' have the same parity, i.e., they both are either scalar or pseudoscalar mesons. If they have opposite parities, then, $(-)^{l+L+L'} = +1$ for a positive parity baryon B and $(-)^{l+L+L'} = -1$ for a negative parity B.

Eq.(3.7) can be inverted to solve for the partial-wave matrix element $M_{lL'L}^{S'J'SJ}(q,p';k)$. We have

$$M_{lL'L}^{S'J'SJ}(q,p';k) = \sum i^{L'+l-L}\frac{8\pi^2}{2J+1}\sqrt{\frac{2L+1}{4\pi}}(SM_SL0|JM_J)$$
$$\times (S'M_{S'}L'M_{L'}|J'M_{J'})(J'M_{J'}lm_l|JM_J)$$
$$\times \int d\Omega_{p'}Y^*_{L'M_{L'}}(\hat{p}')\int_{-1}^{+1} d(\cos(\theta_q))Y^*_{lm_l}(\theta_q,0)\,\langle S'M_{S'}|\hat{M}(\vec{q},\vec{p}';\vec{k})|SM_S\rangle \ , \quad (3.8)$$

where, without loss of generality, the z-axis is chosen along $\vec{k}$ and $\vec{q}$ in the xz-plane; $\cos(\theta_q) \equiv \hat{q}\cdot\hat{k}$. The summation is over all quantum numbers not specified in the l.h.s. of the equation.

The most general structure of the reaction amplitude can be extracted from Eq.(3.7) as

$$\hat{M}(\vec{q},\vec{p}';\vec{k}) = \sum_{S'SM_SM_{S'}} |S'M_{S'}\rangle\,\langle S'M_{S'}|\hat{M}(\vec{q},\vec{p}';\vec{k})|SM_S\rangle\,\langle SM_S| \ . \quad (3.9)$$

Inserting Eq.(3.7) into Eq.(3.9) and re-coupling gives [1]

$$\hat{M}(\vec{q},\vec{p}';\vec{k}) = \sum i^{L-L'-l}(-)^{L'+l+2J+2S'}[J'][J]^2 M_{lL'L}^{S'J'SJ}(q,p';k)$$
$$\times \sum_{\alpha\beta}[\beta]\begin{Bmatrix} S' & L' & J' \\ l & J & \beta \end{Bmatrix}\begin{Bmatrix} S & L & J \\ \beta & S' & \alpha \end{Bmatrix}[B_S\otimes A_{S'}]^\alpha\cdot[X_{L\,(L'l)\beta}]^\alpha \ , \quad (3.10)$$

where we have used the notations $B_{S-M_S} \equiv (-)^{S+M_S}\langle SM_S|$, $A_{S'M_{S'}} \equiv |S'M_{S'}\rangle$, and $[J] \equiv \sqrt{2J+1}$. Also, $[X_{L\,(L'l)\beta}]^\alpha$ is defined as

$$[X_{L\,(L'l)\beta}]^\alpha \equiv \left[Y_L(\hat{k})\otimes D_\beta^{L'l}(\hat{p}',\hat{q})\right]^\alpha \ , \quad (3.11)$$

where

$$D_{\beta M}^{L'l} = D_{\beta M}^{L'l}(\hat{p}',\hat{q}) \equiv [Y_{L'}(\hat{p}')\otimes Y_l(\hat{q})]_M^\beta \ , \quad (3.12)$$

and contains all the information on the angular dependence of the reaction amplitude.

The outer summation in Eq. (3.10) is over the quantum numbers S, L, L', l, and J. In the

[1] In Eq. (50) of Ref. [83], a factor of $[\beta]$ is missing. The following equations are, however, correct. Also, the difference in the phase factors is due to the different coupling scheme adopted here for convenience $[(J'M_{J'}lm_l|JM_J)$ as compared to $(lm_lJ'M_{J'}|JM_J)$, $[B_S\otimes A_{S'}]^\alpha$ as compared to $[A_{S'}\otimes B_S]^\alpha$, and $[X_{L\,(L'l)\beta}]^\alpha$ as compared to $[X_{(lL')\beta\,L}]^\alpha$.

above equation S is either 1/2 or 3/2 so that α takes the values 0, 1, and 2, and denotes the rank of the corresponding tensor. In the above equation it should be understood that the matrix elements of the meson creation and photon annihilation operators have already been taken.

The rest of this calculation is done for the $J = 1/2$ Ξ which means $S' = 1/2$, but the procedure extends to Ξ of any spin. We now expand $[B_S \otimes A_{\frac{1}{2}}]^\alpha$, for each tensor of rank α, in terms of the complete set of available spin operators in the problem, i.e., the photon polarization vector $\vec{\epsilon}$ and the Pauli spin matrix $\vec{\sigma}$ together with the identity matrix. The result is [83]

$$
\begin{aligned}
[B_S \otimes A_{\frac{1}{2}}]^0 &= \frac{1}{\sqrt{6}}\ \vec{\sigma}\cdot\vec{\epsilon}\ , \\
[B_S \otimes A_{\frac{1}{2}}]^1 &= \frac{1}{\sqrt{6}}\delta_{S,\frac{1}{2}}\left\{-\vec{\epsilon} + i(\vec{\sigma}\times\vec{\epsilon})\right\} - \frac{1}{\sqrt{3}}\delta_{S,\frac{3}{2}}\left\{\vec{\epsilon} + \frac{i}{2}(\vec{\sigma}\times\vec{\epsilon})\right\}\ , \\
[B_S \otimes A_{\frac{1}{2}}]^2 &= \frac{1}{\sqrt{2}}[\vec{\sigma}\otimes\vec{\epsilon}]^2\ ,
\end{aligned}
\tag{3.13}
$$

where the numerical factors are uniquely determined such that the spin matrix elements of the right-hand side (r.h.s.) in the above equations equal the corresponding matrix elements of the l.h.s.

Analogously, $[X_{L\,(lL')\beta}]^\alpha$ can be expressed in terms of the three momenta available in the problem, namely, the photon-nucleon relative momentum $\vec{k}$, meson momentum $\vec{q}$, and the $K'\Xi$ relative momentum $\vec{p}\,'$. Here a remark is in order concerning the choice of the set of momenta to form a basis. Since there exist three momenta in the problem, we have a choice of taking any two of them to form a basis of three momentum-vectors. Here, we choose the pair $(\vec{k},\ \vec{q})$ with $\vec{k}$ in the $+z$-direction and $\vec{q}$ in the xz-plane, such that,

$$
\hat{n}_1 \equiv \frac{(\hat{k}\times\hat{q})\times\hat{k}}{|(\hat{k}\times\hat{q})\times\hat{k}|} = \hat{n}_2\times\hat{k} = \hat{x}\ , \qquad\qquad \hat{n}_2 \equiv \frac{\hat{k}\times\hat{q}}{|\hat{k}\times\hat{q}|} = \hat{y}\ ,
\tag{3.14}
$$

and $\hat{k} = \hat{z}$ form a basis of mutually orthogonal vectors. Of course, in principle, any choice of the pair of available momenta to form a basis is equally valid. In practice, however, the suitability of the choice to define the basis vectors depends on the particular kinematical situation of the problem at hand. If we are looking at the limit of $\vec{p}\,' \to 0$, then, the choice of the pair $(\vec{k},\ \vec{q})$, as above, is the appropriate one, while for $\vec{q} \to 0$, the appropriate choice would be the pair $(\vec{k},\ \vec{p}\,')$. As we

discuss in Sec. 3.2.3, the transformation from one choice to another is straightforward and trivial. When $\vec{q} = \vec{p}\,' = 0$ or both of them are non-vanishing, either of the choices is equally suited. As mentioned above, in this section we consider the choice $(\vec{k}, \vec{q})$. From Eq. (3.11), we, then, have

$$
\begin{aligned}
[X_{L\,(L'l)\beta}]^0 &= a^{\beta 0}_{L(L'l)}\ , \\
[X_{L\,(L'l)\beta}]^1 &= a^{\beta 1}_{L(L'l)}\,\hat{k} + b^{\beta 1}_{L(L'l)}\,\hat{n}_1 + c^{\beta 1}_{L(L'l)}\,\hat{n}_2\ , \\
[X_{L\,(L'l)\beta}]^2 &= a^{\beta 2}_{L(L'l)}\,[\hat{k}\otimes\hat{k}]^2 + b^{\beta 2}_{L(L'l)}\,[\hat{n}_1\otimes\hat{n}_1]^2 + c^{\beta 2}_{L(L'l)}\,[\hat{k}\otimes\hat{n}_1]^2 \\
&\qquad + a'^{\beta 2}_{L(L'l)}\,[\hat{k}\otimes\hat{n}_2]^2 + b'^{\beta 2}_{L(L'l)}\,[\hat{n}_1\otimes\hat{n}_2]^2\ , \qquad (3.15)
\end{aligned}
$$

where the coefficients $a^{\beta 0}_{L(L'l)}$, $a^{\beta 1}_{L(L'l)}$, $b^{\beta 1}_{L(L'l)}$, and $c^{\beta 1}_{L(L'l)}$ are derived in Appendix 3.5.1 and the coefficients $a^{\beta 2}_{L(L'l)}$, $b^{\beta 2}_{L(L'l)}$, etc, in Appendix 3.5.2. Note that $[\hat{n}_2\otimes\hat{n}_2]^2$ is not independent from those appearing in the last equality above.

Inserting Eqs.(3.13,3.15) into Eq.(3.10) we have

$$
\begin{aligned}
\hat{M}(\vec{q},\vec{p}\,';\vec{k}) &= \mathcal{M}_1\vec{\epsilon}\cdot\vec{\sigma} + \mathcal{M}_2\vec{\epsilon}\cdot\hat{k} + \mathcal{M}_3\vec{\epsilon}\cdot\hat{n}_1 + \mathcal{M}_4\vec{\epsilon}\cdot\hat{n}_2 \\
&\quad + \tilde{\mathcal{M}}_2\vec{\epsilon}\cdot(\hat{k}\times\vec{\sigma}) + \tilde{\mathcal{M}}_3\vec{\epsilon}\cdot(\hat{n}_1\times\vec{\sigma}) + \tilde{\mathcal{M}}_4\vec{\epsilon}\cdot(\hat{n}_2\times\vec{\sigma}) \\
&\quad + \mathcal{M}_8[\vec{\sigma}\otimes\vec{\epsilon}]^2\cdot[\hat{k}\otimes\hat{k}]^2 + \mathcal{M}_9[\vec{\sigma}\otimes\vec{\epsilon}]^2\cdot[\hat{n}_1\otimes\hat{n}_1]^2 + \mathcal{M}_{10}[\vec{\sigma}\otimes\vec{\epsilon}]^2\cdot[\hat{k}\otimes\hat{n}_1]^2 \\
&\quad + \mathcal{M}_{11}[\vec{\sigma}\otimes\vec{\epsilon}]^2\cdot[\hat{k}\otimes\hat{n}_2]^2 + \mathcal{M}_{12}[\vec{\sigma}\otimes\vec{\epsilon}]^2\cdot[\hat{n}_1\otimes\hat{n}_2]^2\ . \qquad (3.16)
\end{aligned}
$$

Using the identity

$$
3[\ \vec{\sigma}\otimes\vec{\epsilon}\ ]^2\cdot[\ \hat{a}\otimes\hat{b}\ ]^2 = \frac{3}{2}[\ \vec{\sigma}\cdot\hat{a}\vec{\epsilon}\cdot\hat{b} + \vec{\sigma}\cdot\hat{b}\vec{\epsilon}\cdot\hat{a}\ ] - (\hat{a}\cdot\hat{b})\vec{\sigma}\cdot\vec{\epsilon}\,, \qquad (3.17)
$$

where $\hat{a}$ and $\hat{b}$ stand for arbitrary unit vectors, Eq. (3.16) can be rewritten as

$$
\begin{aligned}
\hat{M}(\vec{q},\vec{p}\,';\vec{k}) &= F_1\,\vec{\sigma}\cdot\vec{\epsilon} + F_2\,\vec{\epsilon}\cdot\hat{k} + F_3\,\vec{\epsilon}\cdot\hat{n}_1 + F_4\,\vec{\epsilon}\cdot\hat{n}_2 + F_5\,\vec{\sigma}\cdot\hat{k}\,\vec{\epsilon}\cdot\hat{k} + F_6\,\vec{\sigma}\cdot\hat{n}_1\,\vec{\epsilon}\cdot\hat{n}_1 \\
&\quad + F_7\,[\vec{\sigma}\cdot\hat{k}\vec{\epsilon}\cdot\hat{n}_1] + F_8\,[\vec{\sigma}\cdot\hat{n}_1\vec{\epsilon}\cdot\hat{k}] + F_9\,[\vec{\sigma}\cdot\hat{n}_2\vec{\epsilon}\cdot\hat{k}] + F_{10}\,[\vec{\sigma}\cdot\hat{k}\vec{\epsilon}\cdot\hat{n}_2] \\
&\quad + F_{11}\,[\vec{\sigma}\cdot\hat{n}_1\vec{\epsilon}\cdot\hat{n}_2] + F_{12}\,[\vec{\sigma}\cdot\hat{n}_2\vec{\epsilon}\cdot\hat{n}_1]\ , \qquad (3.18)
\end{aligned}
$$

where

$$
\begin{aligned}
F_1 &\equiv \mathcal{M}_1 - \frac{1}{3}\left(\mathcal{M}_8 + \mathcal{M}_9\right) \ , \\
F_i &\equiv \mathcal{M}_i \qquad (i = 2, 3, 4) \ , \\
F_{5,6} &\equiv \mathcal{M}_{8,9} \\
F_{7,8} &\equiv \frac{1}{2}\mathcal{M}_{10} \pm \tilde{\mathcal{M}}_4 \\
F_{9,10} &\equiv \frac{1}{2}\mathcal{M}_{11} \pm \tilde{\mathcal{M}}_3 \\
F_{11,12} &\equiv \frac{1}{2}\mathcal{M}_{12} \pm \tilde{\mathcal{M}}_2
\end{aligned}
\tag{3.19}
$$

Equation (3.18) is the most general form of the two spinless-meson production amplitude in photon-induced reaction, consistent with symmetry principles. It is valid for both real and virtual photons. The coefficients $F_i(\tilde{F}_i)$ are functions of the energy of the system and scattering angle θ_q of one of the two mesons (K) relative to the photon direction, in addition to the relative momentum $\vec{p}\,'$ of the other meson with baryon, $K'\Xi$. These coefficients are different for a positive- and negative-parity Ξ as seen in Appendix 3.5.4. For certain scattering angles, half of these amplitudes are identically zero and the parity of the produce Ξ can be deduced.

3.2.1 Two-meson photoproduction

For photoproduction, due to the transversality of the photon, the amplitude in Eq. (3.18) reduces to eight structures with eight independent amplitudes,

$$
\begin{aligned}
\hat{M} = {} & F_1\, \vec{\sigma}\cdot\vec{\epsilon} + F_3\, \vec{\epsilon}\cdot\hat{n}_1 + F_4\, \vec{\epsilon}\cdot\hat{n}_2 + F_6\, \vec{\sigma}\cdot\hat{n}_1\, \vec{\epsilon}\cdot\hat{n}_1 \\
& + F_7\left[\vec{\sigma}\cdot\hat{k}\vec{\epsilon}\cdot\hat{n}_1\right] + F_{10}\left[\vec{\sigma}\cdot\hat{k}\vec{\epsilon}\cdot\hat{n}_2\right] + F_{11}\left[\vec{\sigma}\cdot\hat{n}_1\vec{\epsilon}\cdot\hat{n}_2\right] + F_{12}\left[\vec{\sigma}\cdot\hat{n}_2\vec{\epsilon}\cdot\hat{n}_1\right] \ ,
\end{aligned}
\tag{3.20}
$$

For a linearly polarized photon with $\vec{\epsilon} = \vec{\epsilon}_\perp \equiv \hat{n}_2$, we have

$$\hat{M}^\perp = F_4 + F_{11}\,\sigma_1 + F_1\,\sigma_2 + F_{10}\,\sigma_3 \equiv \sum_{i=0}^{3} M_i^\perp \sigma_i \tag{3.21}$$

with four independent amplitudes. $\sigma_0 \equiv 1$, $\sigma_1 = \sigma_x$, etc.

For $\vec{\epsilon} = \vec{\epsilon}_\parallel \equiv \hat{n}_1$,

$$\hat{M}^\parallel = F_3 + (F_1 + F_6)\,\sigma_1 + F_{12}\,\sigma_2 + F_7\,\sigma_3 \equiv \sum_{i=0}^{3} M_i^\parallel \sigma_i \tag{3.22}$$

with five amplitudes. Here, one cannot measure F_1 and F_6 individually, only $F_1 + F_6$ without using different photon polarization. Combining both $\hat{M}^\perp$ and $\hat{M}^\parallel$ results in eight of the original twelve amplitudes being measurable. In electro-production with a virtual photon with longitudinal polarization would be able to access the other four amplitudes in Eq. 3.18.

From the amplitudes in the form given by Eqs. (3.21,3.22), we can calculate all the observables in this reaction straightforwardly with the help of the results in Appendix 3.5.5. We have ($\lambda = \perp, \parallel$)

$$\begin{aligned}
\frac{d\sigma^\lambda}{d\Omega} &= |M_0^\lambda|^2 + |M_1^\lambda|^2 + |M_2^\lambda|^2 + |M_3^\lambda|^2 \ , \\
\frac{d\sigma^\lambda}{d\Omega} K_{xx}^\lambda &= |M_0^\lambda|^2 + |M_1^\lambda|^2 - |M_2^\lambda|^2 - |M_3^\lambda|^2 \ , \\
\frac{d\sigma^\lambda}{d\Omega} K_{yy}^\lambda &= |M_0^\lambda|^2 - |M_1^\lambda|^2 + |M_2^\lambda|^2 - |M_3^\lambda|^2 \ , \\
\frac{d\sigma^\lambda}{d\Omega} K_{zz}^\lambda &= |M_0^\lambda|^2 - |M_1^\lambda|^2 - |M_2^\lambda|^2 + |M_3^\lambda|^2 \ , \\
\frac{d\sigma^\lambda}{d\Omega}(T_i^\lambda + P_i^\lambda) &= 4Re[M_0^\lambda M_i^{\lambda^*}] \ , \qquad \frac{d\sigma^\lambda}{d\Omega}(T_i^\lambda - P_i^\lambda) = 4Im[M_j^\lambda M_k^{\lambda^*}] \ , \\
\frac{d\sigma^\lambda}{d\Omega}(K_{jk}^\lambda - K_{kj}^\lambda) &= 4\epsilon_{jki} Im[M_0^\lambda M_i^{\lambda^*}] \ , \qquad \frac{d\sigma^\lambda}{d\Omega}(K_{jk}^\lambda + K_{kj}^\lambda) = 4Re[M_j^\lambda M_k^{\lambda^*}] \ ,
\end{aligned} \tag{3.23}$$

where i, j, k can be any of $(x, y, z) = (1, 2, 3)$.

The above results reveal that one is required to measure the single- and double-spin observables for each of the two photon polarization states ($\vec{\epsilon}_\perp$ and $\vec{\epsilon}_\parallel$) in order to determine the amplitudes M_i^λ. This is, of course, an extremely difficult task experimentally.

3.2.2 Parity Determination

Here we will discuss the consequences of the Ξ parity on the spin structure, F_i. Eqs. 3.11, 3.15, 3.16, and 3.19 show that F_i depends on $D^{L'l}_{\beta M}$. The tensor $D^{L'l}_{\beta M}$ is complex in general but each F_i only depends on $\mathrm{Re}\left[D^{L'l}_{\beta M}\right]$ *or* $\mathrm{Im}\left[D^{L'l}_{\beta M}\right]$, and never on both. In fact, for each possibility of the parity of the Ξ, π_Ξ, half the F_i depend on $\mathrm{Re}\left[D^{L'l}_{\beta M}\right]$ and the other half on $\mathrm{Im}\left[D^{L'l}_{\beta M}\right]$. See Appendix 3.5.4 for more detail. Table 3.1 displays the dependence of each spin structure coefficient. There are now two cases to consider, identical kaon production and non-identical kaon production.

Non-identical Kaons

We first discuss the case with non-identical kaons. Here, $\mathrm{Im}\left[D^{L'l}_{\beta M}\right] = 0$ when all three final particles are produced in the same plane, i.e., the scattering plane. To make this more explicit, $\hat{p}' \cdot \hat{n}_2 = 0$, or $\phi_{p'} = 0$. The result is that all the F_i's which depended on $\mathrm{Im}\left[D^{L'l}_{\beta M}\right]$ are identically zero. This means that

$$\hat{M}^{\perp} = F_{11}\,\sigma_1 + F_{10}\,\sigma_3 \equiv \sum_{i=0}^{3} M_i^{\perp}\sigma_i \tag{3.24}$$

and

$$\hat{M}^{\parallel} = F_3 + F_{12}\,\sigma_2 \equiv \sum_{i=0}^{3} M_i^{\parallel}\sigma_i \tag{3.25}$$

for $\pi_\Xi = +1$. Here it is obvious to see that $\hat{M}^{\perp}$ and $\hat{M}^{\parallel}$ have the same spin structure as $\bar{K} + N \to K + \Xi$ for $J = 1/2$ Ξ. Here, $\hat{M}^{\parallel}$ and $\hat{M}^{\perp}$ share the spin structure of $\pi_\Xi = +1$ and -1 respectively, i.e., $M_2^{\perp} = M_0^{\perp} = M_1^{\parallel} = M_3^{\parallel} = 0$. This can be seen in Eqs. 2.4.

The case for $\pi_\Xi = -1$ results in

$$\hat{M}^{\perp} = F_4 + F_1\,\sigma_2 \equiv \sum_{i=0}^{3} M_i^{\perp}\sigma_i \tag{3.26}$$

and

$$\hat{M}^{\parallel} = (F_1 + F_6)\,\sigma_1 + F_7\sigma_3 \equiv \sum_{i=0}^{3} M_i^{\parallel}\sigma_i\,. \tag{3.27}$$

Again, the structures of Eqs. 2.4 are seen but now $\hat{M}^{\parallel}$ and $\hat{M}^{\perp}$ share the $\pi_\Xi = -1$ and π_Ξ result respectively, i.e., $M_1^{\perp} = M_3^{\perp} = M_0^{\parallel} = M_2^{\parallel} = 0$ here.

Table 3.1: Here we show which spin structure coefficients, F_i, depend on the real or imaginary part of $D^{L'l}_{\beta M}$ for a given parity, π_Ξ, of the produced Ξ.

	$\mathrm{Re}\left[D^{L'l}_{\beta M}\right]$	$\mathrm{Im}\left[D^{L'l}_{\beta M}\right]$
$\pi_\Xi = +1$	F_2, F_3, F_9, F_{10}, F_{11}, F_{12}	F_1, F_4, F_5, F_6, F_7, F_8
$\pi_\Xi = -1$	F_1, F_4, F_5, F_6, F_7, F_8	F_2, F_3, F_9, F_{10}, F_{11}, F_{12}

This means that the parity of Ξ can be analyzed in the same way that it was in Section 2.1. For a photon beam with polarization $\lambda = \{\perp, \|\}$,

$$K^\lambda_{yy} = \frac{T^\lambda_y}{P^\lambda_y} = \frac{K^\lambda_{xx}}{K^\lambda_{zz}} = -\frac{K^\lambda_{xz}}{K^\lambda_{zx}} = \zeta^\lambda \pi_\Xi \,, \tag{3.28}$$

where $\zeta^\| = 1$ and $\zeta^\perp = -1$. These results are the same as in Ref. [125] for one meson photoproduction. The spin-density matrix elements of Section 2.1 obey

$$(-1)^{\frac{1}{2}-\lambda_2} \frac{\rho^{\lambda,1}_{\lambda_1,\lambda_2}}{\rho^{\lambda,3}_{\lambda_1,-\lambda_2}} = (-1)^{\frac{1}{2}-\lambda_2} \frac{i\rho^{\lambda,2}_{\lambda_1,\lambda_2}}{\rho^{\lambda,0}_{\lambda_1,-\lambda_2}} = \zeta^\lambda \pi_\Xi \,. \tag{3.29}$$

Here $\rho^{\lambda,i}_{\lambda_1,\lambda_2}$ represents the SDM elements associated with a photon beam of polarization $\vec{\epsilon}_\lambda = \vec{\epsilon}_\perp$ or $\vec{\epsilon}_\|$ and the initial nucleon polarized in the $\hat{n}_i$ direction. The set of subscripts λ_1, λ_2 represent which SDM element you are dealing with and are related to the Ξ helicity. In fact, Eq. 2.36 applies here as well for arbitrary J.

$$(-1)^{J-\lambda_2} \frac{\rho^{\lambda,1}_{\lambda_1,\lambda_2}}{\rho^{\lambda,3}_{\lambda_1,-\lambda_2}} = (-1)^{J-\lambda_2} \frac{i\rho^{\lambda,2}_{\lambda_1,\lambda_2}}{\rho^{\lambda,0}_{\lambda_1,-\lambda_2}} = \zeta^\lambda \pi_\Xi \,. \tag{3.30}$$

It should be restated that this spin structure and therefore these results are only valid when all three particles in the final state are produced in the same reaction plane but are independent of their direction in the plane. This structure is a direct result of the mirror symmetry discussed in Section 2.1.

Identical Kaons

If the reaction includes identical kaons in the final state, the amplitude should be symmetric under their exchange. This added symmetry means that the findings for non-identical kaons can be extended to production angles where the relative momentum of the two kaons is perpendicular to the reaction plane, i.e., $\hat{p}' \cdot \hat{n}_2 = \pm 1$. This symmetry is most clearly seen if one couples the kaons, KK, in the final state instead of coupling the cascade with a kaon, $K\Xi$. Once the amplitude has been made symmetric, all terms with odd L' must be zero. Because of this, $\mathrm{Im}\left[D^{L'l}_{\beta M}\right] = 0$ when $\hat{p}' \cdot \hat{n}_2 = \pm 1$ and the results of Eq. 3.28 are valid again. Note that Eq. 3.28 is still true for scattering in the reaction plane, $\hat{p}' \cdot \hat{n}_2 = 0$. Production of identical kaons is therefore more readily analyzed in this way because it offers additional kinematic regions to employ these results.

3.2.3 Hard and soft meson photoproductions

In the previous section, we have considered two-meson photoproduction off a nucleon in its generality. In this section, we consider the case of a hard and a soft kaon production. Hard kaon production means that one of the two kaons, K, carries most of the momentum and, consequently, the (other) kaon-cascade pair ($K'\Xi$) is in the S-wave ($\vec{p}' \to 0$). The soft meson production means the other way around, i.e., one of the two kaons has low momentum ($\vec{q} \to 0$), basically in the s-wave, and the kaon-cascade pair ($K'\Xi$) carries most of the momentum. These correspond to the low- and high-energy region, respectively, in the $K'\Xi$ invariant mass distribution.

Let's first consider the hard meson production case. From the considerations in Appendix 3.5.4, we see that the coefficients $a^{\beta 0}_{L(L'l)}$ (Eq. (3.76)), $c^{\beta 1}_{L(L'l)}$ (Eq. (3.83)) $a^{\beta 2}_{L(L'l)}$, $b^{\beta 2}_{L(L'l)}$ and $c^{\beta 2}_{L(L'l)}$ (Eq. (3.88)), all vanish when $\vec{p}' \to 0$, i.e., they contain no $L' = 0$ partial waves. These lead to $F_i = 0$ ($i = 1, 4, 8, 9, 10$) and $\tilde{F}_4 = 0$ in Eq. (3.20). So, in this limit, the two-kaon photoproduction amplitude reduces to

$$\hat{M} = F_3\, \vec{\epsilon} \cdot \hat{n}_1 + \tilde{F}_2\, \vec{\epsilon} \cdot (\hat{k} \times \vec{\sigma}) + \tilde{F}_3\, \vec{\epsilon} \cdot (\hat{n}_1 \times \vec{\sigma}) + F_{11}\, \vec{\sigma} \cdot \hat{k} \vec{\epsilon} \cdot \hat{n}_2 + F_{12} \left[\vec{\sigma} \cdot \hat{n}_1 \vec{\epsilon} \cdot \hat{n}_2 + \vec{\sigma} \cdot \hat{n}_2 \vec{\epsilon} \cdot \hat{n}_1\right] , \quad (3.31)$$

and we are left with only four independent amplitudes $\{F_i\}$ to be determined. [2]

As discussed in Sec. 3.2, in the case of $\vec{q} = 0$ and $\vec{p}' \neq 0$, we should use the vectors $\vec{k}$ and $\vec{p}'$ to form a basis of three mutually orthogonal vectors instead of the vectors $\vec{k}$ and $\vec{q}$ as have been used so far in the present note. This means that the soft kaon production amplitude is given by Eq. (3.31) with the momenta $\vec{q}$ and $\vec{p}'$ interchanged everywhere ($\vec{q} \leftrightarrow \vec{p}'$), including in the definitions of $\hat{n}_1$ and $\hat{n}_2$ given by Eq. (3.14). Alternatively, we may just call $\vec{p}'$ the momentum of one of the produced kaons (K) and, $\vec{q}$ the relative momentum of the other meson with the cascade ($K'\Xi$) in all the expressions in this note.

3.3 Modeling the Photoproduction Amplitude

3.3.1 Modeling the Reaction $N \to K + K + \Xi$

In the present work, the amplitude, $\bar{T}$, for the reaction $N(p) \to K(q_1) + K(q_2) + \Xi(p')$ is simply obtained from the $\bar{K}$-induced reaction process of the previous section, by first turning the $\bar{K}$ leg around in the amplitude given by Eq. (3.33) (cf. Fig. 3.4), in addition to reversing the direction of the arrow. Then, the corresponding reaction amplitude is given as

$$\bar{T} = \bar{T}_r + \bar{T}_c \ . \tag{3.32}$$

A diagrammatic representation of $\bar{T}$ is given in Fig. 3.3.

The operation of turning one of the kaon legs and reversing the direction of the arrow corresponds to $|jm\rangle \to (-)^{j-m} \langle j - m|$, where $j = 1/2$ and m denote the isospin and its projection of that kaon, so that, $|K^-\rangle \to -\langle K^+|$ and $|\bar{K}^0\rangle \to \langle K^0|$. In addition, one should reverse the direction of the kaon momentum corresponding to the leg turned around. The amplitude $\bar{T}_r$ may be obtained directly by calculating the Feynman diagram of Fig. 3.3.

Let's now derive explicitly the amplitude $\bar{T}$ from T of the previous section. To this end we start

[2] The structure in Eq. (3.31) is equivalent (as it should be) to that given in Eq. (16) of Ref. [83] for a single pseudoscalar-meson photoproduction when the final state baryon B has a negative parity. Note that, in Ref. [83], the amplitude has been expanded using the set of momenta $(\hat{k}, \hat{q}, \hat{n}_2)$ instead of the set $(\hat{k}, \hat{n}_1, \hat{n}_2)$ used in this work. The two sets are related to each other by $\hat{q} = \cos\theta_q \hat{k} + \sin\theta_q \hat{n}_1$.

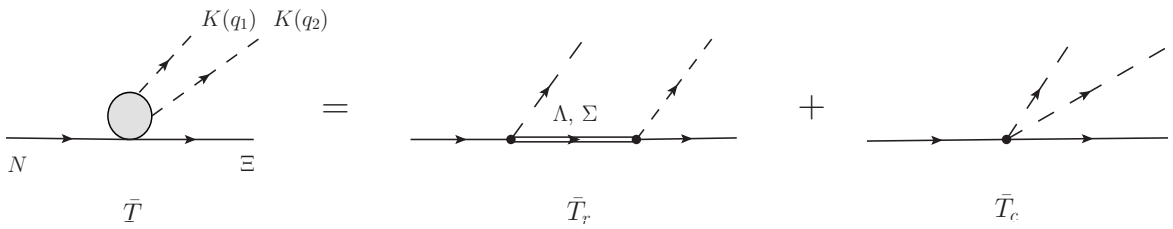

Figure 3.3: $\bar{T}_r$: Λ and Σ hyperon exchange amplitude obtained from T_r of Fig. 3.4. $\bar{T}_c$: contact amplitude obtained from T_c of Fig. 3.4. Symmetrization of the two kaons are not shown but it is implied.

with the reaction $\bar{K} + N \to K + \Xi$ and write the amplitude T as

$$T = T_r + T_c \ , \tag{3.33}$$

where T_r stands for the sum of the s- and u-channel Feynman diagrams as depicted in Fig. 3.4 and, T_c, for the phenomenological contact term also depicted in Fig. 3.4.

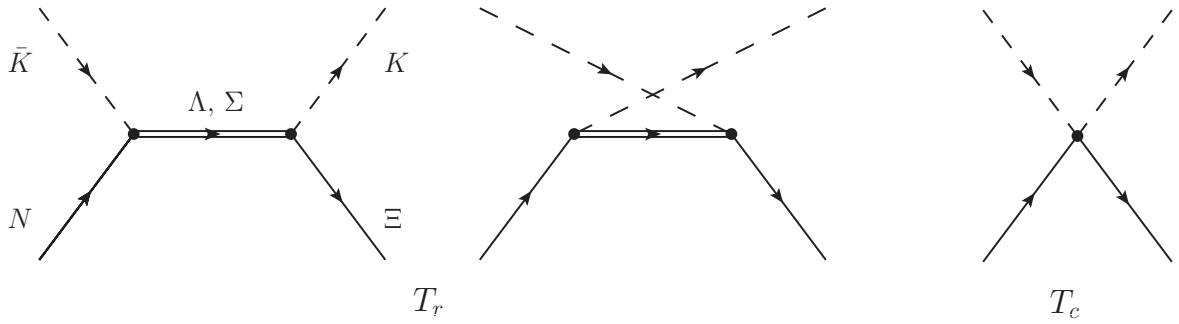

Figure 3.4: Diagrams included in the model of Ref. [122] and Section 2.2.1. T_r : s- plus u-channel Λ and Σ hyperon exchange amplitude. T_c: contact amplitude.

The partial wave decomposition of T in the center-of-momentum (c.m.) frame of the system is

$$\langle \frac{1}{2} m_{s'} \big| T(\vec{p}\,', \vec{p}) \big| \frac{1}{2} m_s \rangle = \sum (\frac{1}{2} m_{s'} L' M_{L'} \big| J M_J)(\frac{1}{2} m_s L M_L \big| J M_J)\ Y_{L'M_{L'}}(\hat{p}')\ Y^*_{LM_L}(\hat{p})\ T^{JT}_{L'L}(p', p) \hat{P}_T \ , \tag{3.34}$$

where the summation in Eq. (3.34) runs over all the quantum numbers not appearing on the left-hand-side of the equation. It should be noted that $L' = L$ by symmetry, but we keep them

distinguished for later convenience. $\hat{P}_I$ stands for the total isospin projection operator. Explicitly,

$$\hat{P}_{T=0} \equiv \frac{1}{4}\left(3 - \vec{\tau}_1 \cdot \vec{\tau}_2\right) \ , \qquad \hat{P}_{T=1} \equiv \frac{1}{4}\left(1 + \vec{\tau}_1 \cdot \vec{\tau}_2\right) \ , \tag{3.35}$$

for the total isospin $T = 0$ and $T = 1$, respectively. Note that the spin matrix element given by Eq. (3.34) is still an operator in isospin space. Now we perform the appropriate angular momenta recouplings and reverse the sign of the $\bar{K}$ momentum whose leg is turned around to obtain $\bar{T}$. We begin by writing

$$\begin{aligned} T(\vec{p}\,', \vec{p}) &= \sum_{m_{s'}, m_s} |\frac{1}{2} m_{s'}\rangle \, \langle \frac{1}{2} m_{s'} \big| T(\vec{p}\,', \vec{p}) \big| \frac{1}{2} m_s \rangle \, \langle \frac{1}{2} m_s | \\ &= \sum |JM_J\rangle \, T^{JT}_{L'L}(p', p) \overline{\langle JM_J|} \hat{P}_T \ , \end{aligned} \tag{3.36}$$

where

$$\begin{aligned} |JM_J\rangle &\equiv \sum_{m_{s'}, M_{L'}} (\frac{1}{2} m_{s'} L' M_{L'} | JM_J) \ Y_{L'M_{L'}}(\hat{p}') \ |\frac{1}{2} m_{s'}\rangle \ , \\ \overline{\langle JM_J|} &\equiv \sum_{m_s, M_L} (\frac{1}{2} m_s L M_L | JM_J) \ Y^*_{LM_L}(\hat{p}) \ \langle \frac{1}{2} m_s| \ . \end{aligned} \tag{3.37}$$

Using the identity

$$\begin{aligned} (l0l'0|L0) \frac{\sqrt{4\pi}}{[L]} \ Y_{LM_L}(\hat{p}) &= \frac{4\pi}{[ll']} \sum_{m_l, m_{l'}} (l, m_l l' m_{l'} | LM_L) \ Y_{lm_l}(\hat{p}) \ Y_{l'm_{l'}}(\hat{p}) \\ &= \frac{4\pi}{[ll']} (-)^{l'} \sum_{m_l, m_{l'}} (l, m_l l' m_{l'} | LM_L) \ Y_{lm_l}(\hat{p}) \ Y_{l'm_{l'}}(-\hat{p}) \ , \end{aligned} \tag{3.38}$$

with $[j_1...j_n] \equiv \sqrt{2j+1}...\sqrt{2j_n+1}$, the last quantity in Eq. (3.37) can be rewritten as

$$\begin{aligned}\overline{\langle JM_J|} \equiv \sqrt{4\pi}\frac{[L]}{[ll']}\frac{(-)^{l'}}{(l0l'0|L0)}\sum_{m_s,M_L}(\frac{1}{2}m_sLM_L|JM_J)\ \langle\frac{1}{2}m_s|\sum_{m_l,m_{l'}}(l,m_ll'm_{l'}|LM_L)\ Y^*_{lm_l}(\hat{p})\ Y^*_{l'm_{l'}}(-\hat{p})\\ = \sqrt{4\pi}\frac{[JL]}{[ll']}\frac{(-)^{-J+\frac{1}{2}}}{(l0l'0|L0)}\sum_{M_L}(LM_LL-M_L|00)\Big[\sum_{m_l,m_{l'}}(l,m_ll'm_{l'}|LM_L)\ Y_{lm_l}(\hat{p})\ Y_{l'm_{l'}}(-\hat{p})\Big]\\ \times\sum_{m_s}(\frac{1}{2}m_sJM_J|L-M_L)\ B_{\frac{1}{2}m_s}\ ,\end{aligned} \tag{3.39}$$

where we have introduced the notation $B_{\frac{1}{2}m_s} \equiv (-)^{\frac{1}{2}-m_s}\langle\frac{1}{2}-m_s|$.

Inserting Eq. (3.39) into Eq. (3.36), we obtain

$$\begin{aligned}T(\vec{p}\,',\vec{p}) = \sum\sqrt{4\pi}\frac{[JL]}{[ll']}\frac{(-)^{-J+\frac{1}{2}}}{(l0l'0|L0)}\ T^{JT}_{L'L}(p',p)\hat{P}_T\sum_{M_L}(LM_LL-M_L|00)\\ \times\Big[\sum_{m_l,m_{l'}}(l,m_ll'm_{l'}|LM_L)\ Y_{lm_l}(\hat{p})\ Y_{l'm_{l'}}(-\hat{p})\Big]\Big[\sum_{m_s,M_J}(\frac{1}{2}m_sJM_J|L-M_L)\ B_{\frac{1}{2}m_s}\,|JM_J\rangle\Big]\ .\end{aligned} \tag{3.40}$$

The above form of T is suited for angular momenta recouplings. Performing the appropriate recouplings, we have

$$\begin{aligned}T(\vec{p}\,',\vec{p}) = \sum\sqrt{4\pi}\frac{[JL]}{[ll']}\frac{(-)^{-J-l'-j}}{(l0l'0|L0)}\ T^{JT}_{L'L}(p',p)[jL]\begin{Bmatrix}l & l' & L\\ J & \frac{1}{2} & j\end{Bmatrix}\sum_{m_j}(jm_jj-m_j|00)\\ \times\Big[\sum_{m_{l'}M_J}(l'm_{l'}JM_J|jm_j)\ Y_{l'm_{l'}}(-\hat{p})\,|JM_J\rangle\Big]\Big[\sum_{m_lm_s}(lm_l\frac{1}{2}m_s|j-m_j)\ Y_{lm_l}(\hat{p})\ B_{\frac{1}{2}m_s}\Big]\hat{P}_T\\ = \sum\sqrt{4\pi}\frac{[JL]}{[jll']}\frac{(-)^{-J+L+j}}{(l0l'0|L0)}\ T^{JT}_{L'L}(p',p)[jL]\begin{Bmatrix}l & l' & L\\ J & \frac{1}{2} & L\end{Bmatrix}\\ \times\sum_{m_j}\Big[\sum_{m_{l'}M_J}(l'm_{l'}JM_J|jm_j)\ Y_{l'm_{l'}}(-\hat{p})\,|JM_J\rangle\Big]\Big[\sum_{m_sm_l}(\frac{1}{2}m_slm_l|jm_j)\ Y^*_{lm_l}(\hat{p})\ \langle\frac{1}{2}m_s|\Big]\hat{P}_T\ .\end{aligned} \tag{3.41}$$

Finally, to obtain $\bar{T}$ from T given above, we reverse the direction of the $\bar{K}$ momentum (note that in the c.m. frame of $\bar{K}N$, $\vec{p}$ is the nucleon momentum and, $-\vec{p}$, the $\bar{K}$ momentum). This is

done by using the relation $Y_{l'm_{l'}}(-\hat{p}) = (-)^{l'} Y_{l'm_{l'}}(\hat{p})$. We then have

$$\bar{T}(\vec{q}_1, \vec{q}_2, \vec{p}\,'; \vec{p}) = \sum \left[|\frac{1}{2} m_{s'}\rangle \langle \frac{1}{2} m_s| \right] \hat{P}_T (\frac{1}{2} m_{s'} L' M_{L'} | J M_J) Y_{L'M_{L'}}(\hat{p}') \; (l' m_{l'} J M_J | j m_j) \\ \times Y_{l'm_{l'}}(\hat{q}_1) \; (\frac{1}{2} m_s l m_l | j m_j) Y^*_{lm_l}(\hat{p}) \; \bar{T}^{jJT}_{l'L'l}(q_1, q_2, p'; p) \; , \tag{3.42}$$

with $\vec{q}_1 \equiv \vec{p}$ denoting the momentum of the outgoing kaon (in the c.m. frame of the final $K\Xi$ subsystem) obtained by turning the $\bar{K}$ from the initial state to the final state. $\vec{q}_2 = -\vec{p}\,'$ is the momentum of the other kaon. We have also used Eq. (3.37) for $|JM_J\rangle$. The partial-wave matrix element $\bar{T}^{jJI}_{l'L'l}(q_1, q_2, p'; p)$ in the above equation is given by

$$\bar{T}^{jJT}_{l'L'l}(q_1, q_2, p'; p) = \sqrt{4\pi} \sum_L \frac{[JL]}{[jll']} \frac{(-)^{-J+l'+L+j}}{(l0l'0|L0)} \; T^{JT}_{L'L}(p', p)[jL] \begin{Bmatrix} l & l' & L \\ J & \frac{1}{2} & L \end{Bmatrix} . \tag{3.43}$$

Note that $T^{JI}_{L'L}(p', p)$ is non-vanishing only for $L = L'$, so the summation over L reduces actually to a single term.

Taking the spin matrix element of $\bar{T}$ in Eq. (3.42), we have

$$\langle \frac{1}{2} m_{s'} | \bar{T}(\vec{q}_1, \vec{q}_2, \vec{p}\,'; \vec{p}) | \frac{1}{2} m_s \rangle = \sum (\frac{1}{2} m_{s'} L' M_{L'} | J M_J) \; Y_{L'M_{L'}}(\hat{p}') \; (l' m_{l'} J M_J | j m_j) \; Y_{l'm_{l'}}(\hat{q}_1) \\ \times \bar{T}^{jJT}_{l'L'l}(q_1, q_2, p'; p) \; (\frac{1}{2} m_s l m_l | j m_j) \; Y^*_{lm_l}(\hat{p}) \; \hat{P}_T \; . \tag{3.44}$$

3.3.2 Current from $\bar{T}_r$

As discussed in Section 3.1, the photoproduction amplitude is found by attaching the photon everywhere in the $N \to K + K + \Xi$ amplitude, $\bar{T}$. This amplitude was decomposed into $\bar{T} = \bar{T}_r + \bar{T}_c$. The process of attaching a photon everywhere in $\bar{T}_r$ has been done in Ref. [54] and here we briefly discuss what was done there.

Attaching to the external kaon legs is done via diagrams (a) and (b) in Figure 3.5. Attaching to the external baryon legs is shown in diagrams (c) and (e) with $N' = N$ and $\Xi' = \Xi$. Attaching the photon to the internal structure of $\bar{T}_r$ is shown in diagrams (f), (g), and (d) with $Y' = Y$. It should be pointed out that diagrams with $N' \neq N$, $\Xi' \neq \Xi$, $Y' \neq Y$, and K^* exchanges can

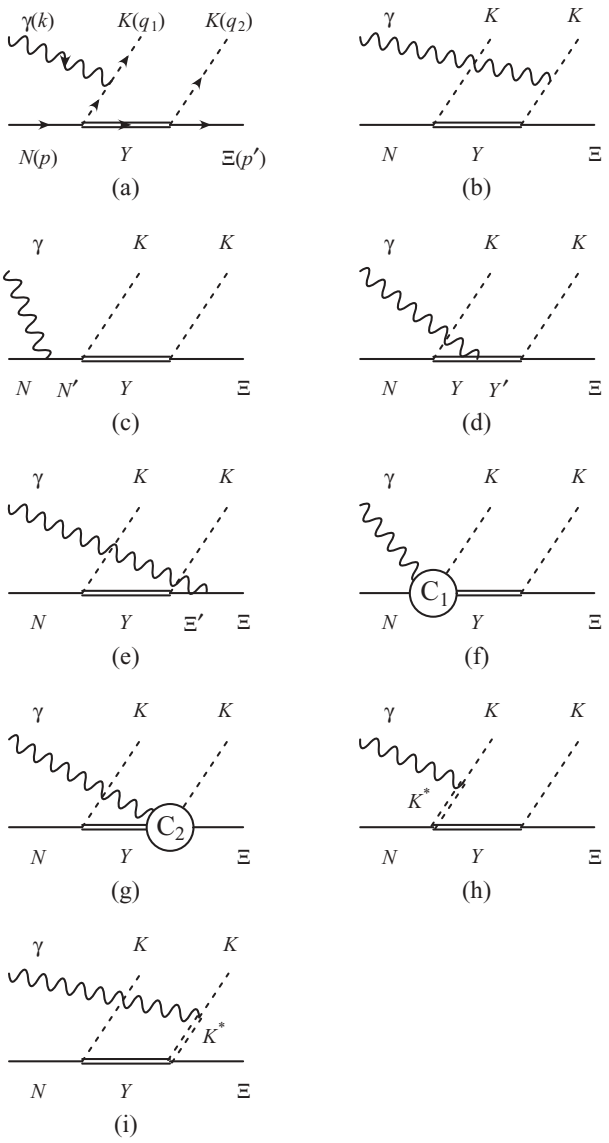

Figure 3.5: Diagrams included in Ref. [54]. The intermediate baryon states are denoted as N' for the nucleon and Δ resonances, Y, Y' for the Λ and Σ resonances, and Ξ' for $\Xi(1318)$ and $\Xi(1530)$. The intermediate mesons in the t channel are K [(a) and (b)] and K^* [(h) and (i)]. The diagrams (f) and (g) contain the generalized contact currents that maintain gauge invariance of $\bar{T}_r$. Diagrams corresponding to (a)$-$(i) with $K(q_1) \leftrightarrow K(q_2)$ are also understood.

not be obtained by the gauge derivative technique described in Section 3.1 but are transverse amplitudes, $k_\mu M^\mu = 0$, and therefore do not disturb the Ward-Takahashi identity. These diagrams

are easily identifiable and are included by hand. The contact terms C_1 and C_2 of (f) and (g) are the generalized 4-point contact terms which arise from form-factors used in the vertices and also include the usual Kroll-Ruderman contact currents. For further detail, see Ref. [54].

3.3.3 External Current from $\bar{T}_c$

Here, we calculate the external currents arising from the photon attaching to the external legs of $\bar{T}_c$ (cf. Fig. 3.1). Since $\bar{T}_c$ is obtained from a direct parametrization of the (physical) on-shell amplitude T_c, there is no information on the matrix elements of $\bar{T}_c$ involving wave functions corresponding to negative-energy particle propagations. We therefore set those contributions to be identically zero in the c.m. frame of the $K\Xi$ pair in the $N \to KK\Xi$ subsystem. Note that this implies that we must evaluate the photoproduction amplitude M_c^μ arising from $\bar{T}_c$ in that frame, where we can drop the negative-energy baryon and kaon propagations in their propagators.

The spin-1/2 baryon propagator can be decomposed into a positive- and a negative-energy propagation part as

$$S_j(p) = \left(\frac{m}{\varepsilon_j(p)}\right) \sum_{m_s} \left(\frac{|u_j(\vec{p}, m_s)\rangle \langle \bar{u}_j(\vec{p}, m_s)|}{p_0 - \varepsilon_j(p) + i\eta} + \frac{|v_j(-\vec{p}, m_s)\rangle \langle \bar{v}_j(-\vec{p}, m_s)|}{p_0 + \varepsilon_j(p) - i\eta} \right) . \tag{3.45}$$

Analogously, the pseudoscalar-meson propagator can be decomposed as

$$\Delta(q) = \frac{1}{2\omega(q)} \left(\frac{1}{q_0 - \omega(q) + i\eta} - \frac{1}{q_0 + \omega(q) - i\eta} \right) . \tag{3.46}$$

Using the above decomposition of the propagators, we have, for the external currents in the c.m. frame of the $K\Xi$ pair in the $N \to KK\Xi$ subsystem, the following:

$$\begin{aligned} \bar{T}^\mu_{cN} &\equiv \langle \bar{u}_\Xi(\vec{p}\,', m_{s'}) \big| \bar{T}_c \; iS_N \; \Gamma^\mu_{NN\gamma} \big| u_N(\vec{p}, m_s) \rangle \\ &= i \frac{m_N}{\varepsilon_N(p'')} \sum_{m_{s''}} \langle \frac{1}{2} m_{s'} \big| \bar{T}_c(\vec{q}_1, \vec{q}_2, \vec{p}\,'; \vec{p}\,'') \big| \frac{1}{2} m_{s''} \rangle \, \frac{1}{p''_0 - \varepsilon_N(p'') + i\eta} \\ &\qquad \times \langle \bar{u}_N(\vec{p}\,'', m_{s''}) \big| \Gamma^\mu_{NN\gamma}(k) \big| u_N(\vec{p}, m_s) \rangle \ , \end{aligned} \tag{3.47}$$

where the intermediate nucleon four-momentum is $p'' = p + k$. Note that, here, $\vec{q}_2 = -\vec{p}\,'$.

$$\bar{T}^{\mu}_{cK_1} \equiv \langle \bar{u}_{\Xi}(\vec{p}',m_{s'})\big|\Gamma^{\mu}_{K_1K_1\gamma}\ i\Delta_{K_1}\bar{T}_c\big|u_N(\vec{p},m_s)\rangle$$
$$= i\frac{1}{2\omega_(q'')}\Gamma^{\mu}_{K_1K_1\gamma}(q_1,q'')\frac{1}{q''_0-\omega(q'')+i\eta}\,\langle\frac{1}{2}m_{s'}\big|\bar{T}_c(\vec{q}'',\vec{q}_2,\vec{p}';\vec{p})\big|\frac{1}{2}m_s\rangle\ , \tag{3.48}$$

where the four-momentum of the intermediate kaon is $q''=q_1-k$. Here also, $\vec{q}_2=-\vec{p}'$.

$$\bar{T}^{\mu}_{cK_2} \equiv \langle \bar{u}_{\Xi}(\vec{p}',m_{s'})\big|\Gamma^{\mu}_{K_2K_2\gamma}\ i\Delta_{K_2}\bar{T}_c\big|u_N(\vec{p},m_s)\rangle$$
$$= i\frac{1}{2\omega_(q'')}\Gamma^{\mu}_{K_2K_2\gamma}(q_2,q'')\frac{1}{q''_0-\omega(q'')+i\eta}\,\langle\frac{1}{2}m_{s'}\big|\bar{T}_c(\vec{q}_1,\vec{q}'',\vec{p}';\vec{p})\big|\frac{1}{2}m_s\rangle\ , \tag{3.49}$$

where the four-momentum of the intermediate kaon is $q''=q_2-k$. Note here that $\vec{q}_1=\vec{p}$.

$$\bar{T}^{\mu}_{c\Xi} \equiv \langle \bar{u}_{\Xi}(\vec{p}',m_{s'})\big|\Gamma^{\mu}_{\Xi\Xi\gamma}\ iS_{\Xi}\ \bar{T}_c\ \big|u_N(\vec{p},m_s)\rangle$$
$$= i\frac{m_{\Xi}}{\varepsilon_{\Xi}(p'')}\sum_{m_{s''}}\langle \bar{u}_{\Xi}(\vec{p}',m_{s'})\big|\Gamma^{\mu}_{\Xi\Xi\gamma}(k)\big|u_{\Xi}(\vec{p}'',m_{s''})\rangle\,\frac{1}{p''_0-\varepsilon_{\Xi}(p'')+i\eta}$$
$$\times\,\langle\frac{1}{2}m_{s''}\big|\bar{T}_c(\vec{q}_1,\vec{q}_2,\vec{p}'';\vec{p})\big|\frac{1}{2}m_s\rangle\ , \tag{3.50}$$

where the intermediate Ξ four-momentum is $p''=p'-k$. Also, $\vec{q}_1=\vec{p}$.

Note that the $\bar{T}^{\mu}_{ci}$ $(i=N,K_1,K_2,\Xi)$ above is Lorentz invariant since $\bar{T}_c$ is Lorentz invariant. Thus, it can be readily obtained in any Lorentz frame once it is evaluated in the c.m. frame of the $K\Xi$ pair in the $N\to KK\Xi$ subsystem.

3.3.4 Phenomenological five-point contact current

In Ref. [53], $\bar{T}^{\mu}_r$ has been constructed (see Fig. 3.1) which satisfies Eq. (3.5). To construct the five point contact current $\bar{T}^{\mu}_c$ – corresponding to the pure phenomenological contact amplitude $\bar{T}_c$ –

that obeys Eq. (3.5), we follow Ref. [123] and make the ansatz

$$\begin{aligned}\bar{T}_c^{\mu} = &-\Big[\bar{T}_c(q_1,q_2,p';p+k) - W(q_1,q_2,p';p,k)\Big]\frac{Q_N(2p+k)^{\mu}}{(p+k)^2-p^2}\\ &-\frac{Q_{\Xi}(2p'-k)^{\mu}}{(p'-k)^2-p'^2}\Big[\bar{T}_c(q_1,q_2,p'-k;p) - W(q_1,q_2,p';p,k)\Big]\\ &-\frac{Q_{K_1}(2q_1-k)^{\mu}}{(q_1-k)^2-q_1^2}\Big[\bar{T}_c(q_1-k,q_2,p';p) - W(q_1,q_2,p';p,k)\Big]\\ &-\frac{Q_{K_2}(2q_2-k)^{\mu}}{(q_2-k)^2-q_2^2}\Big[\bar{T}_c(q_1,q_2-k,p';p) - W(q_1,q_2,p';p,k)\Big]\ , \end{aligned} \tag{3.51}$$

where Q_i denotes the charge operator for particle i and W is a function to be chosen to ensure that each term here is free of propagator singularities. It is trivial to verify that $\bar{T}_c^{\mu}$ given above satisfies Eq. (3.5) due to total charge conservation $Q_N - Q_{\Xi} - Q_{K_1} - Q_{K_2} = 0$.

The simplest choice of the function W in Eq. (3.51) may be

$$\begin{aligned}W(q_1,q_2,p';p,k) =&\bar{T}_c(q_1,q_2,p';p)\\ &+\big[(p+k)^2-p^2\big]\big[(p'-k)^2-p'^2\big]\big[(q_1-k)^2-q_1^2\big]\big[(q_2-k)^2-q_2^2\big]R(q_1,q_2,p';p,k)\ ,\end{aligned} \tag{3.52}$$

where $R(q_1,q_2,p';p,k)$, except for symmetry constraints, is largely arbitrary (and may be equal to zero).

Finally, we should mention that there are diagrams contributing to the photoproduction amplitude that cannot be obtained by the gauge derivative method employed here. However, those diagrams are all transverse currents and, therefore, do not affect gauge invariance of the full amplitude. They are included in our model [53].

3.4 Chapter Summary

The Ward-Takahashi Identity must be satisfied for an amplitude to be gauge invariant. Because our model for $\bar{K}+N \to K+\Xi$ had several independent amplitudes, namely T_r and T_c, the corresponding interaction currents are expected to satisfy the WTI individually for interaction currents and are

thereby constrained by the gauge invariance condition. A general photoproduction model consistent with the $\bar{K}+N \rightarrow K+\Xi$ model used in the previous chapter was presented. The interaction current associated with T_r has been developed in Ref. [53] and this model was adopted here. Following Ref. [123], an interaction current associated with the phenomenological contact amplitude, T_c, was given.

It was shown in the previous chapter that spin observables are important in discerning the spin and parity of produced Ξ or Ξ^*. To that end, we decompose the production amplitude for $\gamma + N \rightarrow K + K + \Xi(\Xi^*)$ into it's most general spin structures and derive the angular dependence of each of these. Parity conservation puts a restriction on the angular dependence of each spin amplitude. Because the reaction has a 3-body final state, this angular dependence is much more complicated than the two-body $\bar{K}$-induced reaction and the reflection symmetry is not as easily exploited. Nonetheless, for certain production angles, this symmetry has serious consequences, especially for the case where two identical Kaons are created. The spin observables are calculated based on these spin amplitudes and a set of observables that is sensitive to the Ξ or Ξ^* parity is given. This analysis is only done for spin-1/2 Ξs but is a general procedure and may be extended to higher spin resonances.

3.5 Appendixes

3.5.1 Appendix F: $a^{\beta 0}_{L(L'l)}$, $a^{\beta 1}_{L(L'l)}$, $b^{\beta 1}_{L(L'l)}$, $c^{\beta 1}_{L(L'l)}$

The quantity $a^{\beta 0}_{L(L'l)}$ in Eq. (3.15) can be calculated directly from the definition of $[X_{l(L'l)\beta}]^{\alpha}$ given by Eq. (3.11). We have

$$a^{\beta 0}_{L(L'l)} = \delta_{\beta L}(L0L0|00)\frac{[L]}{\sqrt{4\pi}}D^{L'l}_{L0} = \delta_{\beta L}\frac{(-)^L}{\sqrt{4\pi}}D^{L'l}_{L0} \ . \tag{3.53}$$

To extract the coefficients $a^{\beta 1}_{L(L'l)}$, $b^{\beta 1}_{L(L'l)}$ and $c^{\beta 1}_{L(L'l)}$ in Eq.(3.55), we start by expanding $[X_{L\,(L'l)\beta}]^1$ in terms of the complete set of mutually orthogonal vectors $\{\hat{e}_m\}$ $(m = 0, \pm 1)$, i.e.,

$$[X_{L\,(L'l)\beta}]^1 = \sum_{m=-1}^{+1} a_m\,\hat{e}_m \ , \tag{3.54}$$

where $a_m = [X_{L\,(L'l)\beta}]^1 \cdot \hat{e}_m$. It is, then, immediate that

$$\begin{aligned}
[X_{L\,(L'l)\beta}]^1 &= \frac{[L]}{\sqrt{4\pi}}\left\{(L0\beta 0|10)D^{L'l}_{\beta 0}\,\hat{e}_0 - (L0\beta 1|11)D^{L'l}_{\beta 1}\,\hat{e}_{-1} - (L0\beta-1|1-1)D^{L'l}_{\beta -1}\,\hat{e}_{+1}\right\} \\
&= \frac{[L]}{\sqrt{4\pi}}\left\{(L0\beta 0|10)D^{L'l}_{\beta 0}\,\hat{e}_0 - (L0\beta 1|11)\left[D^{L'l}_{\beta 1}\,\hat{e}_{-1} + (-)^{L+L'+l}D^{L'l^*}_{\beta 1}\,\hat{e}_{+1}\right]\right\} \\
&= \frac{[L]}{\sqrt{4\pi}}\left\{(L0\beta 0|10)D^{L'l}_{\beta 0}\,\hat{k} - \frac{1}{\sqrt{2}}(L0\beta 1|11)\right. \\
&\qquad \left.\times\left[\left(D^{L'l}_{\beta 1} - (-)^{L+L'+l}D^{L'l^*}_{\beta 1}\right)\hat{n}_1 - i\left(D^{L'l}_{\beta 1} + (-)^{L+L'+l}D^{L'l^*}_{\beta 1}\right)\hat{n}_2\right]\right\} \ ,
\end{aligned} \tag{3.55}$$

where we have used the property

$$D^{L'l}_{\beta -M} = (-)^{L'+l-\beta+M}D^{L'l\ *}_{\beta M} \ . \tag{3.56}$$

From Eq. (3.55), the coefficients $a^{\beta 1}_{L(L'l)}$, $b^{\beta 1}_{L(L'l)}$ and $c^{\beta 1}_{L(L'l)}$ in Eq. (3.15) can be identified as

$$\begin{aligned}
a^{\beta 1}_{L(L'l)} &= \frac{[L]}{\sqrt{4\pi}}(L0\beta 0|10)D^{L'l}_{\beta 0} \ , \\
&= \frac{[L]}{\sqrt{4\pi}}(L0\beta 0|10)\frac{1}{2}\left(D^{L'l}_{\beta 0} + \pi_B D^{L'l^*}_{\beta 0}\right) \ , \\
b^{\beta 1}_{L(L'l)} &= -\frac{[L]}{\sqrt{4\pi}}(L0\beta 1|11)\frac{1}{\sqrt{2}}\left(D^{L'l}_{\beta 1} - (-)^{L+L'+l}D^{L'l^*}_{\beta 1}\right) \ , \\
&= -\frac{[L]}{\sqrt{4\pi}}(L0\beta 1|11)\frac{1}{\sqrt{2}}\left(D^{L'l}_{\beta 1} + \pi_B D^{L'l^*}_{\beta 1}\right) \ , \\
c^{\beta 1}_{L(L'l)} &= -\frac{[L]}{\sqrt{4\pi}}(L0\beta 1|11)\frac{-i}{\sqrt{2}}\left(D^{L'l}_{\beta 1} + (-)^{L+L'+l}D^{L'l^*}_{\beta 1}\right) \ . \\
&= \frac{[L]}{\sqrt{4\pi}}(L0\beta 1|11)\frac{i}{\sqrt{2}}\left(D^{L'l}_{\beta 1} - \pi_B D^{L'l^*}_{\beta 1}\right)
\end{aligned} \tag{3.57}$$

In Appendix 3.5.4, the above results are particularized for the case of a positive and negative baryon B.

3.5.2 Appendix G: $a^{\beta 2}_{L(L'l)}$, $b^{\beta 2}_{L(L'l)}$, $c^{\beta 2}_{L(L'l)}$, $a'^{\beta 2}_{L(L'l)}$, $b'^{\beta 2}_{L(L'l)}$

Taking the scalar product of the last equality in Eq.(3.15) with $[\hat{k}\otimes\hat{k}]^2$, $[\hat{n}_1\otimes\hat{n}_1]^2$, $[\hat{k}\otimes\hat{n}_1]^2$, $[\hat{k}\otimes\hat{n}_2]^2$ and $[\hat{n}_1\otimes\hat{n}_2]^2$, respectively, and using the results

$$\begin{aligned}
[\hat{k}\otimes\hat{k}]^2\cdot[\hat{k}\otimes\hat{k}]^2 &= [\hat{n}_1\otimes\hat{n}_1]^2\cdot[\hat{n_1}\otimes\hat{n}_1]^2 = \frac{2}{3} \ , \\
[\hat{k}\otimes\hat{k}]^2\cdot[\hat{n}_1\otimes\hat{n}_1]^2 &= -\frac{1}{3} \ , \\
[\hat{k}\otimes\hat{n}_1]^2\cdot[\hat{k}\otimes\hat{n}_1]^2 &= \frac{1}{2} \ , \\
[\hat{k}\otimes\hat{n}_2]^2\cdot[\hat{k}\otimes\hat{n}_2]^2 &= \frac{1}{2} \ , \\
[\hat{n}_1\otimes\hat{n}_2]^2\cdot[\hat{n}_1\otimes\hat{n}_2]^2 &= \frac{1}{2} \ ,
\end{aligned} \tag{3.58}$$

with all the other scalar products vanishing identically (because they involve a pair of different parity tensors), we have

$$\begin{aligned} a^{\beta 2}_{L(L'l)} &= 2u + v \ , \\ b^{\beta 2}_{L(L'l)} &= u + 2v \ , \\ c^{\beta 2}_{L(L'l)} &= 2w \ , \\ a'^{\beta 2}_{L(L'l)} &= 2r \ , \\ b'^{\beta 2}_{L(L'l)} &= 2t \ , \end{aligned} \tag{3.59}$$

where

$$\begin{aligned} u &\equiv [Y_L(\hat{k}) \otimes D^{L'l}_{\beta}(\hat{p}', \hat{q})]^2 \cdot [\hat{k} \otimes \hat{k}]^2 \ , \\ v &\equiv [Y_L(\hat{k}) \otimes D^{L'l}_{\beta}(\hat{p}', \hat{q})]^2 \cdot [\hat{n}_1 \otimes \hat{n}_1]^2 \\ w &\equiv [Y_L(\hat{k}) \otimes D^{L'l}_{\beta}(\hat{p}', \hat{q})]^2 \cdot [\hat{k} \otimes \hat{n}_1]^2 \\ r &\equiv [Y_L(\hat{k}) \otimes D^{L'l}_{\beta}(\hat{p}', \hat{q})]^2 \cdot [\hat{k} \otimes \hat{n}_2]^2 \ , \\ t &\equiv [Y_L(\hat{k}) \otimes D^{L'l}_{\beta}(\hat{p}', \hat{q})]^2 \cdot [\hat{n}_1 \otimes \hat{n}_2]^2 \end{aligned} \tag{3.60}$$

Choosing the quantization axis $\hat{z}$ along $\vec{k}$ and $\vec{q}$ in the xz-plane, the quantities u, v, w, r and t can be expressed without loss of generality as (using the relations given in the following subsection in this Appendix)

$$
\begin{aligned}
u &= \frac{1}{\sqrt{4\pi}}\sqrt{\frac{2}{3}}[L](L0\beta 0|20)D^{L'l}_{\beta 0}\ , \\
&= \frac{[L]}{\sqrt{4\pi}}\sqrt{\frac{1}{6}}(L0\beta 0|20)\left(D^{L'l}_{\beta 0}-\pi_B D^{L'l^*}_{\beta 0}\right)\ , \\
v &= \sqrt{\frac{2}{15}}[L]\sum_M (-)^M (L0\beta M|2M)D^{L'l}_{\beta M}Y_{2-M}(\hat{n}_1) \\
&= \sqrt{\frac{2}{15}}[L]\left[(L0\beta 0|20)\,Y_{20}(\hat{n}_1)D^{L'l}_{\beta 0}-(L0\beta 1|21)\,Y_{21}(\hat{n}_1)\left(D^{L'l}_{\beta 1}+(-)^{L+L'+l}D^{L'l^*}_{\beta 1}\right)\right. \\
&\qquad\qquad \left.+(L0\beta 2|22)\,Y_{22}(\hat{n}_1)\left(D^{L'l}_{\beta 2}+(-)^{L+L'+l}D^{L'l^*}_{\beta 2}\right)\right]\ , \\
&= \frac{[L]}{\sqrt{4\pi}}\left[-\frac{1}{\sqrt{6}}(L0\beta 0|20)D^{L'l}_{\beta 0}+\frac{1}{2}(L0\beta 2|22)\left(D^{L'l}_{\beta 2}-\pi_B D^{L'l^*}_{\beta 2}\right)\right]\ , \\
w &= \frac{[L]}{\sqrt{3}}\sum_M (-)^M (L0\beta M|2M)(101M|2M)D^{L'l}_{\beta M}Y_{1-M}(\hat{n}_1) \\
&= \frac{[L]}{\sqrt{3}}\left[(L0\beta 0|20)(1010|20)D^{L'l}_{\beta 0}Y_{10}(\hat{n}_1)-(L0\beta 1|21)(1011|21)\left(D^{L'l}_{\beta 1}+(-)^{L+L'+l}D^{L'l^*}_{\beta 1}\right)Y_{11}(\hat{n}_1)\right]\ , \\
&= -\frac{[L]}{\sqrt{4\pi}}\frac{1}{2}(L0\beta 1|21)\left(D^{L'l}_{\beta 1}-\pi_B D^{L'l^*}_{\beta 1}\right)\ , \\
r &= \frac{[L]}{\sqrt{3}}\sum_M (-)^M (L0\beta M|2M)(101M|2M)D^{L'l}_{\beta M}Y_{1-M}(\hat{n}_2) \\
&= \frac{[L]}{\sqrt{3}}\left[(L0\beta 0|20)(1010|20)D^{L'l}_{\beta 0}Y_{10}(\hat{n}_2)-(L0\beta 1|21)(1011|21)\left(D^{L'l}_{\beta 1}-(-)^{L+L'+l}D^{L'l^*}_{\beta 1}\right)Y_{11}(\hat{n}_2)\right]\ , \\
&= i\frac{[L]}{\sqrt{4\pi}}\frac{1}{2}(L0\beta 1|21)\left(D^{L'l}_{\beta 1}+\pi_B D^{L'l^*}_{\beta 1}\right)\ , \\
t &= \frac{\sqrt{4\pi}}{3}[L]\sum_M (-)^M (L0\beta M|2M)D^{L'l}_{\beta M}[Y_1(\hat{n}_1)\otimes Y_1(\hat{n}_2)]^2_{-M} \\
&= \frac{\sqrt{4\pi}}{3}[L]\left[(L0\beta 0|20)D^{L'l}_{\beta 0}[Y_1(\hat{n}_1)\otimes Y_1(\hat{n}_2)]^2_0-(L0\beta 1|21)\left(D^{L'l}_{\beta 1}-(-)^{L+L'+l}D^{L'l^*}_{\beta 1}\right)[Y_1(\hat{n}_1)\otimes Y_1(\hat{n}_2)]^2_1\right. \\
&\qquad\qquad \left.+(L0\beta 2|22)\left(D^{L'l}_{\beta 2}-(-)^{L+L'+l}D^{L'l^*}_{\beta 2}\right)[Y_1(\hat{n}_1)\otimes Y_1(\hat{n}_2)]^2_2\right] \\
&= -i\frac{[L]}{\sqrt{4\pi}}\frac{1}{2}(L0\beta 2|22)\left(D^{L'l}_{\beta 2}+\pi_B D^{L'l^*}_{\beta 2}\right)\ .
\end{aligned}
\tag{3.61}
$$

In Appendix 3.5.4, the above results are particularized for the case of a hyperon $\Xi(\Xi^*)$ with parity π_B.

3.5.3 Appendix H: $\mathcal{M}_i$

The coefficients $\mathcal{M}_i$ in Eq. (3.16) are given by

$$\mathcal{M}_1 = \frac{\pi_B}{2\sqrt{3}} \sum i^{L-L'-l}(-)^{J+\frac{1}{2}}[J'][J]^2 M_{lL'L}^{\frac{1}{2}J'\frac{1}{2}J}(q,p';k) \begin{Bmatrix} \frac{1}{2} & L' & J' \\ l & J & L \end{Bmatrix} a^{L0}_{L(L'l)} \ , \tag{3.62}$$

$$\mathcal{M}_2 = \sum i^{L-L'-l}(-)^{L'+l+1}[J'][J]^2 M_{lL'L}^{\frac{1}{2}J'SJ}(q,p';k) \times \sum_\beta [\beta] \begin{Bmatrix} \frac{1}{2} & L' & J' \\ l & J & \beta \end{Bmatrix} \left[\frac{1}{\sqrt{6}} \begin{Bmatrix} \frac{1}{2} & L & J \\ \beta & \frac{1}{2} & 1 \end{Bmatrix} \delta_{S,\frac{1}{2}} + \frac{1}{\sqrt{3}} \begin{Bmatrix} \frac{3}{2} & L & J \\ \beta & \frac{1}{2} & 1 \end{Bmatrix} \delta_{S,\frac{3}{2}} \right] a^{\beta 1}_{L(L'l)} \ , \tag{3.63}$$

$$\mathcal{M}_3 = \sum i^{L-L'-l}(-)^{L'+l+1}[J'][J]^2 M_{lL'L}^{\frac{1}{2}J'SJ}(q,p';k) \times \sum_\beta [\beta] \begin{Bmatrix} \frac{1}{2} & L' & J' \\ l & J & \beta \end{Bmatrix} \left[\frac{1}{\sqrt{6}} \begin{Bmatrix} \frac{1}{2} & L & J \\ \beta & \frac{1}{2} & 1 \end{Bmatrix} \delta_{S,\frac{1}{2}} + \frac{1}{\sqrt{3}} \begin{Bmatrix} \frac{3}{2} & L & J \\ \beta & \frac{1}{2} & 1 \end{Bmatrix} \delta_{S,\frac{3}{2}} \right] b^{\beta 1}_{L(L'l)} \ , \tag{3.64}$$

$$\mathcal{M}_4 = \sum i^{L-L'-l}(-)^{L'+l+1}[J'][J]^2 M_{lL'L}^{\frac{1}{2}J'SJ}(q,p';k) \times \sum_\beta [\beta] \begin{Bmatrix} \frac{1}{2} & L' & J' \\ l & J & \beta \end{Bmatrix} \left[\frac{1}{\sqrt{6}} \begin{Bmatrix} \frac{1}{2} & L & J \\ \beta & \frac{1}{2} & 1 \end{Bmatrix} \delta_{S,\frac{1}{2}} + \frac{1}{\sqrt{3}} \begin{Bmatrix} \frac{3}{2} & L & J \\ \beta & \frac{1}{2} & 1 \end{Bmatrix} \delta_{S,\frac{3}{2}} \right] c^{\beta 1}_{L(L'l)} \ , \tag{3.65}$$

$$\tilde{\mathcal{M}}_2 = \sum i^{L-L'-l}(-)^{L'+l+\frac{1}{2}}[J'][J]^2 M_{lL'L}^{\frac{1}{2}J'SJ}(q,p';k) \times \sum_\beta [\beta] \begin{Bmatrix} \frac{1}{2} & L' & J' \\ l & J & \beta \end{Bmatrix} \left[\frac{1}{\sqrt{6}} \begin{Bmatrix} \frac{1}{2} & L & J \\ \beta & \frac{1}{2} & 1 \end{Bmatrix} \delta_{S,\frac{1}{2}} - \frac{1}{2\sqrt{3}} \begin{Bmatrix} \frac{3}{2} & L & J \\ \beta & \frac{1}{2} & 1 \end{Bmatrix} \delta_{S,\frac{3}{2}} \right] a^{\beta 1}_{L(L'l)} \ , \tag{3.66}$$

$$\tilde{\mathcal{M}}_3 = \sum i^{L-L'-l}(-)^{L'+l+\frac{1}{2}}[J'][J]^2 M_{lL'L}^{\frac{1}{2}J'SJ}(q,p';k) \times \sum_\beta [\beta] \begin{Bmatrix} \frac{1}{2} & L' & J' \\ l & J & \beta \end{Bmatrix} \left[\frac{1}{\sqrt{6}} \begin{Bmatrix} \frac{1}{2} & L & J \\ \beta & \frac{1}{2} & 1 \end{Bmatrix} \delta_{S,\frac{1}{2}} - \frac{1}{2\sqrt{3}} \begin{Bmatrix} \frac{3}{2} & L & J \\ \beta & \frac{1}{2} & 1 \end{Bmatrix} \delta_{S,\frac{3}{2}} \right] a^{\beta 1}_{L(L'l)} \ , \tag{3.67}$$

$$\tilde{\mathcal{M}}_4 = \sum i^{L-L'-l}(-)^{L'+l+\frac{1}{2}}[J'][J]^2 M_{lL'L}^{\frac{1}{2}J'SJ}(q,p';k) \times \sum_\beta [\beta] \begin{Bmatrix} \frac{1}{2} & L' & J' \\ l & J & \beta \end{Bmatrix} \left[\frac{1}{\sqrt{6}} \begin{Bmatrix} \frac{1}{2} & L & J \\ \beta & \frac{1}{2} & 1 \end{Bmatrix} \delta_{S,\frac{1}{2}} - \frac{1}{2\sqrt{3}} \begin{Bmatrix} \frac{3}{2} & L & J \\ \beta & \frac{1}{2} & 1 \end{Bmatrix} \delta_{S,\frac{3}{2}} \right] c^{\beta 1}_{L(L'l)} \ , \tag{3.68}$$

$$\mathcal{M}_8 = \frac{1}{\sqrt{2}} \sum i^{L-L'-l} (-)^{L+l} [J'][J]^2 M^{J'SJ}_{lL'L}(q,p';k) \sum_\beta [\beta] \begin{Bmatrix} \frac{1}{2} & L' & J' \\ l & J & \beta \end{Bmatrix} \begin{Bmatrix} S & L & J \\ \beta & \frac{1}{2} & 2 \end{Bmatrix} a^{\beta 2}_{L(L'l)} \ , \tag{3.69}$$

$$\mathcal{M}_9 = \frac{1}{\sqrt{2}} \sum i^{L-L'-l} (-)^{L+l} [J'][J]^2 M^{J'SJ}_{lL'L}(q,p';k) \sum_\beta [\beta] \begin{Bmatrix} \frac{1}{2} & L' & J' \\ l & J & \beta \end{Bmatrix} \begin{Bmatrix} S & L & J \\ \beta & \frac{1}{2} & 2 \end{Bmatrix} b^{\beta 2}_{L(L'l)} \ , \tag{3.70}$$

$$\mathcal{M}_{10} = \frac{1}{\sqrt{2}} \sum i^{L-L'-l} (-)^{L+l} [J'][J]^2 M^{J'SJ}_{lL'L}(q,p';k) \sum_\beta [\beta] \begin{Bmatrix} \frac{1}{2} & L' & J' \\ l & J & \beta \end{Bmatrix} \begin{Bmatrix} S & L & J \\ \beta & \frac{1}{2} & 2 \end{Bmatrix} c^{\beta 2}_{L(L'l)} \ , \tag{3.71}$$

$$\mathcal{M}_{11} = \frac{1}{\sqrt{2}} \sum i^{L-L'-l} (-)^{L+l} [J'][J]^2 M^{J'SJ}_{lL'L}(q,p';k) \sum_\beta [\beta] \begin{Bmatrix} \frac{1}{2} & L' & J' \\ l & J & \beta \end{Bmatrix} \begin{Bmatrix} S & L & J \\ \beta & \frac{1}{2} & 2 \end{Bmatrix} a'^{\beta 2}_{L(L'l)} \ , \tag{3.72}$$

$$\mathcal{M}_{12} = \frac{1}{\sqrt{2}} \sum i^{L-L'-l} (-)^{L+l} [J'][J]^2 M^{J'SJ}_{lL'L}(q,p';k) \sum_\beta [\beta] \begin{Bmatrix} \frac{1}{2} & L' & J' \\ l & J & \beta \end{Bmatrix} \begin{Bmatrix} S & L & J \\ \beta & \frac{1}{2} & 2 \end{Bmatrix} b'^{\beta 2}_{L(L'l)} \ , \tag{3.73}$$

where the coefficients $a^{\beta\alpha}_{L(L'l)}$, $b^{\beta\alpha}_{L(L'l)}$, etc, are derived in Appendices A and B, and particularized for the case of a positive- and negative-parity baryon B in Appendix 3.5.4.

3.5.4 Appendix I: Coefficients for Positive and Negative Parity Ξ

In the following, we choose the quantization axis $\hat{z}$ along $\vec{k}$ and $\vec{q}$ to be in the xz-plane, as have been chosen in Eq. (3.8), without loss of generality.

As stated at the end of the paragraph below Eq. (3.7), for a positive parity baryon B, total parity conservation demands that $(-)^{L+L'+l} = -1$. Likewise, for a negative parity B, we have $(-)^{L+L'+l} = +1$. Let's see what do these conditions imply for $[X_{L\,(lL')\beta}]^\alpha$ in Eq. (3.11).

For $\alpha = 0$ (Eq. (3.53)) :

We see from Eq. (3.56) that $D^{L'l}_{L0}$ must be purely imaginary for a positive parity baryon B. Note that $Y_{lm_l}(\hat{q}) = Y_{lm_l}(\theta_q, \phi_q = 0)$ is real, so the complex nature of $D^{L'l}_{L0}$ is determined solely by $Y_{L'M_{L'}}(\hat{p}')$ alone. Now, $Y_{L'M_{L'}}(\hat{p}' = \hat{z}) \left(= \delta_{M_{L'}0}[L']/\sqrt{4\pi}\right)$, $Y_{L'M_{L'}}(\theta_{p'}, \phi_{p'} = 0)$ and $Y_{L'0}(\hat{p}')$ are all real. This implies that

$$D^{L'l}_{L0} = \sum_{M_{L'}} (L'M_{L'}l - M_{L'}|L0) Y_{L'M_{L'}}(\hat{p}') Y_{l-M_{L'}}(\hat{q}) \ , \tag{3.74}$$

vanishes when $\hat{p}' = \hat{z}$, $\phi_{p'} = 0$ or $M_{L'} = 0$ for a positive parity baryon. For $D^{L'l}_{L0}$ not to vanish for $\phi_{p'} \neq 0$, one should necessarily have $M_{L'} \neq 0$ and, consequently, $L', l > 0$. Note also that $D^{L'l}_{L0}$ vanishes identically unless $L > 0$. These features of $D^{L'l}_{L0}$ for a positive parity baryon can be made explicit by rewriting it as

$$D^{L'l}_{L0} = \left[\frac{1}{\sin\theta_{p'} \sin\phi_{p'}} D^{L'l}_{L0} \right] (\hat{p}' \cdot \hat{n}_2) \ . \tag{3.75}$$

On the other hand, for a negative parity baryon B, $D^{L'l}_{L0}$ must be purely real, which implies just the opposite conditions discussed above for a positive parity baryon. In particular, $L, L', l = 0$ are allowed. We, therefore, leave $D^{L'l}_{L0}$ in the original form given by Eq. (3.74).

Summarizing, for a positive parity baryon B, we write

$$a^{\beta 0}_{L(L'l)} = \delta_{\beta L} \frac{(-)^L}{\sqrt{4\pi}} \left[\frac{1}{\sin\theta_{p'} \sin\phi_{p'}} D^{L'l}_{L0} \right] (\hat{p}' \cdot \hat{n}_2) \ , \tag{3.76}$$

and, for a negative parity baryon,

$$a^{\beta 0}_{L(L'l)} = \delta_{\beta L} \frac{(-)^L}{\sqrt{4\pi}} D^{L'l}_{L0} \ . \tag{3.77}$$

For $\alpha = 1$ (Eq. (3.55)) :

First, for the coefficient $a^{\beta 1}_{L(L'l)}$ in Eq. (3.57), we see that $(L0\beta 0|10) \neq 0$ only for $\beta = L \pm 1$. Combining this with Eq. (3.56), it implies that $D^{L'l}_{\beta 0}$ is purely real(imaginary) for a positive(negative) parity baryon B. Therefore, for a positive parity B, $D^{L'l}_{\beta 0}$ in Eq. (3.57) is left in its original form, while, for a negative parity B, it is rewritten in the form given by Eq. (3.76) (with L replaced by

β), i.e.,

$$D^{L'l}_{\beta 0} = \left[\frac{1}{\sin\theta_{p'}\sin\phi_{p'}} D^{L'l}_{\beta 0}\right](\hat{p}'\cdot\hat{n}_2) \ . \tag{3.78}$$

Note that since $\beta = L \pm 1$, one difference from $D^{L'l}_{L0}$ discussed above for $\alpha = 0$ is that, here, $D^{L'l}_{\beta 0}$ does allow $L = 0$.

Next, the coefficients $b^{\beta 1}_{L(L'l)}$ and $c^{\beta 1}_{L(L'l)}$ in Eq. (3.57) involve the terms of the form

$$\begin{aligned}
\frac{1}{\sqrt{2}}\left[Y_{L'M_{L'}}(\hat{p}') + Y^*_{L'M_{L'}}(\hat{p}')\right] &= \sqrt{2}N_{L'M_{L'}}P^{M_{L'}}_{L'}(\cos\theta_{p'})\cos(M_{L'}\phi_{p'}) \ , \\
\frac{-i}{\sqrt{2}}\left[Y_{L'M_{L'}}(\hat{p}') - Y^*_{L'M_{L'}}(\hat{p}')\right] &= \sqrt{2}N_{L'M_{L'}}P^{M_{L'}}_{L'}(\cos\theta_{p'})\sin(M_{L'}\phi_{p'}) \ ,
\end{aligned} \tag{3.79}$$

where

$$N_{L'M_{L'}} \equiv \frac{[L']}{\sqrt{4\pi}}\sqrt{\frac{(L'-M_{L'})!}{(L'+M_{L'})!}} \ . \tag{3.80}$$

Equation (3.79), then, can be rewritten as

$$\begin{aligned}
\frac{1}{\sqrt{2}}\left[D^{L'l}_{\beta 1} + D^{L'l*}_{\beta 1}\right] &= \mathcal{A}^{L'l}_{\beta 1} \ , \\
\frac{-i}{\sqrt{2}}\left[D^{L'l}_{\beta 1} - D^{L'l*}_{\beta 1}\right] &= \mathcal{S}^{L'l}_{\beta 1}\ (\hat{p}'\cdot\hat{n}_2) \ ,
\end{aligned} \tag{3.81}$$

where

$$\begin{aligned}
\mathcal{A}^{L'l}_{\beta M} &\equiv \sqrt{2}\left[\sum_{M_{L'}m_l}(L'M_{L'}lm_l|\beta M)Y_{lm_l}(\hat{q})N_{L'M_{L'}}P^{M_{L'}}_{L'}(\cos\theta_{p'})\cos(M_{L'}\phi_{p'})\right] \ , \\
\mathcal{S}^{L'l}_{\beta M} &\equiv \sqrt{2}\left[\frac{1}{\sin\theta_{p'}\sin\phi_{p'}}\sum_{M_{L'}m_l}(L'M_{L'}lm_l|\beta M)Y_{lm_l}(\hat{q})N_{L'M_{L'}}P^{M_{L'}}_{L'}(\cos\theta_{p'})\sin(M_{L'}\phi_{p'})\right] \ .
\end{aligned} \tag{3.82}$$

Therefore, summarizing, for a positive parity baryon B, we have

$$
\begin{aligned}
a^{\beta 1}_{L(L'l)} &= \frac{[L]}{\sqrt{4\pi}}(L0\beta 0|10)D^{L'l}_{\beta 0} \ , \\
b^{\beta 1}_{L(L'l)} &= -\frac{[L]}{\sqrt{4\pi}}(L0\beta 1|11)\mathcal{A}^{L'l}_{\beta 1} \ , \\
c^{\beta 1}_{L(L'l)} &= -\frac{[L]}{\sqrt{4\pi}}(L0\beta 1|11)\mathcal{S}^{L'l}_{\beta 1}\ (\hat{p}'\cdot\hat{n}_2) \ ,
\end{aligned}
\tag{3.83}
$$

and for a negative baryon B,

$$
\begin{aligned}
a^{\beta 1}_{L(L'l)} &= \frac{[L]}{\sqrt{4\pi}}(L0\beta 0|10)\left[\frac{1}{\sin\theta_{p'}\sin\phi_{p'}}D^{L'l}_{\beta 0}\right](\hat{p}'\cdot\hat{n}_2) \ , \\
b^{\beta 1}_{L(L'l)} &= -\frac{[L]}{\sqrt{4\pi}}(L0\beta 1|11)\mathcal{S}^{L'l}_{\beta 1}\ (\hat{p}'\cdot\hat{n}_2) \ , \\
c^{\beta 1}_{L(L'l)} &= -\frac{[L]}{\sqrt{4\pi}}(L0\beta 1|11)\mathcal{A}^{L'l}_{\beta 1} \ .
\end{aligned}
\tag{3.84}
$$

We note that $\mathcal{S}^{L'l}_{\beta 1}$ does allow both $l=0$ and $L=0$.

For $\alpha = 2$ (Eqs. (3.59,3.61)) :

For u in Eq. (3.61), we see that $(L0\beta 0|20) \neq 0$ only for $\beta = L, L\pm 2$. Combining this with Eq. (3.56), it implies that $D^{L'l}_{\beta 0}$ is purely imaginary(real) for a positive(negative) parity baryon B, like in the case of $\alpha = 0$. Therefore, for a positive parity B, $D^{L'l}_{\beta 0}$ in Eq. (3.61) is rewritten in the form given by Eq. (3.78), while for a negative parity B, it left in its original form. $D^{L'l}_{\beta 0}$ appears also in v and t.

In Eq. (3.61), the same combinations of $D^{L'l}_{\beta 1}$ as given by Eq. (3.81) also appear in w and r, while similar combinations of $D^{L'l}_{\beta 2}$ appear in v and t. They are

$$
\begin{aligned}
\frac{1}{\sqrt{2}}\left[D^{L'l}_{\beta 2} + D^{L'l*}_{\beta 2}\right] &= \mathcal{A}^{L'l}_{\beta 2} \ , \\
\frac{-i}{\sqrt{2}}\left[D^{L'l}_{\beta 2} - D^{L'l*}_{\beta 2}\right] &= \mathcal{S}^{L'l}_{\beta 2}\ (\hat{p}'\cdot\hat{n}_2) \ ,
\end{aligned}
\tag{3.85}
$$

where the quantities in the l.h.s. are defined in Eq. (3.82).

Putting together, for a positive-parity baryon B, we have

$$
\begin{aligned}
u &= \frac{1}{\sqrt{4\pi}}\sqrt{\frac{2}{3}}[L](L0\beta 0|20)\left[\frac{1}{\sin\theta_{p'}\sin\phi_{p'}}D^{L'l}_{\beta 0}\right](\hat{p}'\cdot\hat{n}_2)\ , \\
v &= -\frac{1}{2}\frac{1}{\sqrt{4\pi}}\sqrt{\frac{2}{3}}[L]\left[(L0\beta 0|20)\left[\frac{1}{\sin\theta_{p'}\sin\phi_{p'}}D^{L'l}_{\beta 0}\right] - i\sqrt{3}(L0\beta 2|22)\mathcal{S}^{L'l}_{\beta 2}\right](\hat{p}'\cdot\hat{n}_2)\ , \\
w &= i\sqrt{\frac{3}{4\pi}}\frac{[L]}{\sqrt{10}}(L0\beta 1|21)\mathcal{S}^{L'l}_{\beta 1}\,(\hat{p}'\cdot\hat{n}_2)\ , \\
r &= i\sqrt{\frac{3}{4\pi}}\frac{[L]}{\sqrt{10}}(L0\beta 1|21)\mathcal{A}^{L'l}_{\beta 1}\ , \\
t &= -i\frac{1}{\sqrt{4\pi}}\frac{[L]}{\sqrt{2}}(L0\beta 2|22)\mathcal{A}^{L'l}_{\beta 2}\ ,
\end{aligned}
\tag{3.86}
$$

and, for a negative-parity baryon,

$$
\begin{aligned}
u &= \frac{1}{\sqrt{4\pi}}\sqrt{\frac{2}{3}}[L](L0\beta 0|20)D^{L'l}_{\beta 0}\ , \\
v &= -\frac{1}{2}\frac{1}{\sqrt{4\pi}}\sqrt{\frac{2}{3}}[L]\left[(L0\beta 0|20)D^{L'l}_{\beta 0} - \sqrt{3}(L0\beta 2|22)\mathcal{A}^{L'l}_{\beta 2}\right]\ , \\
w &= \sqrt{\frac{3}{4\pi}}\frac{[L]}{\sqrt{10}}(L0\beta 1|21)\mathcal{A}^{L'l}_{\beta 1}\ , \\
r &= -\sqrt{\frac{3}{4\pi}}\frac{[L]}{\sqrt{10}}(L0\beta 1|21)\mathcal{S}^{L'l}_{\beta 1}\,(\hat{p}'\cdot\hat{n}_2)\ , \\
t &= \frac{1}{\sqrt{4\pi}}\frac{[L]}{\sqrt{2}}(L0\beta 2|22)\mathcal{S}^{L'l}_{\beta 2}\,(\hat{p}'\cdot\hat{n}_2)\ .
\end{aligned}
\tag{3.87}
$$

The respective coefficients $a^{\beta 2}_{L(L'l)}$, $b^{\beta 2}_{L(L'l)}$, etc, are, then, (from Eq. (3.59))

$$\begin{aligned}
a^{\beta 2}_{L(L'l)} &= \frac{1}{\sqrt{8\pi}}[L]\left[\sqrt{3}(L0\beta 0|20)\left[\frac{1}{\sin\theta_{p'}\sin\phi_{p'}}D^{L'l}_{\beta 0}\right] + i(L0\beta 2|22)\mathcal{S}^{L'l}_{\beta 2}\right](\hat{p}'\cdot\hat{n}_2)\ , \\
b^{\beta 2}_{L(L'l)} &= i\frac{1}{\sqrt{2\pi}}[L](L0\beta 2|22)\mathcal{S}^{L'l}_{\beta 2}\,(\hat{p}'\cdot\hat{n}_2)\ , \\
c^{\beta 2}_{L(L'l)} &= i\sqrt{\frac{3}{4\pi}}\sqrt{\frac{2}{5}}[L](L0\beta 1|21)\mathcal{S}^{L'l}_{\beta 1}\,(\hat{p}'\cdot\hat{n}_2)\ , \\
a'^{\beta 2}_{L(L'l)} &= i\sqrt{\frac{3}{4\pi}}\sqrt{\frac{2}{5}}[L](L0\beta 1|21)\mathcal{A}^{L'l}_{\beta 1}\ , \\
b'^{\beta 2}_{L(L'l)} &= -i\frac{1}{\sqrt{2\pi}}[L](L0\beta 2|22)\mathcal{A}^{L'l}_{\beta 2}\ ,
\end{aligned} \tag{3.88}$$

for a positive-parity baryon B, and

$$\begin{aligned}
a^{\beta 2}_{L(L'l)} &= \frac{1}{\sqrt{8\pi}}[L]\left[\sqrt{3}(L0\beta 0|20)D^{L'l}_{\beta 0} + (L0\beta 2|22)\mathcal{A}^{L'l}_{\beta 2}\right]\ , \\
b^{\beta 2}_{L(L'l)} &= \frac{1}{\sqrt{2\pi}}[L](L0\beta 2|22)\mathcal{A}^{L'l}_{\beta 2}\ , \\
c^{\beta 2}_{L(L'l)} &= \sqrt{\frac{3}{4\pi}}\sqrt{\frac{2}{5}}[L](L0\beta 1|21)\mathcal{A}^{L'l}_{\beta 1}\ , \\
a'^{\beta 2}_{L(L'l)} &= -\sqrt{\frac{3}{4\pi}}\sqrt{\frac{2}{5}}[L](L0\beta 1|21)\mathcal{S}^{L'l}_{\beta 1}\,(\hat{p}'\cdot\hat{n}_2)\ , \\
b'^{\beta 2}_{L(L'l)} &= \frac{1}{\sqrt{2\pi}}[L](L0\beta 2|22)\mathcal{S}^{L'l}_{\beta 2}\,(\hat{p}'\cdot\hat{n}_2)\ ,
\end{aligned} \tag{3.89}$$

for a negative-parity baryon.

The coefficients, $a^{\beta\alpha}_{L(L'l)}$, have been determined to be either purely real or purely imaginary for a given π_Ξ. Eqs. 3.76(3.77), 3.83(3.84), and 3.88(3.89), for positive(negative) π_Ξ, along with Eqs. 3.62-3.73 can be applied to Eq. 3.19 to determine which spin-structure coefficients, F_i, depend on Re $\left[D^{L'l}_{\beta M}\right]$ or Im $\left[D^{L'l}_{\beta M}\right]$. These results are shown in Table 3.1.

3.5.5 Appendix J: Spin Observables

Using the photoproduction amplitude in the form

$$\hat{M}^{\lambda} \equiv \sum_{m=0}^{3} M_m^{\lambda} \sigma_m \ , \tag{3.90}$$

with $\sigma_0 = 1$, $\sigma_1 = \sigma_x$, etc, any observable corresponding to the photon polarization $\vec{\epsilon}_\lambda$ can be calculated straightforwardly. The cross section with the polarization of the photon $\vec{\epsilon}_\lambda$ incident on an unpolarized target is given by

$$\frac{d\sigma^{\lambda}}{d\Omega} \equiv \frac{1}{2} Tr\left[\hat{M}^{\lambda}\hat{M}^{\lambda\dagger}\right] = \sum_{m=0}^{3} |M_m^{\lambda}|^2 \ . \tag{3.91}$$

For a given photon polarization $\vec{\epsilon}_\lambda$, and target nucleon spin in the i-direction ($i = x, y, z$), the corresponding spin-correlation coefficient T_i^{λ} can be expressed as

$$\begin{aligned} \frac{d\sigma^{\lambda}}{d\Omega} T_i^{\lambda} &\equiv \frac{1}{2} Tr[\hat{M}^{\lambda}\sigma_i \hat{M}^{\lambda\dagger}] \\ &= 2Re[M_0^{\lambda} M_i^{\lambda *}] + 2Im[M_j^{\lambda} M_k^{\lambda *}] \ , \end{aligned} \tag{3.92}$$

where the subscripts (i, j, k) run cyclically, i.e., (1,2,3), (2,3,1), (3,1,2).

Similarly, the polarization, P_i^{λ}, of the outgoing nucleon in the i-direction induced by a photon beam with polarization $\vec{\epsilon}_\lambda$ is given by

$$\begin{aligned} \frac{d\sigma^{\lambda}}{d\Omega} P_i^{\lambda} &\equiv \frac{1}{2} Tr[\hat{M}^{\lambda}\hat{M}^{\lambda\dagger}\sigma_i] \\ &= 2Re[M_0^{\lambda} M_i^{\lambda *}] - 2Im[M_j^{\lambda} M_k^{\lambda *}] \ , \end{aligned} \tag{3.93}$$

where the subscripts (i, j, k) run cyclically.

Another spin observable is the spin transfer coefficient induced by a polarized photon beam,

K_{ij}^{λ}, which is given by

$$\begin{aligned}\frac{d\sigma^{\lambda}}{d\Omega}K_{ij}^{\lambda} &\equiv \frac{1}{2}Tr[\hat{M}^{\lambda}\sigma_i\hat{M}^{\lambda\dagger}\sigma_j] \\ &= \left(2|M_0^{\lambda}|^2 - \frac{d\sigma^{\lambda}}{d\Omega}\right)\delta_{ij} + 2Re[M_i^{\lambda}M_j^{\lambda *}] - 2\epsilon_{ijk}Im[M_k^{\lambda}M_0^{\lambda *}] \ , \end{aligned} \tag{3.94}$$

where ϵ_{ijk} denotes the Levi-Civita antisymmetric tensor and (i,j,k) may take any of the values $(1,2,3)$. The diagonal terms reduce to

$$\frac{d\sigma^{\lambda}}{d\Omega}K_{jj}^{\lambda} = |M_0^{\lambda}|^2 + |M_j^{\lambda}|^2 - \sum_{k\neq j}|M_k^{\lambda}|^2 \ . \tag{3.95}$$

In terms of the individual cross sections K_{jj}^{λ} may be written as

$$K_{jj}^{\lambda} = \frac{[\sigma_j^{\lambda}(+,+) + \sigma_j^{\lambda}(-,-)] - [\sigma_j^{\lambda}(+,-) + \sigma_j^{\lambda}(-,+)]}{[\sigma_j^{\lambda}(+,+) + \sigma_j^{\lambda}(-,-)] + [\sigma_j^{\lambda}(+,-) + \sigma_j^{\lambda}(-,+)]} \ , \tag{3.96}$$

where $\sigma_j^{\lambda}(+,-)$, for example, corresponds to the cross section induced by a photon beam with polarization $\vec{\epsilon}_{\lambda}$ on a target nucleon spin in the positive$(+)$ j-direction and leading to the recoil nucleon spin in the negative$(-)$ j-direction. Given the spin structure of the amplitude, Eq. (3.96) is often helpful in determining the characteristics of K_{jj}^{λ}.

Eqs. (3.91,3.92,3.93,3.94) exhaust all the possible observables in photoproduction with a polarized photon beam. Other observables may be constructed by appropriate linear combinations of them. The completely unpolarized cross section is given by

$$\frac{d\sigma}{d\Omega} \equiv \left(\frac{1}{2}Tr\left[\hat{M}\hat{M}^{\dagger}\right]\right) = \sum_{\lambda}\frac{d\sigma^{\lambda}}{d\Omega} = \sum_{\lambda}\sum_{m=0}^{3}|M_m^{\lambda}|^2 \ . \tag{3.97}$$

The photon asymmetry is given by

$$\begin{aligned}\frac{d\sigma}{d\Omega}\Sigma &\equiv \frac{d\sigma^{\lambda_1}}{d\Omega} - \frac{d\sigma^{\lambda_2}}{d\Omega} \\ &= \sum_{m=0}^{3}\left(|M_m^{\lambda_1}|^2 - |M_m^{\lambda_2}|^2\right) \ , \end{aligned} \tag{3.98}$$

where λ_1 and λ_2 stands for the two independent state of polarization of the photon, $\vec{\epsilon}_{\lambda_1}$ and $\vec{\epsilon}_{\lambda_2}$, to be specified. Note that the factor 1/2 in the above equation is due to the fact that we have multiplied the beam asymmetry Σ by the completely unpolarized cross section $d\sigma/d\Omega$. The same observation holds for the spin observables defined below. In Refs. [83,125] $d\sigma/d\Omega$ is defined without the factor of 1/2.

The target nucleon asymmetry, T_i, obtained using an unpolarized photon beam on a target nucleon polarized in the i-direction, is given by

$$\begin{aligned} \frac{d\sigma}{d\Omega}T_i &\equiv \frac{1}{2}Tr[\hat{M}\sigma_i\hat{M}^\dagger] \\ &= \sum_\lambda \frac{d\sigma^\lambda}{d\Omega}T_i^\lambda = \sum_\lambda \Big(2Re[M_0^\lambda M_i^{\lambda *}] + 2Im[M_j^\lambda M_k^{\lambda *}]\Big) \ , \end{aligned} \tag{3.99}$$

where again, the subscripts (i,j,k) run cyclically.

Similarly, the polarization observable, P_i, of the recoil nucleon with an unpolarized photon beam is given by

$$\begin{aligned} \frac{d\sigma}{d\Omega}P_i &\equiv \frac{1}{2}Tr[\hat{M}M^\dagger\sigma_i] \\ &= \sum_\lambda \frac{d\sigma^\lambda}{d\Omega}P_i^\lambda = \sum_\lambda \Big(2Re[M_0^\lambda M_i^{\lambda *}] - 2Im[M_j^\lambda M_k^{\lambda *}]\Big) \ . \end{aligned} \tag{3.100}$$

The spin transfer coefficient using an unpolarized photon beam is given by

$$\begin{aligned} \frac{d\sigma}{d\Omega}K_{ij} &\equiv \frac{1}{2}Tr[\hat{M}\sigma_i\hat{M}^\dagger\sigma_j] \ , \\ &= \sum_\lambda \frac{d\sigma^\lambda}{d\Omega}K_{ij}^\lambda = \sum_\lambda \left\{ \left(2|M_0^\lambda|^2 - \frac{d\sigma^\lambda}{d\Omega}\right)\delta_{ij} + 2Re[M_i^\lambda M_j^{\lambda *}] - 2\epsilon_{ijk}Im[M_k^\lambda M_0^{\lambda *}] \right\} \end{aligned} \tag{3.101}$$

where (i,j,k) may take any of the values $(1,2,3)$ as in Eq.(3.94). The diagonal terms reduce to

$$\frac{d\sigma}{d\Omega}K_{jj} = |M_0|^2 + |M_j|^2 - \sum_{k\neq j}|M_k|^2 \ , \tag{3.102}$$

with $|M_i|^2 = \sum_\lambda |M_i^\lambda|^2$.

Chapter 4

Summary and Outlook

There is a global effort to understand confinement. To that end, hadronic resonances offer a unique opportunity to study the non-perturbative region of QCD. To compare scattering data with fundamental QCD-based quark calculations, a good reaction theory is needed. Such a reaction theory should distill resonance properties, such as mass, width, spin, parity, among others, from scattering data. It is these properties that are compared with the QCD calculations. This work focuses on the $S = -2$ hyperon sector. The $\bar{K} + N \rightarrow K + \Xi(\Xi^*)$ reaction was studied via a model-independent analysis. This analysis allowed us to list a minimum set of spin observables which determine the reaction amplitude completely and the J^P of the produced Ξ or Ξ^*. A model calculation for this same reaction was conducted and contributions from Y^* hyperons were investigated. A number of Y^* states were needed to reproduce the existing data and their parameters were reported. In addition, yet-to-be-measured spin observables were predicted based on these results. The $\gamma + N \rightarrow K + K + \Xi$ reaction was also investigated in a model-independent manner and its spin structure analyzed. Again, the parity of the produced Ξ can be determined by analyzing the spin observables in certain angular regions. Gauge-invariance of the photoproduction amplitude was discussed and its constraints on our model were determined.

A continuation of this work would be the model calculation of the $\gamma + N \rightarrow K + K + \Xi$ according to the model described in Section 3.3. Past work has concluded that high spin resonances were necessary to fit existing photoproduction data [54]. While these results appear to be consistent

with our findings for $\bar{K} + N \to K + \Xi$, a simultaneous analysis of both reactions is called for and underway. Also, new data is expected in the coming years for both these reactions and others, and should be analyzed along the same lines described in this work. In addition, the simple model described here violates unitarity. A general procedure for guaranteeing unitary within the models based on Effective Lagrangian approaches has been developed by our group [126] and could be implemented in the present model calculations. In this method, a complex phase would be introduced in a systematic way to ensure unitarity and spin-observables will be very sensitive to this phase. This will shed light on the contributions from coupled channels that we are currently excluding. Because resonances couple to different channels, the ultimate goal should still be a full dynamical coupled-channel (DCC) calculation.

In addition to improving our calculation toward a full DCC approach, new data is expected soon in these reactions and others. $\bar{K}$-induced reactions at J-PARC will offer new and improved data for $K\Xi$ as well as other $S = -1$ channels. The newly upgraded facility at J-Lab will be providing new data on $\gamma + N \to K + K + \Xi$ as well as $K + K + K + \Omega^-$. This new data for $K\Xi$, $\pi\Lambda$, $\pi\Sigma$, $KK\Xi$, $KKK\Omega^-$ and other final states should provide new insights into the multi-strangeness hyperon physics.

Bibliography

[1] H. Fritzsch, M. Gell-Mann and H. Leutwyler, Phys. Lett. B 47, 365 (1973).

[2] A. Bondar *et al.* [Belle Collaboration], Phys. Rev. Lett. 108, 122001 (2012).

[3] I. Adachi *et al.* [Belle Collaboration], arXiv:1209.6450v2 [hep-ex].

[4] I. Adachi *et al.* [Belle Collaboration], arXiv:1207.4345v1 [hep-ex].

[5] N. Brabilla, *et al.* Eur. Phys. J. C **71** 1534 (2011)

[6] K. A. Olive *et al.* (Particle Data Group), Chin. Phys. C **38**, 090001 (2014).

[7] J. Kogut, L. Susskind, Phys. Rev. D **10**, 3468 (1974); 11, 3594 (1975).

[8] E. Witten, Nucl. Phys. **B149**, 285 (1979); Ann. Phys. (N.Y.) **128**, 363 (1980).

[9] G. 't Hooft, Phys. Rep. **142**, 357 (1986).

[10] S. Weinberg, Phys. Rev. D **11**, 3583 (1975).

[11] G. t Hooft, Phys. Rev. Lett. **37**, 8 (1976).

[12] E. Witten, Nucl. Phys. **B156**, 269 (1979).

[13] G. Veneziano, Nucl. Phys. **B159**, 213 (1979).

[14] G. Christos, Phys. Rep. **116**, 251 (1984).

[15] M. Gell-Mann, Y. Ne'eman, Frontiers in physics. W.A. Benjamin, 1964.

[16] www.learner.org/courses/physics/visual/visual.html?shortname=mesons_baryons.

[17] Siegfried Bethke, Eur. Phys. J. C **64**, 689 (2009)

[18] K. G. Wilson, Phys. Rev. D 10, 2445 (1974).

[19] Hadron Spectrum Collaboration, R. G. Edwards, N. Mathur, D. G. Richards, and S. J. Wallace, Phys. Rev. D **87**, 054506 (2013).

[20] BGR [Bern-Graz-Regensburg] Collaboration, G. P. Engel, C. B. Lang, D. Mohler, and A. Schäfer, Phys. Rev. D **87**, 074504 (2013).

[21] S. Du?rr, Z. Fodor, J. Frison, C. Hoelbling, R. Hoffmann, S. D. Katz, S. Krieg and T. Kurth *et al.*, Science 322, 1224 (2008).

[22] J. J. Dudek, R. G. Edwards, M. J. Peardon, D. G. Richards and C. E. Thomas, Phys. Rev. Lett. 103, 262001 (2009).

[23] G. P. Engel *et al.* [BGR [Bern-Graz-Regensburg] Collaboration], Phys. Rev. D 82, 034505 (2010).

[24] J. Bulava, R. G. Edwards, E. Engelson, B. Joo, H-W. Lin, C. Morningstar, D. G. Richards and S. J. Wallace, Phys. Rev. D 82, 014507 (2010).

[25] C. B. Lang and V. Verduci, Phys. Rev. D 87, no. 5, 054502 (2013).

[26] G. P. Engel, C. B. Lang, D. Mohler and A. Schafer, Phys. Rev. D 87, 074504 (2013).

[27] C. Alexandrou, J. W. Negele, M. Petschlies, A. Strelchenko and A. Tsapalis, Phys. Rev. D 88, 031501 (2013).

[28] R. G. Edwards, N. Mathur, D. G. Richards and S. J. Wallace, Phys. Rev. D 87, 054506 (2013).

[29] M. Döring, M. Mai and U.-G. Meißner, Phys. Lett. B 722, 185 (2013).

[30] S. Capstick and W. Roberts, Prog. Part. Nucl. Phys. **45**, S241 (2000).

[31] M. Ronniger and B. C. Metsch, Eur. Phys. J. A **47**, 162 (2011).

[32] N. Isgur, G. Karl, Phys. Rev. D **18** 4187 (1978)

[33] S. Capstick and N. Isgur, Phys. Rev. D **34**, 2809 (1986).

[34] D. J. Wilson, I. C. Cloet, L. Chang, and C. D. Roberts, Phys. Rev. C **85**, 025205 (2012).

[35] Y. Oh, Phys. Rev. D **75**, 074002 (2007).

[36] E. Oset and A. Ramos, Eur. Phys. J. A **44**, 445 (2010).

[37] M. Mai, P. C. Bruns, and U.-G. Meissner, Phys. Rev. D **86**, 094033 (2012).

[38] E. Klempt and J.-M. Richard, Rev. Mod. Phys. **82**, 1095 (2010).

[39] Volker Crede, Winston Roberts, arXiv:1302.7299v2 [nucl-ex]

[40] S. Weinberg Physica A **96**, 327 (1979).

[41] V. K. Magas, A. Feijoo, and A. Ramos, AIP Conf. Proc. **1606**, 208 (2014); arXiv:1402.3971v1 [hep-ph].

[42] J. Caro Ramon, N. Kaiser, S. Wetzel, and W. Weise, Nucl. Phys. **A672**, 249 (2000).

[43] U. G. Meißner and J. A. Oller, Nucl. Phys. **A673**, 311 (2000).

[44] V. E. Barnes, P. L. Connolly, D. J. Crennell, B. B. Culwick, W. C. Delaney, W. B. Fowler, P. E. Hagerty and E. L. Hart *et al.*, Phys. Rev. Lett. 12, 204 (1964).

[45] BABAR Collaboration, B. Aubert *et al.*, Phys. Rev. Lett. **97**, 112001 (2006).

[46] Particle Data Group, J. Beringer *et al.*, Phys. Rev. D **86**, 010001 (2012), http://pdg.lbl.gov.

[47] CLAS Collaboration, L. Guo *et al.*, Phys. Rev. C **76**, 025208 (2007).

[48] High-Energy Reactions Analysis Group, V. Flaminio, W. G. Moorhead, D. R. O. Morrison, and N. Rivoire, CERN Report No. CERN-HERA-83-02 (1983).

[49] H.-Y. Ryu, A. Hosaka, H. Haberzettl, H.-C. Kim, K. Nakayama, and Y. Oh, PoS **Hadron2013**, 140 (2013), [arXiv:1401.3804v1 [hep-ph]].

[50] J. Bono, PhD. Dissertation, Florida International University, 2014

[51] J. Bono, PoS XLASNPA (2014) 039

[52] The Very Strange Collaboration, A. Afanasev *et al.*, JLab. Report No. JLAB-PR-12-008 (2012).

[53] K. Nakayama, Y. Oh, and H. Haberzettl, Phys. Rev. C **74**, 035205 (2006).

[54] J. K. S. Man, Y. Oh, and K. Nakayama, Phys. Rev. C **83**, 055201 (2011).

[55] V. Flaminio, W. G. Moorhead, D. R. O. Morrison, and N. Rivoire (High-Energy Reactions Analysis Group), CERN Report No. CERN-HERA-83-02.

[56] J. K. Ahn, J. Korean Phys. Soc. **49**, 2276 (2006).

[57] H. Takahashi, Nucl. Phys. **A914**, 553 (2013).

[58] The $\overline{\text{P}}$ANDA Collaboration, W. Erni *et al.*, arXiv:0903.3905v1 [hep-ex].

[59] K.-T. Chao, N. Isgur, and G. Karl, Phys. Rev. D **23**, 155 (1981).

[60] M. Pervin and W. Roberts, Phys. Rev. C **77**, 025202 (2008).

[61] L. Ya. Glozman and D. O. Riska, Phys. Rep. **268**, 263 (1996).

[62] C. E. Carlson and C. D. Carone, Phys. Lett. B **484**, 260 (2000).

[63] C. L. Schat, J. L. Goity, and N. N. Scoccola, Phys. Rev. Lett. **88**, 102002 (2002).

[64] J. L. Goity, C. Schat, and N. N. Scoccola, Phys. Lett. B **564**, 83 (2003).

[65] N. Matagne and Fl. Stancu, Phys. Rev. D **71**, 014010 (2005).

[66] N. Matagne and Fl. Stancu, Phys. Rev. D **74**, 034014 (2006).

[67] F. X. Lee and X. Liu, Phys. Rev. D **66**, 014014 (2002).

[68] D. Jido and M. Oka, arXiv:hep-ph/9611322v2.

[69] D. D. Carmony, G. M. Pjerrou, P. E. Schlein, W. E. Slater, D. H. Stork, and H. K. Ticho, Phys. Rev. Lett. **12**, 482 (1964).

[70] J. P. Berge, P. Eberhard, J. R. Hubbard, D. W. Merrill, J. Button-Shafer, F. T. Solmitz, and M. L. Stevenson, Phys. Rev. **147**, 945 (1966).

[71] M. Haque *et al.* (Birmingham-Glasgow-London(I.C.)-Oxford-Rutherford Collaboration), Phys. Rev. **152**, 1148 (1966).

[72] G. W. London, R. R. Rau, N. P. Samios, S. S. Yamamoto, M. Goldberg, S. Lichtman, M. Prime, and J. Leitner, Phys. Rev. **143**, 1034 (1966).

[73] T. G. Trippe and P. E. Schlein, Phys. Rev. **158**, 1334 (1967).

[74] G. Burgun *et al.*, Nucl. Phys. B **8**, 447 (1968).

[75] W. P. Trower, J. R. Ficenec, R. I. Hulsizer, J. Lathrop, J. N. Snyder, and W. P. Swanson, Phys. Rev. **170**, 1207 (1968).

[76] P. M. Dauber, J. P. Berge, J. R. Hubbard, D. W. Merrill, and R. A. Muller, Phys. Rev. **179**, 1262 (1969).

[77] J. C. Scheuer *et al.* (S.A.B.R.E. Collaboration), Nucl. Phys. B **33**, 61 (1971).

[78] A. de Bellefon *et al.*, Nuovo Cim. A **7**, 567 (1972).

[79] R. Rader *et al.*, Nuovo Cim. A **16**, 178 (1973).

[80] J. Griselin *et al.*, Nucl. Phys. B **93**, 189 (1975).

[81] E. Briefel *et al.*, Phys. Rev. D **16**, 2706 (1977).

[82] J. R. Carlson, H. F. Davis, D. E. Jauch, N. D. Sossong, and R. Ellsworth, Phys. Rev. D **7**, 2533 (1973).

[83] K. Nakayama and W. G. Love, Phys. Rev. C **72**, 034603 (2005).

[84] M. Jacob and G. C. Wick, Ann. Phys. (N.Y.) **7**, 404 (1959).

[85] A. Bohr, Nucl. Phys. **10**, 486 (1959).

[86] G. R. Satchler, *Direct Nuclear Reactions*, (Oxford University Press, New York, 1983).

[87] K. Nakayama, Y. Oh, and H. Haberzettl, Phys. Rev. C **85**, 042201(R) (2012).

[88] S. M. Deen, Rutherford Laboratory Preprint, RPP/H/68 (1968), (Rutherford High Energy Laboratory, Chilton, Didcot, Berkshire),

[89] A. Brandstetter *et al.*, Nucl. Phys. **B39**, 13 (1972).

[90] W.-T. Chiang and F. Tabakin, Phys. Rev. C **55**, 2054 (1997).

[91] S. U. Chung, CERN Report No. CERN-71-08 (1971), revised version (Aug 2, 2013).

[92] S. F. Biagi *et al.*, Z. Phys. C **34**, 175 (1987).

[93] K. Moriya *et al.* Phys. Rev. Lett. **112** (2014), 082004.

[94] D. A. Sharov, V. L. Korotkikh, and D. E. Lanskoy, Eur. Phys. J. A **47**, 109 (2011).

[95] R. Shyam, O. Scholten, and A. W. Thomas, Phys. Rev. C **84**, 042201 (2011).

[96] H. Kamano, S. X. Nakamura, T.-S. H. Lee, and T. Sato, arXiv:1407.6839v1 [nucl-th]

[97] C. B. Dover and A. Gal, Ann. Phys. (N.Y.) **146**, 309 (1983).

[98] Y. Yamamoto, T. Motoba, T. Fukuda, M. Takahashi, and K. Ikeda, Prog. Theor. Phys. Suppl. **117**, 281 (1994).

[99] S. Tadokoro, H. Kobayashi, and Y. Akaishi, Phys. Rev. C **51**, 2656 (1995).

[100] M. Kohno and S. Hashimoto, Prog. Theor. Phys. **123**, 157 (2010).

[101] B. Jackson, Y. Oh, H. Haberzettl, and K. Nakayama, Phys. Rev. C **89**, 025206 (2014).

[102] M. Döring and K. Nakayama, Phys. Lett. B **683**, 145 (2010).

[103] A. Ramos and E. Oset, Phys. Lett. B **727**, 287 (2013).

[104] H.-Y. Ryu, A. I. Titov, A. Hosaka, and H.-C. Kim, Prog. Theor. Exp. Phys. **2014**, 023D03 (2014).

[105] H. Ryu, A. Hosaka, H.-C. Kim, and A. I. Titov, Int. J. Mod. Phys. Conf. Ser. **26**, 1460055 (2014).

[106] D. Plümper, J. Flender, and M. F. Gari, Phys. Rev. C **49**, 2370 (1994).

[107] R. Shyam and O. Scholten, Phys. Rev. C **78**, 065201 (2008).

[108] L. Guo *et al.* (CLAS Collaboration), Phys. Rev. C **76**, 025208 (2007).

[109] K. Schilling, P. Seyboth, and G. Wolf, **B18**, 332(E) (1970).

[110] A. R. Edmonds, *Angular Momentum in Quantum Mechanics*, (Princeton University Press, 1957).

[111] G. Källén, *Elementary Particle Physics*, (Addison-Wesley, Reading, MA, 1964), Ch. 17.

[112] S. Gasiorowicz, *Elementary Particle Physics*, (John Wiley & Sons, New York, 1966), Ch. 32.

[113] K. Nakayama and H. Haberzettl, Phys. Rev. C **69**, 065212 (2004).

[114] K. Nakayama and H. Haberzettl, Phys. Rev. C **73**, 045211 (2006).

[115] K. Nakayama, Y. Oh, and H. Haberzettl, J. Korean Phys. Soc. **59**, 224 (2011).

[116] S.-J. Chang, Phys. Rev. **161**, 1308 (1967).

[117] J. C. Ward, Phys. Rev. **78**, 182 (1950)

[118] Y. Takahashi, Nuovo Cimento, Ser. 10, 370 (1957)

[119] H. Haberzettl, Phys. Rev. C **56**, 2041 (1997).

[120] E.O. Alt, P. Grassberger, and W. Sandhas, Nucl. Phys. **B2**, 167 (1967).

[121] W. Sandhas, Acta Physica Austriaca, Suppl. IX, 57 (1972).

[122] B. C. Jackson, Y. Oh, H. Haberzettl, and K. Nakayama, arXiv:1503.00845 [nucl-th].

[123] H. Haberzettl and K. Nakayama, Phys. Rev. C **85**, 064001 (2012).

[124] K. Moriya *et al.* (CLAS Collaboration), Phys. Rev. Lett. **112**, 082004 (2014).

[125] K. Nakayama and W. G. Love, Phys. Rev. **C70**, 01220(R) (2004).

[126] S. Razavi, K. Nakayama, to be published